SPATIAL AND SPECTRAL BEHAVIOR OF SPECKLE IN AN IMAGING SYSTEM

Thesis by

Richard Devern Samuels Melville, Jr.

In Partial Fulfillment of the Requirements

For the Degree of

Doctor of Philosophy

California Institute of Technology

Pasadena, California

1975

(Submitted February 18 1975)

Acknowledgments

I wish to thank my thesis advisor, Dr. Nicholas George, for his suggestion of the research topic and for his continued support and guidance throughout the conduct of the work.

In addition, I acknowledge the continuing influence of Professor Emeritus Austin R. Frey of the United States Naval Postgraduate School, and I am also most grateful for the help of Professor Charles H. Papas and Dr. William B. Bridges during the course of this work.

I am especially grateful for the constant encouragement and support of my wife, Jean, and the others of my family who have endured substantial disruption of their lives because of my studies.

Finally, I thank the Institute, the U. S. Air Force, and the Northrop Aircraft Corporation for the financial support I have received.

ABSTRACT

When coherent illumination is reflected from or transmitted through a medium which causes random phase changes in the illumination, a random interference pattern termed speckle results.

We have studied speckle in an imaging system and have described and measured the effect of polarization of the illumination, the first order statistics of speckle intensity, and the autocorrelation of speckle intensity as a function of space and wavelength variables.

We have measured the relationship between the amount of depolarization of a plane polarized input in transmission through opal glass diffusers of various thicknesses and the effect of this phenomenon on the first and second order statistics of speckle intensity. A relationship between diffuser thickness and the probability density function for speckle intensities has been calculated and measured. The autocorrelation of speckle intensities has been calculated and measured as a function of both the spatial dimension of the speckle pattern and the wavelength of the illumination. We find that the spatial behavior of the autocorrelation depends upon the limiting aperture of the optical system, while the wavelength dependence is a function of the roughness of the diffuser and is only very slightly influenced by the imaging system.

TABLE OF CONTENTS

CHAPTER I

INTRODUCTION

1.1 Speckle

Whenever coherent light is reflected from or transmitted through a random diffusing medium which is sufficiently rough so as to produce localized phase retardations in the direction of propagation, the wave upon leaving the medium will consist of randomized regions of high and low field. A pattern of such light and dark regions due to the interference of the various random phases exiting the diffuser we term speckle, or a speckle pattern. Clearly, a detailed understanding of the characteristics of speckle phenomena will be important in the use of any coherent optical system and although speckle is described here in terms of a visible optical phenomenon, the same random interference effect is found in infrared optical systems, radar and acoustic imaging or detection systems. We emphasize that speckle results from coherent irradiation of a rough object. With normal white light illumination of a diffuse surface at optical frequencies, the phases at each point on the object are changing randomly on the order of 10^{10} times per second, thus typical viewing systems (such as the eye) average the random phases over many fluctuations and the speckle disappears.

1.2 Review of Speckle Studies

The random interference effect which we call speckle has been observed and studied for many years [1,2]. The early statistical calculations found in reference [1], while given in terms of acoustics,

provide a direct basis for the theory of the statistics of speckle.

Since the invention of the laser, the widespread use of coherent optical systems has made the study of speckle increasingly important. Almost immediately upon the advent of the He-Ne laser, speckle was observed and reported in the literature by a number of authors [3,4,5]. An analysis was presented showing that the average size of the light and dark areas in the speckle pattern is a function of the transfer function of the viewing system [3]. It was further pointed out that the laser speckle phenomenon is analogous to radar "clutter" which occurs in the reflection of radar signals from raindrops or other random media [4].

An early treatment of the statistics of laser speckle patterns used a set of randomly positioned antennae as a model for a diffuse surface [6]. With this model, calculations of the first and second order statistics of speckle intensity were made. Here we also find the first discussion of the wavelength dependence of speckle. A different calculation of the spatial autocorrelation function of speckle intensity was made for coherent light transmitted through a pure phase diffuser [7]. In this diffuser model, the phase of a plane wave illumination beam is randomized by scatterers arranged in "checkerboard" fashion across the diffuser surface. The amount of phase retardation for each scattering area was a random variable uniformly distributed over $0 - 2\pi$. It was determined theoretically and experimentally verified that the spatial autocorrelation in the Fresnel zone was equal to the two-dimensional Fourier transform of the illumination spot distribution on the diffuser surface.

In the field of holography, speckle occurred as an unwanted noise phenomenon, displeasing in pictorial holography and nearly ruinous in micro-holography where the speckles are approximately the size of the objects to be studied. Therefore, a number of workers advanced ideas for the reduction of speckle in holography. One technique for recording a hologram with greatly reduced granulation was that of making a superposition hologram of the same object illuminated by light passed through a large number of different diffusers [8]. Photographs of holograms made with a superposition of 25 different illuminations show marked improvement in image quality.

Another method, appropriate for reduction of speckle in holograms of planar objects, such as photographic transparencies, was the use of spatially phase modulated illumination [9]. Experimentally, significant speckle reduction was demonstrated using a pure phase diffuser in very close contact with the transparency to provide the spatial phase modulation in the illumination of the object. It was also shown theoretically that the illumination of a planar object could be optimized to produce low-noise holograms [10]. A pseudo-random diffuser resembling ground glass, but specifically designed with certain constraints given by the optimization was used to modulate the phase of the illumination. Still another technique for speckle reduction in holograms was that of using a grating in a collimated laser beam to provide multiple illumination of a planar transparency [11]. In this way it was possible to reduce speckle, but still make a hologram relatively insensitive to dust and scratches, such as one made by diffuse illumination.

In a study of the noise-like structure in the image of a diffusely reflecting object, the diffused object was considered to be a planar array of independent point scatterers, and from this model, the average intensity of the image, the standard deviation of the speckle fluctuations and the autocorrelation of image intensity were calculated [12]. Since the phases of the reflected wave were assumed to be uniformly distributed over $0 - 2\pi$, the average intensity and standard deviation of intensity were found to be equal. The autocorrelation was found to be proportional to the impulse response of the image system. *Using the same physical model for a diffuser in an image system*, but mathematically modelling the diffuser as a narrow-band noise source, the same calculations were made using linear system theory to describe the image system [13]. The calculations made using the linear system approach were substantially simpler and the results were in agreement with those in [12].

Not all of the interest in speckle has been directly oriented toward its elimination. For example, it has been found possible to achieve nearly diffraction limited resolution in large astronomical telescopes by Fourier analyzing speckle intensity patterns in star images [14]. When the radiation from a star propagates through a turbulent atmosphere, the image which results in a telescope incorporating a narrow-band spectral filter is a speckle pattern. If a sequence of these speckle patterns are recorded photographically, with exposure times short compared to the changes in the turbulence, each will contain a different speckle distribution, but the information

about the star is present in each. By superposing these images in an optical processor, the random data tend to be smoothed, while the desired stellar information is enhanced in an additive way. This technique has been used to measure the diameter of some previously unresolved stars as well as previously unresolved binary spacings [15].

Another use of speckle has been demonstrated in the direct visual observation of surface "in-plane" vibration nodal patterns [16]. It was shown that if a vibrating surface is illuminatd with a speckle pattern, where the surface motion is large the speckle is averaged by the vibration, while at nodes of the vibration the speckle is distinct. Thus it is possible to make an immediate visual assessment of surface vibrational characteristics. Indeed this area of interest has come to be called laser speckle metrology and a number of ideas for measurement of small surface displacements and deformations have been advanced e.g., [17,18].

Speckle reduction in imagery with laser illumination has been achieved by use of moving diffusers in the laser beam [19,20].

Now, in most of the theoretical and all of the experimental work previously described attention was given primarily to the spatial character of the speckle patterns, and the effects of wavelength variation, diffuser correlations and depolarization were largely ignored. However, it has been found that the effect of speckle in imagery may be reduced by the use of multicolor illumination [21,22]. In the images of various microscope specimens it was found that photographs produced by a multiple exposure using 6 narrow illumination wavelengths spread over 1500Å were comparable to those taken with white light [23].

Calculations were also made to establish that two speckle patterns produced by the same diffuse surface would be uncorrelated if the wavelengths used to illuminate the surface were spaced by an amount proportional to the square of the mean wavelength divided by the standard deviation of the heights of the scatterers on the surface. A number of experimental results have been given to support this calculation [24,25]. Recent significant steps in the understanding of speckle were the introduction into the theory of the concept of fractional roughness [26,27] and the inclusion of correlation length along the diffuser [28,29].

In this thesis, the entire speckle phenomenon is studied, generalizing on the concept of varying roughness of a scattering surface. In the analysis, herein, the diffuser model is also generalized to include a function describing the correlation between the heights of the scatterers on the diffuse surface. Calculations of the autocorrelation of speckle intensity in the output of the linear system as a function of both spatial and temporal frequency variables show that the spatial dependence of the speckle is primarily determined by the linear system transfer function, while the spectral dependence is determined by the roughness of the diffuse surface. A number of experimental tests have also been made to support the analyses.

An outline of this work is as follows: Chapter II contains a restatement of the theory for the characterization of speckle in a linear, space-invariant system. In Chapter III, the effects of polarization on speckle patterns are measured and analyzed. Chapter IV gives theory and experiment relating to the first order statistics

of speckle. In Chapter V, the multidimensional spatial and spectral autocorrelation function of speckle intensity is measured.

REFERENCES

1. Lord Rayleigh: Phil. Mag. X, 73 (1880).
2. vonLaue, M.: Sitzungsber Kgl. Preuss. Akad. Wiss. 47, 1144 (1914).
3. Rigden, J. O. and Gordon, E. I.: IRE Proc. 50, 2367 (1962).
4. Langmuir, R. V.: App. Phys. Lett. 2, 29 (1963).
5. Oliver, B. M.: IEEE Proc. 51, 220 (1963).
6. Goodman, J. W.: Stanford U. Elec. Labs. Tech. Report SEL-63-140, (1963).
7. Goldfischer, L. I., JOSA 55, 247 (1965).
8. Martiessen, W. and Spiller, S.: Phys. Lett. 24A, 126 (1967).
9. Upatnieks, J.: Appl. Opt. 6, 1905 (1967).
10. Leith, E. N. and Upatnieks, J.: Appl. Opt. 7, 2085 (1968).
11. Gerritsen, H. J., Hannan, W. J. and Ramberg, E. J.: Appl. Opt. 7, 2301 (1968).
12. Enloe, L. H.: Bell Sys. Tech. J. 46, 1479 (1967).
13. Burckhardt, C. B.: Bell Sys. Tech. J. 49, 309 (1970).
14. Labeyrie, A.: Astron. & Astrophys. 6, 85 (1970).
15. Gezari, D. Y., Labeyrie, A., and Stachnik, R. V.: Astrophys. J. 173, L1 (1972).
16. Archbold, E., Burch, J. M., Ennos, A. E. and Taylor, P. A.: Nature 222, 263 (1969).
17. Archbold, E., Burch, J. M. and Ennos, A. E.: Optica Acta 17, 883 (1970).
18. Butters, J. N. and Leendertz, J. A.: J. Phys. E. 4, 277 (1971).
19. Lowenthal, S., Arsenault, H. and Joyeux, D.: Application of Holography (Besancon Conference 6-11 July 1970), p. 2-2.
20. Arsenault, H. and Lowenthal, S.: Optics Comm. II, 451 (1970).

21. Elbaum, M., Greenbaum, M. and King, M.: Opt. Comm. 5, 171 (1972).

22. George, N. and Jain, A.: JOSA 62, 1356A (1972).

23. George, N. and Jain, A.: Opt. Comm. 6, 253 (1972).

24. George, N. and Jain, A.: JOSA 63, 480A (1972).

25. George, N. and Jain, A.: Proc. SPIE 41, 161 (1973).

26. George, N. and Jain, A.: Appl. Opt. 12, 1202 (1973).

27. Jain, A.: Ph.D. Thesis: "A Wavelength Diversity Technique for Smoothing of Speckle", California Institute of Technology, 1974.

28. George, N. and Jain, A.: App. Phys. 1, (1974).

29. Asakura, T., Fujii, H. and Jurata, K.: Optica Acta 19, 273 (1972).

CHAPTER II

SPECKLE IN A SPACE-INVARIANT LINEAR SYSTEM

2.1 Statement of the Problem

In this chapter we will calculate the autocorrelation of the output intensity of an imaged speckle pattern as a function of spatial and spectral variables. However, in this section we present and describe a simple model for the phenomenon.

The term imaged speckle refers to an experiment as shown in figure (2-1), in which a coherently illuminated diffuser is placed in the input plane of the optical system and the output intensity is observed in the plane which is normally associated with production of an image of the input. Using the idea of reciprocity, we describe the system physically in a manner inverse to that normally thought of in imaging systems. That is, we consider the output field at a point to be the resultant of a sum of fields emanating from within a resolution diameter in the input plane. From this viewpoint, we can describe both the spectral and spatial behavior of the output speckle and estimate the form of the autocorrelation function.

We examine one resolution diameter of a phase object as in figure (2-2). Assume that the object is a diffuser such as ground glass which creates local phase disturbances in the electric field at the diffuser surface. The amplitude of the electric field is constant over the surface. Call the phase at a point $\phi(x)$. Now

$$\phi(x) = kn_3h(x) \tag{2.1}$$

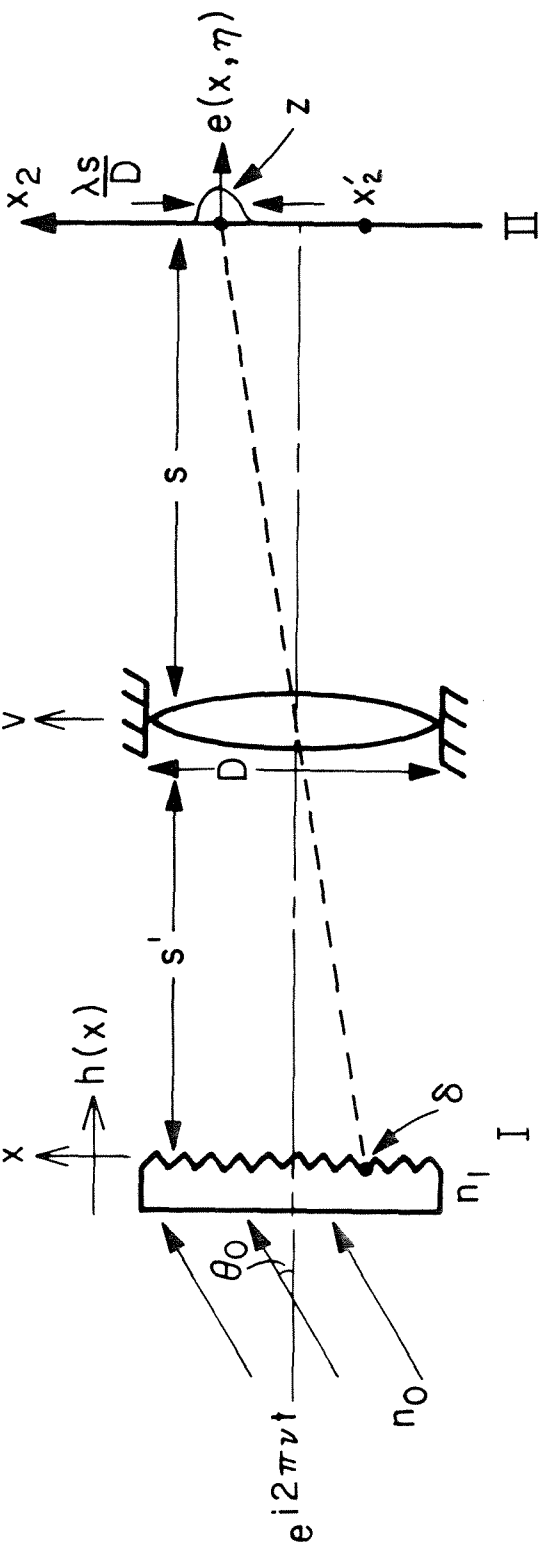

$$\eta = \frac{2\pi n_3 \nu}{c}$$

$$n_3 = n_1/\cos\theta_1 - n_0/\cos\theta_0$$

Fig. 2-1: Imaged speckle. Diffuser at plane I is coherently illuminated and the speckle pattern is observed at plane II. Z represents the impulse response of the lens.

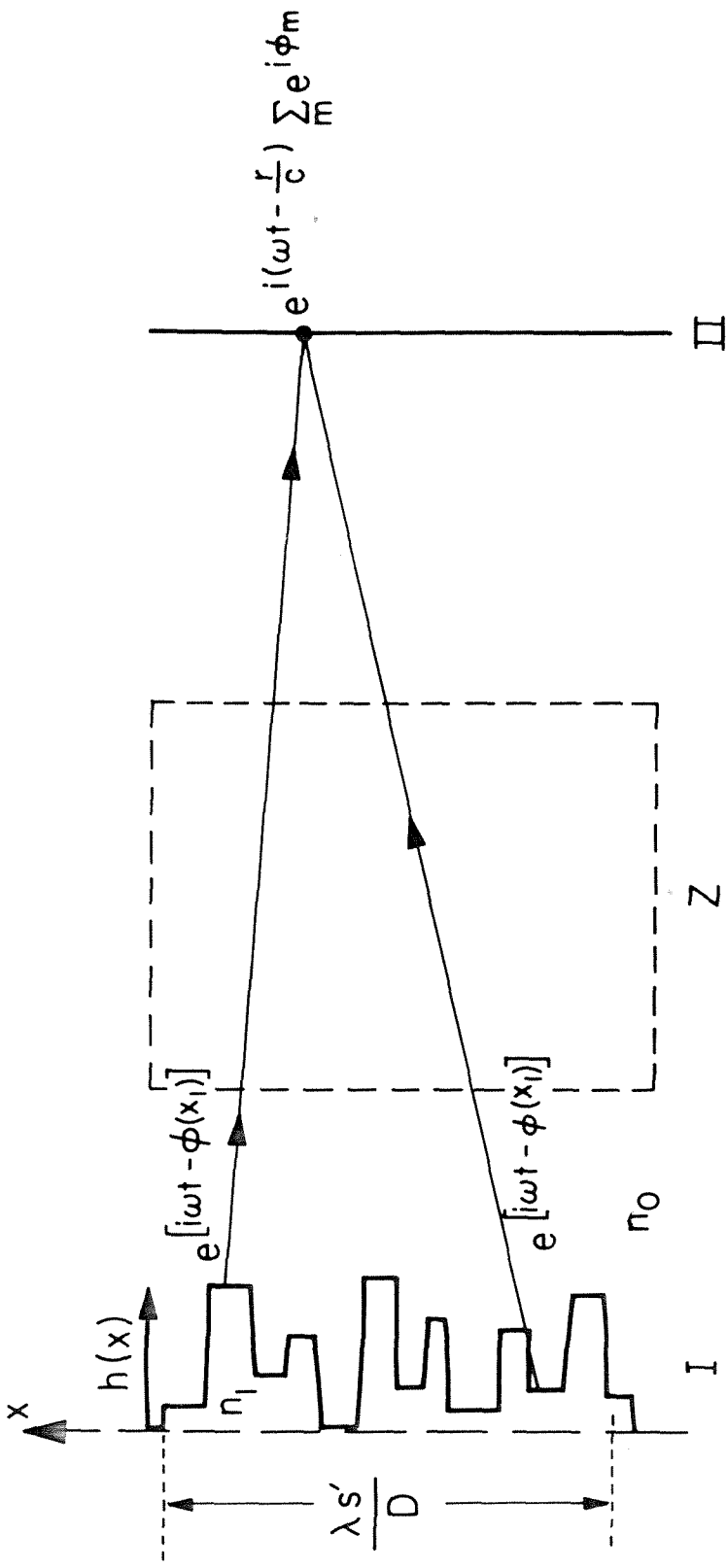

Fig. 2-2: Field at plane II shown as the sum of fields over the dimension $\lambda s'/D$ in the input plane. Z represents the optical system.

where n_3 is the difference in refractive index between the glass and the air, k is the wave number and $h(x)$ is the height of glass at x measured from the minimum height as shown. We consider cases in which there are ten or more distinct heights in a resolution diameter. Now, by decorrelation with wavelength, we mean: by how much would we expect to change the wavelength of the illumination on the diffuser in order to change the intensity at a point in the speckle pattern where we observe the interference of the various phases coming from the resolution cell? Since the intensity variations are caused only by the interference, we examine $\phi(x)$. From equation (2.1) we see that $\phi(x)$ is a product of the height and the wave number. Therefore, if the heights in the resolution cell are large, a small change in k causes large changes in $\phi(x)$, whereas if the heights are small it requires a much larger change in k to produce a comparable change in $\phi(x)$. Since the intensity in the output depends on the specific summation of the $\phi(x)$ from the resolution cell, the change in $\phi(x)$ due to the wavelength change will determine the change in output intensity. If *we pick as a criterion for decorrelation of the speckle that the* <u>average</u> phase difference between any two points on the diffuser surface, $\Delta\phi(x) = \phi(x_1) - \phi(x_2)$, changes by π then we see that the frequency change required is

$$\frac{\Delta\nu}{c} \simeq \frac{1}{2n_3\,\sigma(h)} \tag{2.2}$$

where $\sigma(h)$ is the standard deviation of heights in a resolution cell.

Equation (2.2) differs only by a factor π from results previously given in the literature [1,2,3]. Thus, we expect that the change in optical frequency required to decorrelate the speckle pattern is primarily a function of the roughness of the diffuser as characterized by $\sigma(h)$

A similar physical reasoning can be applied to estimate the spatial autocorrelation of the speckle pattern. We consider an imaging system of unity magnification and ask: how far from the point x_2 in the output must we move before the intensity we measure at a new point x_2' is uncorrelated with that at x_2? Referring to figure (2-1), we see that if the intensity were measured by scanning an intensity measuring instrument slowly from x_2 to x_2' the specific set of phase scatterers on the diffuser contributing to the output at each intermediate position x is constantly changing. However, it is not until x_2' is at least one resolution diameter away from x_2 that we have removed from the field of view all of the scatterers belonging to the observation at x_2. We therefore contend that the autocorrelation of speckle intensity at constant wavelength is a function of the limiting aperture of the system, which determines the size of the resolution cell. This result is generally accepted [4,5].

We now proceed to calculate the spatial and spectral correlation function for the speckle intensity using a linear system formalism.

2.2 Characterization of Input Fields

We consider the characteristics of speckle intensity produced in the image plane of an optical system as shown in figure (2-1). Following the format of George and Jain [3] we will calculate the autocorrelation of the speckle intensity as a function of spatial and spectral variables. In this section a description of the interaction between illumination and the diffuse transmissive surface is given. This interaction is the randomized input to the optical system.

The scalar component of electric field at a point on a rough transmissive diffuser will be written

$$g(x,\eta) = a(x,\eta) \exp(-i\eta\, h(x)) \tag{2.3}$$

where x is a spatial variable in the plane of the diffuser and

$$\eta = \frac{2\pi\nu}{c}\left(\frac{n_1}{\cos\theta_1} - \frac{n_o}{\cos\theta_o}\right) \tag{2.4}$$

is a normalized wave number, a function of n_1 and n_o the indices of refraction of the diffuser and ambient medium respectively, and θ_1 and θ_o, the angles in the same media measured from the normal. $h(x)$ is a random variable representing the height of the diffuser surface and $a(x,\eta)$ is the amplitude of the field on the diffuser surface which may also be a random variable.

2.3 Autocorrelation of the Output Intensity

In the space-invariant system shown conceptually in figure (2-3) we denote the input field by $g(x,\eta)$ as before. The impulse response of the system is $z(x,\eta)$, and the output electric field is given by $e(x,\eta)$. Presuming coherent illumination, the output speckle intensity is

$$u(x,\eta) = e(x,\eta)\, e^*(x,\eta) \tag{2.5}$$

where the asterisk connotes complex conjugation. We write the autocorrelation of output intensity

$$R_u(\Delta x,\eta_1,\eta_2) = \langle u(x+\Delta x,\eta_1+\Delta\eta)\, u^*(x,\eta_1)\rangle \tag{2.6}$$

where the brackets $\langle\ \rangle$ are used to denote an expected value, $\Delta\eta = \eta_2 - \eta_1$ and $\Delta x = x_2 - x_1$. As pointed out in [3], the notation $R_u(\Delta x,\eta_1,\eta_2)$ is specifically used to show that the process considered is stationary in the spatial variable x, but not in the normalized wave-number η. This stationarity is determined by the random process $h(x)$. If we choose a diffuser such that $h(x)$ is stationary, then $g(x,\eta)$ is stationary in x, and by the linearity of the spatial convolution between g and z, the output field will be stationary in x. Additionally, if we neglect dispersion $a(x,\eta)$ can be thought of as stationary in x. However, as is seen in equation (2.3), η is a <u>deterministic</u> multiplier of $h(x)$, therefore we expect that the autocorrelation of the output will depend upon both η_1 and η_2 and not simply $\Delta\eta$. This is readily seen by assuming $\eta_1 = 0$ for one set (η_1,η_2).

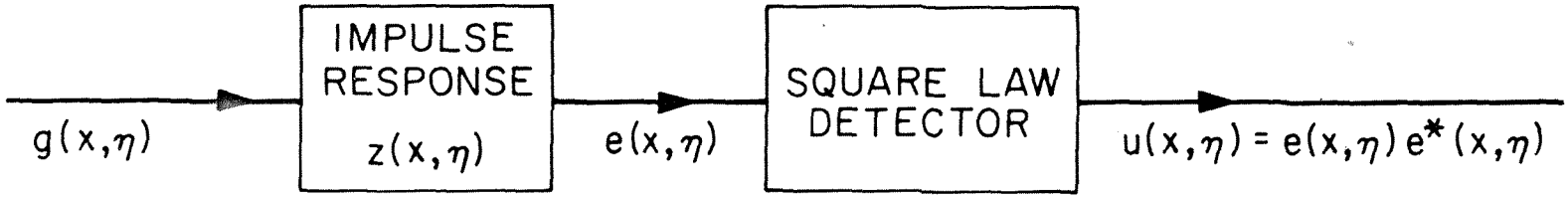

Fig. 2-3: Linear system model for space-invariant optical system.

Using (2.5) and (2.6) we write R_u in terms of the output electric field

$$R_u(\Delta x,\eta_1,\eta_2) = \langle e(x+\Delta x,\eta_1+\Delta\eta)\, e(x,\eta_1) \cdot e^*(x+\Delta x,\eta_1+\Delta\eta)\, e^*(x,\eta_1)\rangle \tag{2.7}$$

Now if we make the assumption that we are dealing with fields which are normally distributed we may apply Reed's [6] theorem relating an n^{th} order central product moment to a sum of products of covariances. Thus

$$R_u(\Delta x,\eta_1,\eta_2) = \langle e(x,\eta_1)\, e^*(x,\eta_1)\rangle \langle e(x+\Delta x,\eta_1+\Delta\eta) \cdot e^*(x+\Delta x,\eta_1+\Delta\eta)\rangle + \langle e(x,\eta_1) \cdot e^*(x+\Delta x,\eta_1+\Delta\eta)\rangle \langle e^*(x_1\eta_1)\, e(x+\Delta x,\eta_1+\Delta\eta)\rangle \tag{2.8}$$

The first two terms of equation (2.8) are recognized as

$$\langle u(x,\eta_1)\rangle \langle u(x+\Delta x,\eta_1+\Delta\eta)\rangle \tag{2.9}$$

and the last two terms may be written

$$|\langle e(x+\Delta x,\eta_1+\Delta\eta)\, e^*(x,\eta_1)\rangle|^2 \tag{2.10}$$

which by analogy to equation (2.6) we write

$$|R_e(\Delta x,\eta_1,\eta_2)|^2 \tag{2.11}$$

Therefore,

$$R_u(\Delta x,\eta_1,\eta_2) = \langle u(x,\eta_1)\rangle \langle u(x+\Delta x,\eta_1+\Delta\eta)\rangle + |R_e(\Delta x,\eta_1,\eta_2)|^2 \tag{2.12}$$

Now for the space-invariant system where the output field is written as the convolution of the input with the impulse response of the system

$$e(x,\eta) = g(x,\eta) * z(x,\eta) \tag{2.13}$$

it is easily shown that

$$R_e(\Delta x,\eta_1,\eta_2) = R_g(\Delta x,\eta_1,\eta_2) * R_z(\Delta x,\eta_1,\eta_2) \tag{2.14}$$

where R_g is the autocorrelation of the <u>input</u> field and R_z is the autocorrelation of the impulse response, and the asterisk again denotes convolution.

Thus, the general result for the autocorrelation of the output intensity where we assume normally distributed random processes in the input for the space invariant linear system is

$$R_u(\Delta x,\eta_1,\eta_2) = \langle u(x,\eta_1)\rangle \langle u(x+\Delta x,\eta_1+\Delta\eta)\rangle + |R_g(\Delta x,\eta_1,\eta_2) * R_z(\Delta x,\eta_1,\eta_2)|^2 \tag{2.15}$$

In this formulation we see that in order to predict the form of the function R_u and its behavior with respect to the spatial and spectral variables, we must calculate the autocorrelation of the input field for various diffuser classes. The expected intensities at (x,η_1) and at $(x+\Delta x,\eta_1+\Delta\eta)$ can be obtained from $R_g * R_z$ and the impulse

response $z(x,\eta)$ will be a deterministic function of the spatial variable x only. Following [3] we calculate R_g for a pure phase diffuser and show a new calculation for a thin variable amplitude diffuser.

2.4 Autocorrelation of $g(x,\eta)$ Resulting from a Thin Pure Phase Diffuser

We define a thin pure phase diffuser as one which does not attenuate input illumination, but merely retards the phase of the illumination at the surface as determined by the product $\eta h(x)$. Therefore, from equation (2.3), setting $a(x,\eta) \equiv 1$ we have the input field

$$g(x,\eta) = \exp(-i\eta h(x)) \tag{2.16}$$

We define the random process $h(x)$ by a joint probability density function $f(h(x), h(x+\Delta x))$ and solve for R_g:

$$\begin{aligned} R_g(\Delta x,\eta_1,\eta_2) &= \langle g(x+\Delta x,\eta_1+\Delta\eta)\, g^*(x,\eta_1)\rangle \\ &= \int_{-\infty}^{\infty}\int \exp[i\eta_1 h(x)] \exp[-i(\eta_1+\Delta\eta)\, h(x+\Delta x)] \\ &\quad \cdot f(h(x),h(x+\Delta x))\, dh(x)\, dh(x+\Delta x) \end{aligned} \tag{2.17}$$

From the definition of the two-dimensional characteristic function for the process h

$$F(p,q) = \int_{-\infty}^{\infty}\int \exp(-iph_1 - iqh_2)\, f(h_1,h_2)\, dh_1 dh_2 \tag{2.18}$$

we see that the integral in equation (2.17) is the characteristic

function for the diffuser heights expressed as a function of η_1 and η_2

$$R_g(\Delta x,\eta_1,\eta_2) = F(-\eta_1,\eta_2) \tag{2.19}$$

Using this result it is possible to solve for the desired R_u by knowledge of the characteristic function of the diffuser.

2.5 Autocorrelation of $g(x,\eta)$ from a Thin Amplitude Diffuser

We characterize a pure amplitude diffuser as one with a random amplitude transmittance, but without a phase changing property. Then

$$g(x,\eta) = a(x,\eta) \tag{2.20}$$

We further assume that the function $a(x,\eta)$ is achromatic and is normally distributed in x. We then write the joint density for $a(x_1)$ and $a(x_2)$ with correlation coefficient $r(x_2-x_1)$,

$$f(a(x_1),a(x_2)) = \frac{1}{2\pi\sigma_1\sigma_2\sqrt{1-r^2}}$$

$$\times \exp\Big[-\frac{1}{2(1-r^2)}\Big\{\frac{(a(x_1)-\langle a(x_1)\rangle)^2}{\sigma_1^2}$$

$$-\frac{2r(a(x_1)-\langle a(x_1)\rangle)(a(x_2)-\langle a(x_2)\rangle)}{\sigma_1\sigma_2}$$

$$+\frac{(a(x_2)-\langle a(x_2)\rangle)^2}{\sigma_2^2}\Big\}\Big] \tag{2.21}$$

We choose

$$\sigma_1 = \sigma_2 = \sigma$$

$$\langle a(x_1)\rangle = \langle a(x_2)\rangle = a \tag{2.22}$$

and solve for

$$R_g(\Delta x,\eta_1,\eta_2) = \langle a(x_1)\, a(x_2)\rangle \tag{2.23}$$

Using the notation $a(x_1) = a_1$ and $a(x_2) = a_2$ and the assumptions of equation (2.20) the autocorrelation of the input field is

$$R_g(\Delta x,\eta_1,\eta_2) = \frac{1}{2\pi\sigma^2\sqrt{1-r^2}} \int_{-\infty}^{\infty}\int a_1 a_2 \exp\Big[-\frac{1}{2(1-r^2)\sigma^2}$$

$$\cdot \{(a_1-a)^2 - 2r(a_1-a)(a_2-a) + (a_2-a)^2\}\Big]$$

$$\cdot\ da_1\, da_2 \tag{2.24}$$

which can be integrated directly. However, we make use of the identity [7]

$$\langle a_1 a_2\rangle = \langle a_1 \langle a_2|a_1\rangle\rangle \tag{2.25}$$

where $\langle a_2|a_1\rangle$ denotes the conditional expectation of a_2 given a_1. The conditional density of a_2 when given a_1 is

$$f(a_2|a_1) = \frac{1}{\sqrt{2\sigma(1-r^2)}} \exp\left\{-\frac{[(a_2-a) - r(a_1-a)]^2}{2\sigma^2(1-r^2)}\right\} \tag{2.26}$$

Thus

$$\langle a_2|a_1\rangle = \int_{-\infty}^{\infty} \frac{a_2}{\sigma\sqrt{2\pi(1-r^2)}} \exp\left\{-\frac{[(a_2-a) - r(a_1-a)]^2}{2\sigma^2(1-r^2)}\right\} da_2 \tag{2.27}$$

which results in

$$\langle a_2 | a_1 \rangle = a + r(a_1 - a) \tag{2.28}$$

Using (2.28) in (2.25) and (2.23) we see that

$$R_g(\Delta x, \eta_1, \eta_2) = \langle a_1 [a + r(a_1 - a)] \rangle \tag{2.29}$$

which can be solved by inspection.

$$R_g(\Delta x, \eta_1, \eta_2) = \langle a_1 a \rangle + r\langle a_1^2 \rangle - r\langle a_1 a \rangle \tag{2.30}$$

and since $\langle a_1 \rangle = a$ we rewrite

$$R_g(\Delta x, \eta_1, \eta_2) = \langle a_1 \rangle^2 + r(\langle a_1^2 \rangle - \langle a_1 \rangle^2) \tag{2.31}$$

which is simplified to

$$R_g(\Delta x, \eta_1, \eta_2) = a^2 + r\sigma^2 \tag{2.32}$$

This form of the autocorrelation of the input field is appropriate then for a pure amplitude diffuser with jointly normal amplitude variations and correlation coefficient $r(x_1, x_2) = r(\Delta x)$.

2.6 Spatial and Spectral Autocorrelation of Speckle Intensity from a Pure Phase Diffuser

The results of sections 2.3 and 2.4 are used to calculate the autocorrelation function of speckle intensity for a phase diffuser with jointly normal heights in an achromatic viewing system. The heights $h(x) = h_1$ and $h(x + \Delta x) = h_2$ are jointly normal random variables with a correlation coefficient $r(\Delta x)$ between them. The joint density function is [7]

$$f(h_1,h_2) = \frac{1}{2\pi\sigma^2(1-r^2)^{1/2}} \exp\left\{ - \frac{h_1^2 - 2rh_1h_2 + h_2^2}{2\sigma^2(1-r^2)} \right\} \tag{2.33}$$

We have assumed zero means for h_1 and h_2 and a common variance. Since we are assuming an achromatic optical system, the autocorrelation of the impulse response is

$$R_z(\Delta x,\eta_1,\eta_2) = R_z(\Delta x) \tag{2.34}$$

The characteristic function for the diffuser is calculated by taking the Fourier transform of $f(h_1,h_2)$ with respect to the variables $(-\eta_1,\eta_2)$. Substituting (2.33) into (2.16) and integrating yields

$$F(-\eta_1,\eta_2) = \exp\{ - \frac{\sigma^2}{2} (\eta_1^2 - 2r\eta_1\eta_2 + \eta_2^2) \} \tag{2.35}$$

Then from (2.15) we can write the resultant autocorrelation of speckle intensity

$$R_u(\Delta x,\eta_1,\eta_2) = \langle u(x,\eta_1)\rangle \langle u(x+\Delta x,\eta_1+\Delta\eta)\rangle + |\exp\{- \frac{\sigma^2}{2} (\Delta\eta^2 + 2(1-r)\eta_1(\eta_1+\Delta\eta)\} * R_z(\Delta x)|^2 \tag{2.36}$$

Now showing the dependence of r on the spatial variable and writing the convolution integral explicitly, the result is

$$R_u(\Delta x,\eta_1,\eta_2) = \langle u(x,\eta)\rangle \langle u(x+\Delta x,\eta_1+\Delta\eta)\rangle + \left| \int_{-\infty}^{\infty} \exp\{- \frac{\sigma^2}{2} (\Delta\eta^2 + 2(1-r(\xi))\eta_1(\eta_1+\Delta\eta)\} \cdot R_z(\Delta x - \xi)d\xi \right|^2 \tag{2.37}$$

We consider a particular imaging system in one dimension. Using the notation of figure (2-1) the diffuser is placed in the (x,y) plane, a distance s' from the lens, and the output intensity is measured in the (x_2,y_2) plane, a distance s from the lens. We use the image condition $1/s' + 1/s = 1/f$ where f is the focal length of the lens. The standard form [8] for the system transfer function, neglecting slowly varying phase terms is:

$$z(x_2,x) = \frac{s}{s'} \int_{-\infty}^{\infty} A(\lambda s\tilde{v}) \exp[\{i2\pi(x_2 + \frac{s}{s'} x)\} \tilde{v}] \, d\tilde{v} \tag{2.38}$$

where $A(v)$ is the pupil function measured in the lens plane along v and

$$\tilde{v} = \frac{v}{\lambda s} \tag{2.39}$$

Choosing as a pupil function

$$A(v) = \text{rect}(\frac{v}{L_x}) \tag{2.40}$$

where the rect function represents transmissivity one over the range $-L_x/2 \leq v \leq L_x/2$ and transmissivity zero elsewhere, we find that

$$Z(x_2,x) = \frac{L_x}{\lambda s'} \text{sinc}[\frac{L_x}{\lambda s} (x_2 + \frac{s}{s'} x)] \tag{2.41}$$

and

$$R_z(\Delta x_2,\eta_1,\eta_2) \cong \frac{L_x \bar{\nu}}{Cs'} \text{sinc}(\frac{L_x \bar{\nu}}{Cs} \Delta x_2) \tag{2.42}$$

where $\bar{\nu}$ is the mean of ν_1 and ν_2 and the subscript 2 indicates that the spatial variable is in the output plane. The function $\text{sinc}(t)$ is defined by $\sin(\pi t)/\pi t$.

For the correlation coefficient $r(\xi)$ in (2.37) we choose a

Gaussian shape

$$r(\xi) = \exp\{-\xi^2/T^2\} \tag{2.43}$$

which has been used by Asakura et al. [9] in the calculation for speckle intensity in the Fourier transform plane of a lens. T is representative of the correlation length on the diffuser surface. Then (2.37) is expressed

$$R_u(\Delta x_2, \eta_1, \eta_2) = \langle u(x_2, \eta_1)\rangle \langle u(x_2+\Delta x_2, \eta_1+\Delta\eta)\rangle + \left| \int_{-\infty}^{\infty} \exp\left[-\frac{\sigma^2}{2}(\Delta\eta^2 + 2(1 - \exp[-\xi_2^2/T^2])\eta_1(\eta_1+\Delta\eta)\right] \cdot Ma\ \mathrm{sinc}(a\Delta x_2 - a\xi_2)\, d\xi_2 \right|^2 \tag{2.44}$$

The substitutions $M = s/s'$ and $a = L_x\bar{\nu}/Cs$ have been made and it is noted that the correlation length T has been scaled by the factor M for integration in the output plane.

We seek a solution of the integral expressed in equation (2.44). Neglecting the constants and re-arranging the terms

$$I = \exp(-\sigma^2\Delta\eta^2)\exp(-\sigma^2\beta) \cdot \int_{-\infty}^{\infty} \exp[\sigma^2\beta \exp(-\xi^2/T^2)]\ \mathrm{sinc}(a\Delta x - a\xi)d\xi \tag{2.45}$$

where the variables are expressed in the output plane and the substitution

$$\beta = \eta_1(\eta_1 + \Delta\eta) \tag{2.46}$$

has been made. Now expanding the exponential in the integral I' of (2.45)

$$\exp[\sigma^2\beta \exp(-\xi^2/T^2)] = \sum_{m=o}^{\infty} \frac{(\sigma^2\beta)^m}{m!} \exp(-m\xi^2/T^2) \tag{2.47}$$

we express

$$I' = \sum_{m=o}^{\infty} \frac{(\sigma^2\beta)^m}{m!} \int_{-\infty}^{\infty} \exp(-m\xi^2/T^2)\mathrm{sinc}(a\Delta x - a\xi)d\xi \tag{2.48}$$

Equation (2.48) is solved by use of the convolution theorem

$$I' = \sum_{m=o}^{\infty} \frac{(\sigma^2\beta)^m}{m!} \frac{T}{a}\sqrt{\frac{\pi}{m}} \int_{-\infty}^{\infty} \mathrm{rect}(\frac{\alpha}{a})\exp(\frac{-\pi^2T^2}{m}\alpha^2)$$

$$\cdot\exp(i2\pi\Delta x\alpha)\, d\alpha \tag{2.49}$$

Applying the definition of the rect function

$$I' = \sum_{m=o}^{\infty} \frac{(\sigma^2\beta)^m}{m!} \frac{T}{a}\sqrt{\frac{\pi}{m}} \int_{-\frac{a}{2}}^{\frac{a}{2}} \exp(-\frac{\pi^2T^2}{m}\alpha^2 + i2\pi\Delta x\alpha)d\alpha \tag{2.50}$$

Integration of (2.50) and substitution into (2.45) and (2.44) yields (after some algebraic manipulation)

$$R_u(\Delta x,\ \eta_1\eta_2) = \langle u(x,\eta_1)\rangle \langle u(x+\Delta x,\eta_1+\Delta\eta)\rangle$$

$$+ \left| \frac{M}{2} \exp(-\sigma^2\Delta\eta^2)\exp(-\sigma^2\beta) \left\{ 2 + \sum_{m=1}^{\infty} \frac{(\sigma^2\beta)^m}{m!} \right.\right.$$

$$\cdot\exp\left(\frac{-m\Delta x^2}{T^2}\right) \left[\operatorname{erfc}\left(-\frac{\pi T a}{2\sqrt{m}} - i\frac{\sqrt{m}\,\Delta x}{T}\right)\right.$$

$$\left.\left.\left. -\operatorname{erfc}\left(\frac{\pi T a}{2\sqrt{m}} - i\frac{\sqrt{m}\,\Delta x}{T}\right)\right]\right\}\right|^2 \qquad (2.51)$$

Now using equations (2.6) and (2.8) we recognize that

$$\langle u(x,\eta_1)\rangle = R_g(0,\eta_1,\eta_1) * R_z(0,\eta_1,\eta_1) \qquad (2.52)$$

and

$$\langle u(x+\Delta x,\eta_1+\Delta\eta)\rangle = R_g(\Delta x,\eta_2,\eta_2) * R_z(\Delta x,\eta_2,\eta_2) \qquad (2.53)$$

Using (2.52) and (2.53) and (2.15) we define a normalized autocorrelation of the output intensity

$$R_u'(\Delta x,\eta_1,\eta_2) = 1 + \left[\frac{|R_g(\Delta x,\eta_1\eta_2) * R_z(\Delta x,\eta_1,\eta_2)|^2}{(R_g(o,\eta_1,\eta_1)*R_z(o,\eta_1,\eta_1))} \right.$$

$$\left. \cdot \frac{1}{R_g(\Delta x,\ r_2,\eta_2)*R_z(\Delta x,\eta_2,\eta_2)} \right] \qquad (2.54)$$

Using the result of (2.51) in the digital computer, we have made graphs of the normalized autocorrelation function (2.54) for various parameter choices.

In Figs. (2-4), (2-5), and (2-6) we present computer plots of R'_u vs. $\Delta\lambda$ with the spatial variable, $\Delta x = 0$. $\Delta\lambda$ is calculated from Δn with normal incidence and the index of refraction of the diffuser assumed to be 1.5. Figure (2-4) shows the autocorrelation with four values of σ, or roughness. We see that the change in wavelength required to minimize R'_u is strongly dependent on the roughness. Figures (2-5) and (2-6) show the effect of varying the aperture and correlation length respectively. Each of these figures have four curves which are very nearly identical and thus it is seen that the wavelength dependence of the speckle pattern is not a function of aperture size or correlation length on the diffusion surface.

Figures (2-4, 5, 6) were plotted by a direct computation of Eq. (2.51). However, in the solutions for $\Delta x \neq 0$, the arguments in the complex error functions routine, pre-programmed in the computer, rapidly exceeded the maximum allowable value. Rather than re-program with a new routine to handle these large values, a new program was written to solve the convolution integral of Eq. (2.44) directly. The integrals were computed in a program using Simpson's Rule. In this method the limits of integration are set by the user and the range between the limits is divided into successively smaller intervals until the difference between the value of the integral for one number of intervals (N) and the value at the next succeeding number of intervals (2N) is less than a pre-determined value. We have used 10^{-3} as the maximum permissible error. Although the integral in (2.44) has infinite limits, it is clear that most of the contribution will come from the region near $\xi = 0$.

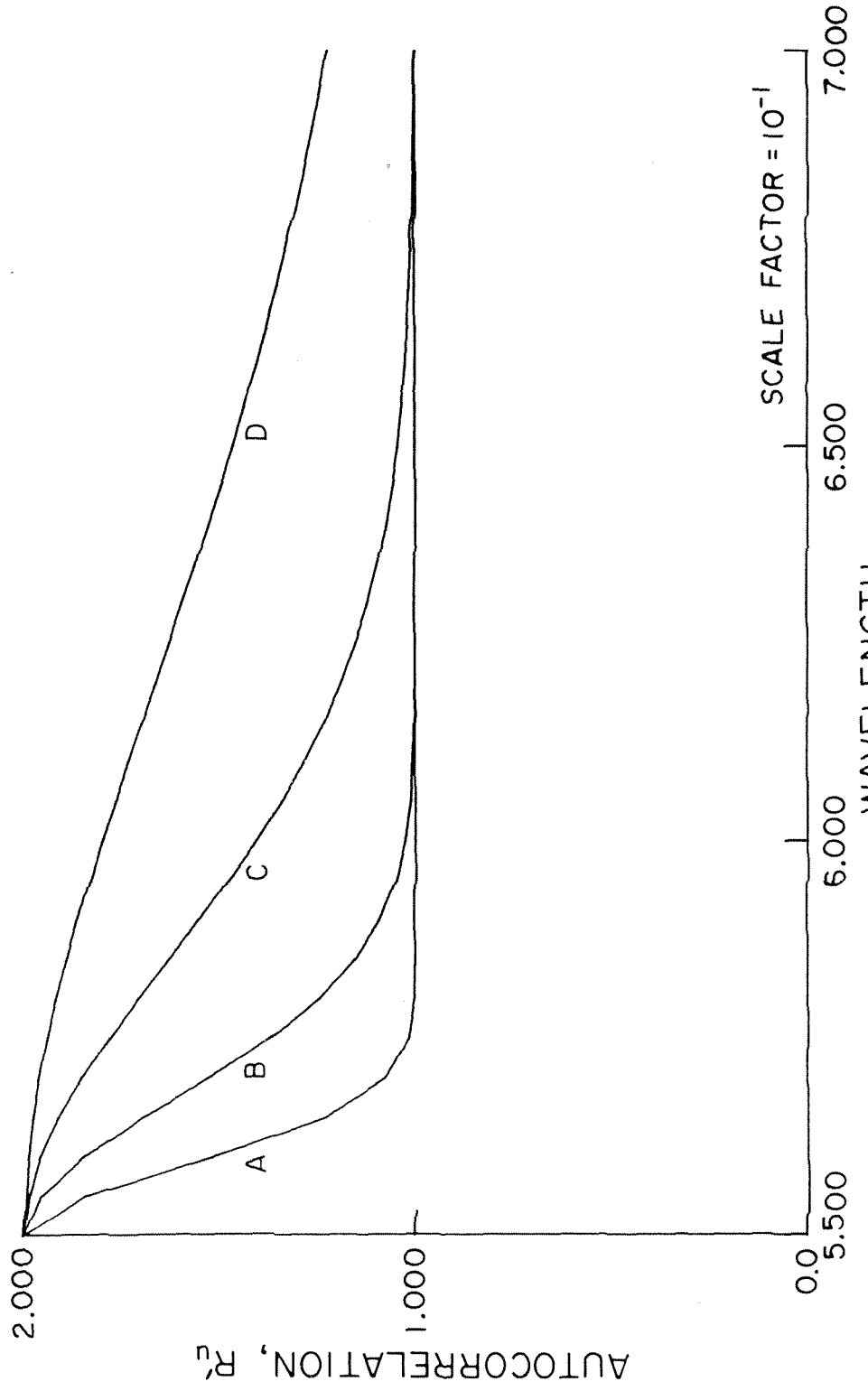

Fig. 2-4: Autocorrelation of speckle intensity vs. wavelength λ_2. λ_1 = .55μm and $\Delta\lambda = \lambda_2 - \lambda_1$. Curves A, B, C, D are for standard deviation of diffuser heights 1, 2, 4 & 8μm respectively. Resolution diameter is 10μm and correlation length for heights on diffuser surface is 2.5μm.

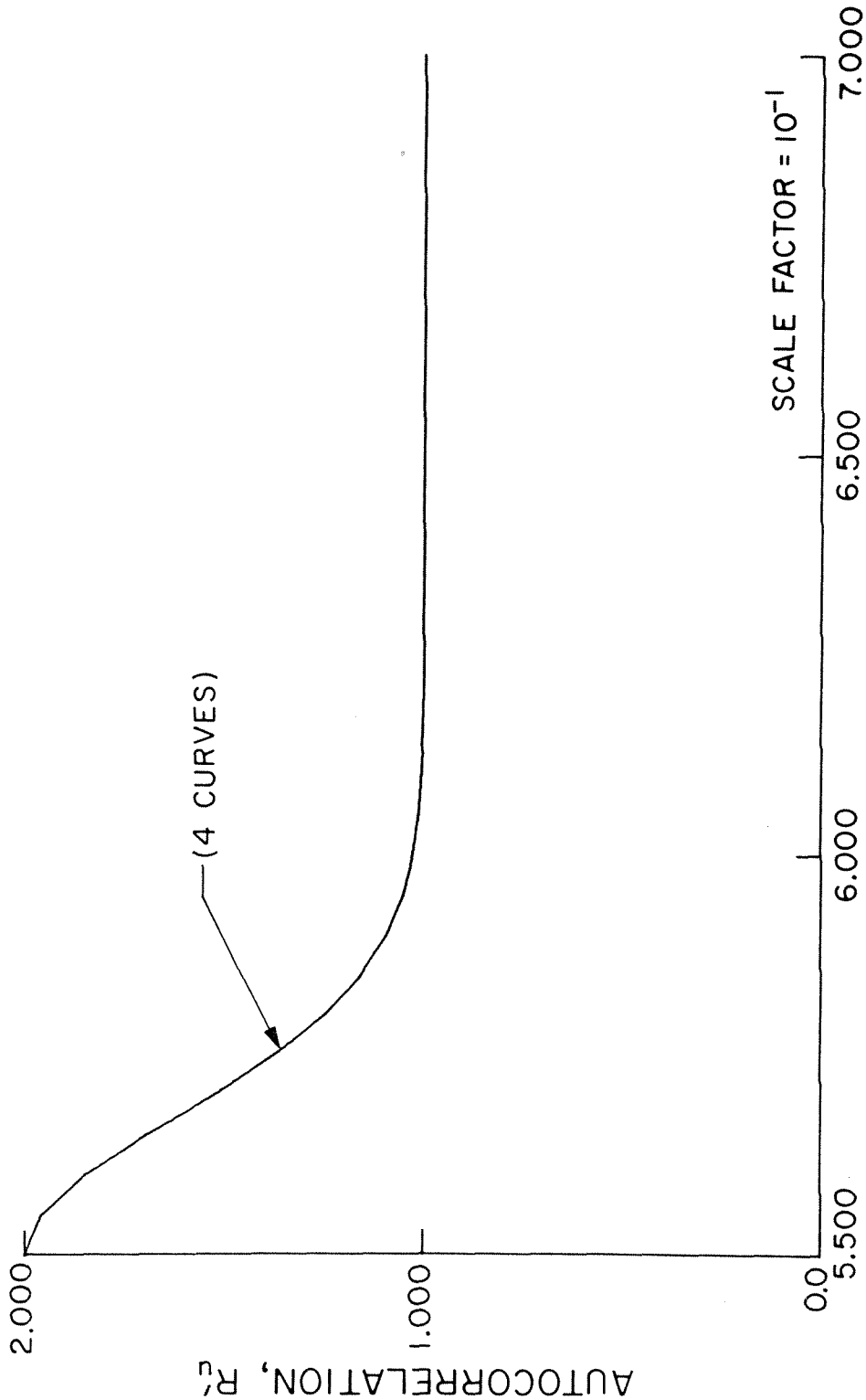

Fig. 2-5: Autocorrelation of speckle intensity vs. wavelength λ_2. λ_1 = .55μm and $\Delta\lambda = \lambda_2 - \lambda_1$. Four curves (nearly identical) are shown for resolution diameters 5, 10, 15 & 20μm. Standard deviation of diffuser heights and correlation distance between them are 2μm and 2.5μm respectively

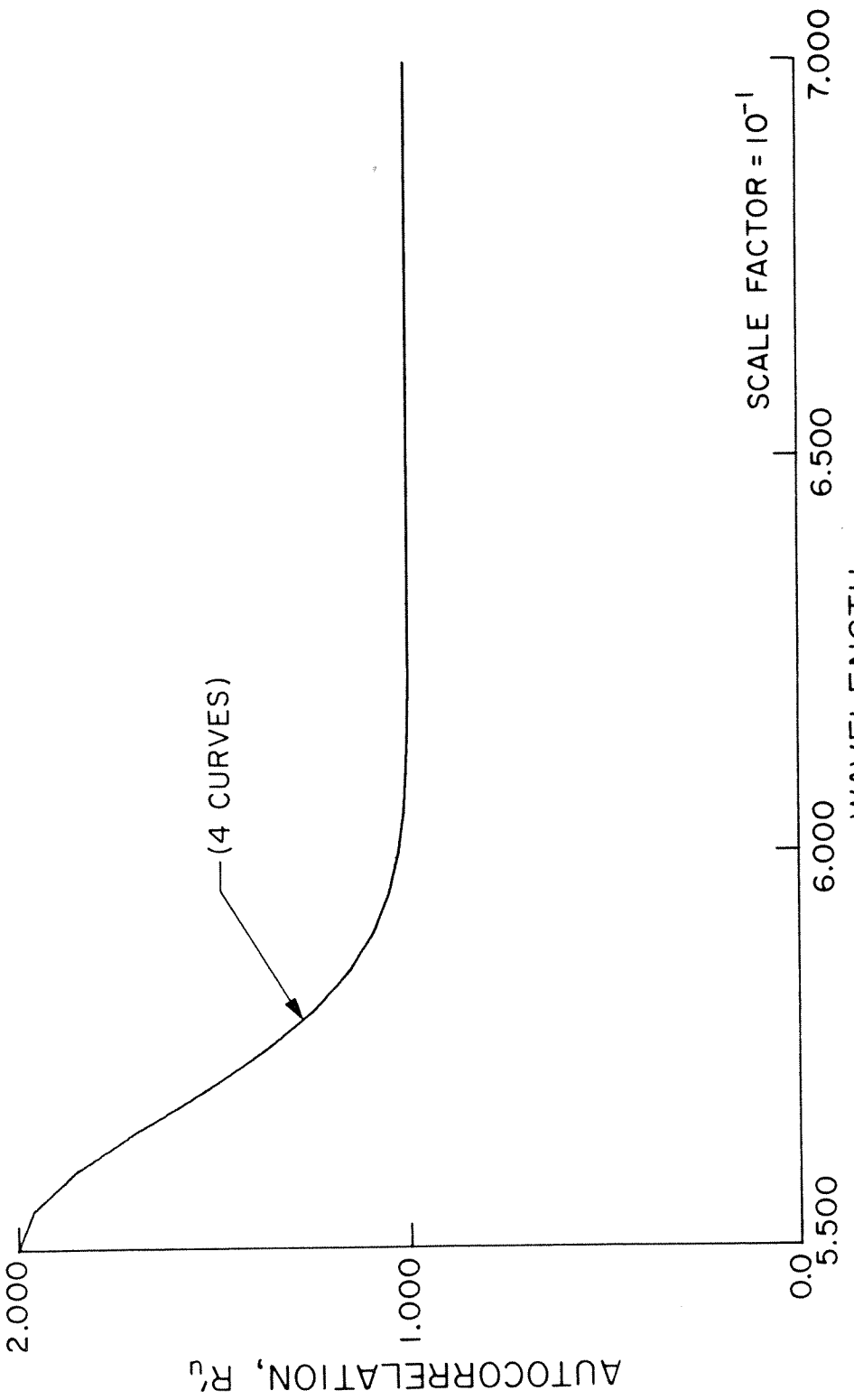

Fig. 2-6: Autocorrelation of speckle intensity vs. wavelength λ_2. λ_1 = .55μm and $\Delta\lambda = \lambda_2 - \lambda_1$. Four curves (nearly identical) are shown for correlation length for diffuser heights 1.25, 2.5, 3.75 and 5μm. Resolution diameter is 10μm and standard deviation of diffuser heights is 2μm.

We have therefore integrated the function numerically using $-2T \leq \xi \leq 2T$ as the limits. The computed maximum value of the integral over this range is .194 for $\Delta x = 0$. We find the remainder or error from the truncation of the limits from the approximation

$$E_{rr} < 2 \int_{2T}^{\infty} \exp[\sigma^2\beta\{\exp[-(\frac{2T}{T})^2] - 1\}] \operatorname{sinc}(\frac{-\xi}{k})\, d\xi \qquad (2.55)$$

The value of (2.55) will always be greater than the true error since we have fixed ξ in the exponential function. The resultant error from this approximation in the worst case is 2.44×10^{-14}. Therefore, the error in the calculation caused by the introduction of finite limits is less than one part in 10^{12}. As a test, we have varied the limits of integration from T/4 to 2T without any measurable change in the result. Additionally we have duplicated the plots for R_u' as a function of wavelength using both the formulation of Eqs. (2.51) and of (2.44) and the results were identical.

Figures (2-7), (2-8) and (2-9) show the computed autocorrelation as a function of the output plane spatial variable Δx with the normalized frequency variable maintained constant. Figure (2-7) shows the effect of the aperture size on the autocorrelation with correlation length T and diffuser roughness (characterized by σ) fixed. The distance Δx required for R_u' to go from maximum to minimum value is proportional to the inverse of the aperture size. This dimension is also a measure of the average speckle size. Thus we see that speckle size is a function of the system aperture. Figure (2-8) presents four curves of R_u vs Δx

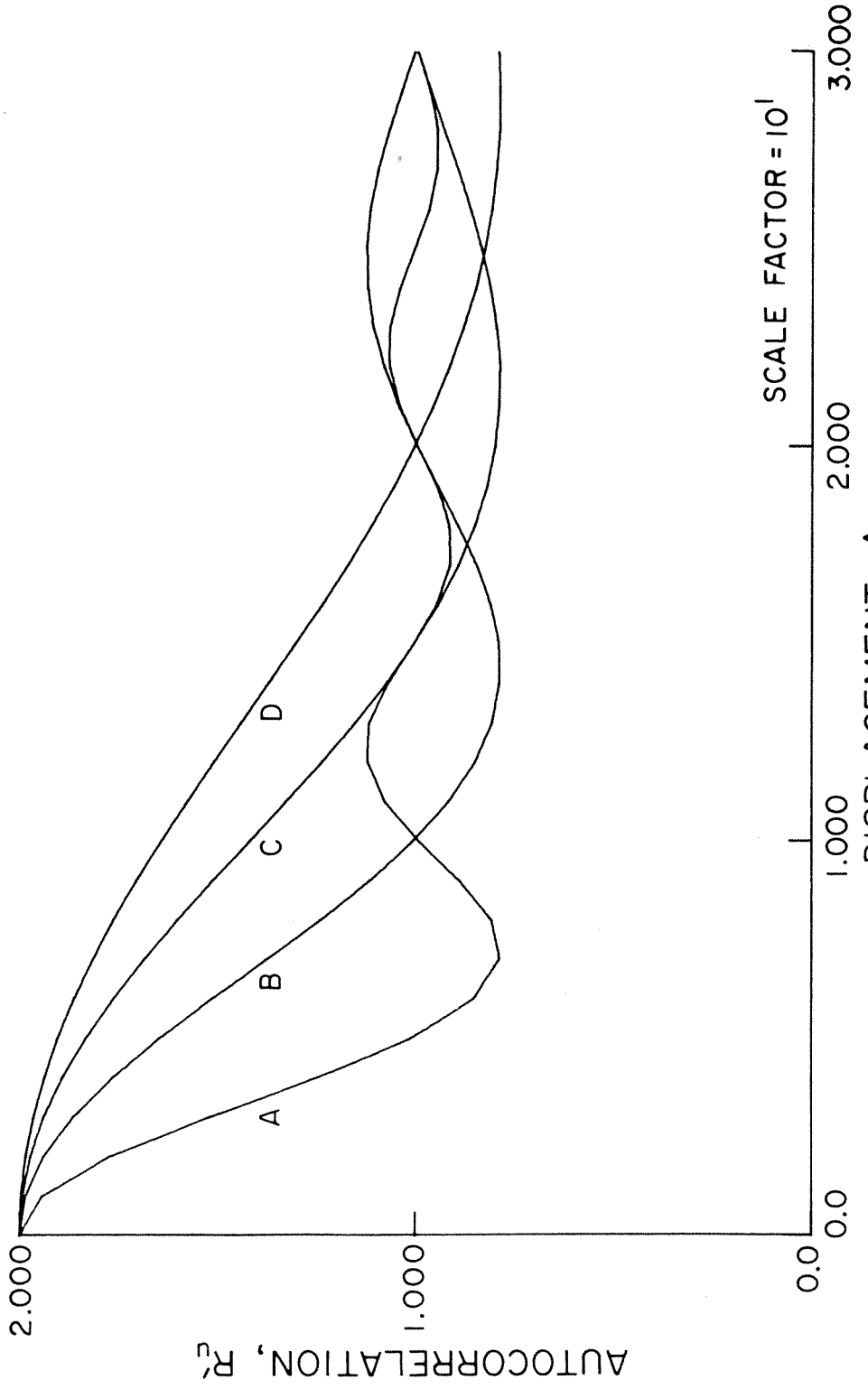

Fig. 2-7: Spatial autocorrelation of speckle intensity. Curves A, B, C, D are for optical resolution distance 5, 10, 15 & 20μm respectively. λ = .55μm, correlation length for heights on the diffuser surface is 2.5μm and standard deviation of heights is 4μm.

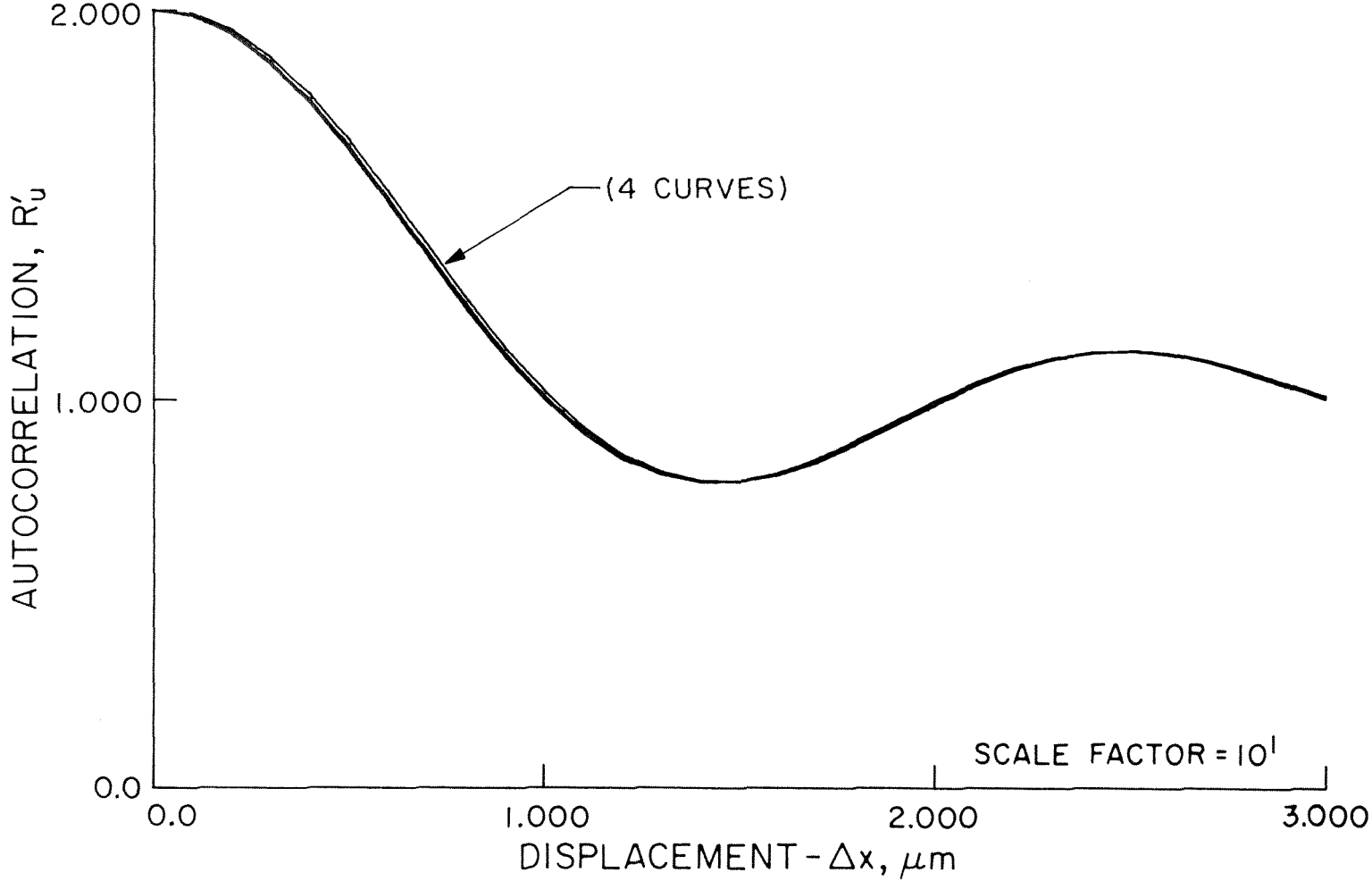

Fig. 2-8: Spatial autocorrelation of speckle intensity. Four curves (nearly identical) have been plotted for standard deviation of diffuser height 1, 2, 4 & 8μm. λ = .55μm, optical resolution diameter is 10μm and correlation length for diffuser heights is 2.5μm.

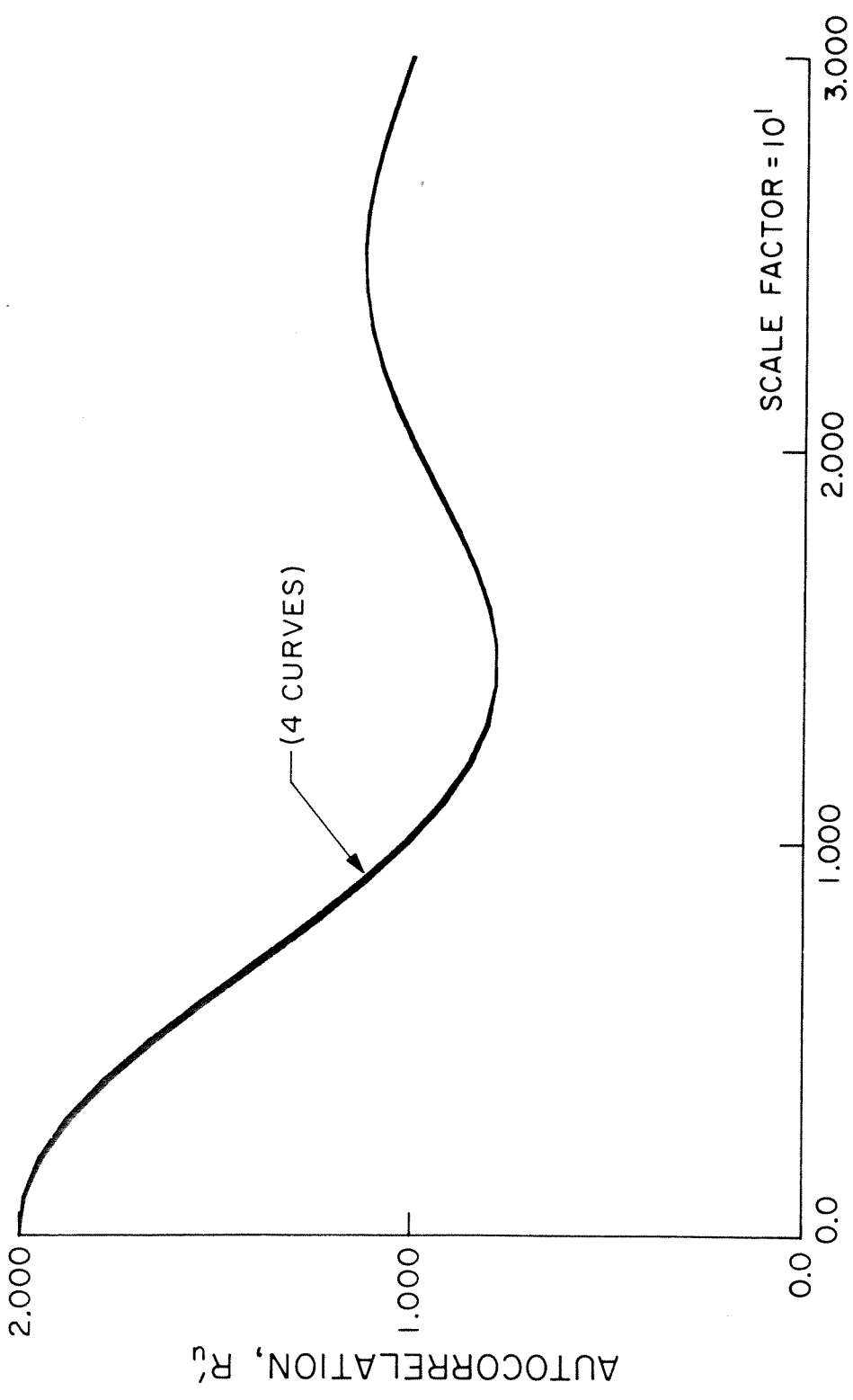

Fig. 2-9: Spatial autocorrelation of speckle intensity. Four curves (nearly identical) have been plotted for correlation length for heights on diffuser surface 1.25, 2.5, 3.75 & 5μm. λ is .55μm, resolution diameter is 10μm and the standard deviation of diffuser heights is 4μm.

for constant aperture, but with four different diffuser heights. We see that the four curves are nearly identical, indicating that the spatial character of the speckle is independent of the roughness of the diffuser. In Fig. (2-9) we have varied the correlation parameter T with fixed aperture and σ. The maximum T considered was 1/2 the resolution diameter as necessitated by our prior assumption of normally distributed fields. Again, we see that the correlation length has little effect upon the spatial autocorrelation function.

2.7 Autocorrelation Function for a Rough Diffuser with Small Correlation Length

The solution to equation (2.44) which we have obtained in (2.51) is general, but tends to obscure the form of the autocorrelation for most of the diffusers we are considering. We therefore seek an approximate solution for the case of a moderately rough diffuser with short correlation length T.

We begin with the assumption

$$\sigma\overline{\eta} >> 1. \tag{2.56}$$

This means that the standard deviation of the heights on the diffuser surface is large on a wavelength scale. It is further assumed that the correlation length on the diffuser surface

$$T << \frac{\lambda S}{L_x} = \frac{1}{a} \tag{2.57}$$

which means that there are many independent scatterers or heights in a resolution diameter on the diffuser surface. Now, it is evident that most of the contribution to the integral in (2.44) representing $R_g * R_z$ will come from values of ξ very near zero. Therefore we approximate

$$\exp(-\frac{\xi^2}{T^2}) \cong 1 - \frac{\xi^2}{T^2} \tag{2.58}$$

and again using the substitution $\beta = \eta_1(\eta_1 + \Delta\eta)$,

we have the approximate form for the integral of (2.44)

$$R_g * R_z \cong Ma \int_{-\infty}^{\infty} \exp(-\frac{\sigma^2\Delta\eta^2}{2}) \exp(\frac{\beta\sigma^2}{T^2})\xi^2 \cdot \operatorname{sinc}(a\Delta x_2 - a\xi_2)\, d\xi_2 \tag{2.59}$$

Making use of the convolution theorem, (2.59) becomes

$$R_g * R_z \cong \frac{MT}{a\sigma}\sqrt{\frac{\pi}{\beta}} \exp[-\frac{\sigma^2\Delta\eta^2}{2}] \int_{-\infty}^{\infty} \operatorname{rect}(\frac{f_x}{a}) \exp[-\frac{\pi^2T^2}{\sigma^2\beta} f_x^2] \cdot \exp[+ i2\pi\, \Delta x\, f_x]\, df_x \tag{2.60}$$

where f_x is a spatial frequency variable. Equation (2.60) is equivalent to

$$R_g * R_z = \frac{MT}{a\sigma}\sqrt{\frac{\pi}{\beta}} \exp[-\frac{\sigma^2\Delta\eta^2}{2}] \int_{-a/2}^{a/2} \exp[-\frac{\pi^2T^2}{\sigma^2\beta} f_x^2 + i2\pi\, \Delta x\, f_x]\, df_x \tag{2.61}$$

Now we examine the behavior of the exponential in f_x^2 over the range of integration and we see that the assumptions of (2.56) and (2.57)

force

$$\exp[-\frac{\pi^2 T^2}{\sigma^2 \beta} f_x^2] \cong 1 \tag{2.62}$$

over the range $-a/2 < f_x < a/2$. Thus integration of (2.61) gives

$$R_g * R_z \cong \frac{M}{\sigma}\sqrt{\frac{\pi}{\beta}} \exp[-\frac{\sigma^2 \Delta\eta^2}{2}] \operatorname{sinc}(a\Delta x) \tag{2.63}$$

Then substituting (2.63) into (2.44) the autocorrelation for the speckle intensity is

$$R_u(\Delta x, \eta_1, \eta_2) \cong \langle u(x,\eta_1)\rangle \langle u(x+\Delta x, \eta_1 + \Delta\eta)\rangle$$

$$+ \frac{\pi M^2}{\sigma^2 \beta} \exp(-\sigma^2 \Delta\eta^2) \operatorname{sinc}^2(a\Delta x) \tag{2.64}$$

The form of (2.64) allows us to predict the behavior of the autocorrelation with respect to either spatial or spectral variables. For example, if the optical frequency is fixed, $\Delta\eta = 0$, the spatial autocorrelation is seen to depend on the limiting aperture of the system contained in the sinc function. This result has been obtained in several different ways by Enloe [4], Goldfischer [10], and others, and is generally accepted. If, on the other hand we consider $\Delta x = 0$ it is seen that the autocorrelation of the speckle at a point in the output is governed by

$$\exp[-\sigma^2 \Delta\eta^2] \tag{2.65}$$

indicating that the spectral sensitivity is a function of the diffuser heights and not of the optical system parameters. These results are essentially the same as those of Section (2.6) and a similar result

has been given by George and Jain [3] for the phase diffuser with the assumed correlation for diffuser heights a triangle function

$$r(\xi) = \begin{vmatrix} 1 - |\frac{\xi}{\alpha}| & |\frac{\xi}{\alpha}| \leq 1 \\ 0 & |\frac{\xi}{\alpha}| \geq 1 \end{vmatrix} \tag{2.66}$$

We re-emphasize that the essential result is that spatial characteristics of imaged speckle patterns from phase diffusers are primarily determined by the limiting aperture of the imaging system, while the spectral behavior is primarily a function of the roughness of the diffuser.

2.8 Autocorrelation Function for Gaussian Apodization of the Image System

In Sections 2.6 and 2.7 we have calculated the autocorrelation of speckle intensity for image systems in which the aperture transmission is assumed to be unity across some length L_x and zero elsewhere. Here we consider a transmission function with Gaussian apodization in which the characteristic width of the aperture is governed by the dimension L_x. Thus we define a one-dimensional transmission function for the lens of focal length F by

$$A(u) = \exp\left[\frac{i\pi u^2}{\lambda F}\right] \exp\left[-\left(\frac{2u}{L_x}\right)^2\right] \tag{2.67}$$

Corresponding to Eq. (2.41) the one-dimensional transfer function is defined by

$$Z(x_2,x) = \frac{1}{\sqrt{\pi}\, W} \exp\left[-\frac{1}{\sqrt{\pi}W}\left(x_2 - \frac{S}{S'}x\right)^2\right] \tag{2.68}$$

where W is an achromatic resolution diameter calculated from the average wavelength $\bar{\lambda}$ by

$$W = \frac{2\bar{\lambda}S}{\pi L_x} \tag{2.69}$$

Again in (2.68) phase terms which vanish in the final result have been neglected. The autocorrelation of the impulse response $z(x_2,x)$ given as a function of lag Δx_2 in the output plane is

$$R_z(\Delta x_2,\eta_1,\eta_2) = \frac{1}{\sqrt{2\pi}\ W} \exp\left\{-\frac{1}{2}\left(\frac{\Delta x}{W}\right)^2\right\} \tag{2.70}$$

Now consider Eq. (2.37) with R_z given by (2.70) and the correlation function for the diffuser heights r(x) the same exponential function as in (2.43). Writing only the integral representing $R_g * R_z$ we have the following:

$$R_g * R_z = \frac{\exp(-\sigma^2\Delta\eta^2)}{\sqrt{2\pi}\ W} \int_{-\infty}^{\infty} \exp\left[-\sigma^2\beta\left\{1-\exp\left(-\frac{\xi^2}{T^2}\right)\right\}\right.$$

$$\left. - \frac{1}{2W^2}(\Delta x_2 - \xi)^2\right] d\xi \tag{2.71}$$

where β is defined by (2.46). Using the expansion of (2.47) and rearranging terms

$$R_g * R_z = \frac{\exp(-\sigma^2\Delta\eta^2)}{\sqrt{2\pi}\ W} \exp(-\sigma^2\beta) \sum_{m=0}^{\infty} \frac{(\sigma^2\beta)^m}{m!}$$

$$\cdot \int_{-\infty}^{\infty} \exp\left\{-\left[\left(\frac{m}{T^2}+\frac{1}{2W^2}\right)\xi^2 - \frac{\Delta x}{W^2}\xi + \frac{\Delta x^2}{2W^2}\right]\right\} d\xi \tag{2.72}$$

Integrating this expression yields

$$R_g * R_z = \exp(-\sigma^2 \Delta\eta^2) \exp(-\sigma^2 \beta) \cdot \sum_{m=0}^{\infty} \left(\frac{T^2}{2mW^2 + T^2} \right)^{1/2} \frac{(\sigma^2 \beta)^m}{m!} \exp \left[- \left(\frac{m \Delta x^2}{2mW^2 + T^2} \right) \right] \tag{2.73}$$

Using (2.73) in (2.54) the result is amenable to digital computer calculation of the dependence of the autocorrelation on space and wavelength variables.

If we make the assumption that $T << W$, i.e. there are many scattering centers in a resolution distance, and set $\eta_1 \equiv \eta_2$ to examine the spatial variation of $R_u'(\Delta x, \eta_1, \eta_2)$, from (2.54) and (2.73) it is seen that

$$R_u'(\Delta x, \Delta\eta = 0) \propto 1 + \exp \left\{ - \frac{\Delta x^2}{2W^2} \right\} \tag{2.74}$$

Thus the spatial variation in R_u' is again only a function of the resolution distance W, which in turn is determined by the aperture size L_x in (2.69). Examination of (2.71) with the assumption $\sigma^2 \beta >> 1$, and substitution into (2.54) shows that

$$R_u'(0, \eta_1 \eta_2) \propto 1 + \exp \left\{ -\sigma^2 \Delta\eta^2 \right\} \tag{2.75}$$

Thus $R_u'(\Delta\eta)$ depends primarily upon the roughness of the diffuser which is characterized by σ^2.

References

1. George, N. and Jain, A.: Opt. Comm. 6, 253 (1972).
2. George, N. and Jain, A.: Appl Opt. 12, 1202 (1973).
3. George, N. and Jain, A.: Appl. Phys. 4, 201 (1974).
4. Enloe, L. H.: Bell Sys. Tech. J. 46, 1479 (1967).
5. Burckhardt, C. B.: Bell Sys. Tech. J. 49, 309 (1970).
6. Reed, I.S.: IRE Trans. Inf. Theory IT-8, 194 (1962).
7. Papoulis, A.: Probability, Random Variables and Stochastic Processes; McGraw-Hill, New York, 1968.
8. Goodman, J. W.: Introduction to Fourier Optics; McGraw-Hill, New York, 1968.
9. Asakura, T., Fujii, H. and Murata, K.: Optica Acta 19, 273 (1972).
10. Goldfischer, L. I.: JOSA 55, 247 (1965).

Chapter III

POLARIZATION PHENOMENA IN SPECKLE PATTERNS

3.1 Introduction

In the previous chapter we have presented an analysis of speckle in an imaging system. Implicit in the development was the assumption of scalar diffraction theory. We now describe some transmission and depolarization properties of a series of opal glass diffusers and demonstrate that both input and output polarization must be controlled in a speckle experiment if agreement with a scalar diffraction theory model is to be realized.

It is known that the state of polarization of an electromagnetic wave may be changed upon reflection from a rough surface [1,2] or by transmission through a random medium [2,3]. If a plane polarized wave interacts with a reflecting medium of surface roughness the order of $\lambda/8$ or greater or passes through a diffuser with local phase retardations of $\lambda/4$ or greater some amount of cross polarization or depolarization will be observed.

Laser speckle patterns are generally produced by the interaction of plane polarized laser beams with various diffuse media. It is therefore expected that depolarization phenomena will be observed in the speckle patterns and must be understood in the analysis of the patterns.

While relatively thin coarse diffusers transmit a beam of light with negligible (down by 30db) cross-polarized component, as the diffuseness increases, the cross-polarized term may become equal

to the component retaining the input polarization. This is of particular interest in the study of laser speckle. Since most theories published, e.g. [4], assume only a scalar component of electric field exits the diffuser, care must be taken in experiments either to use a polarization analyzer in the output field or in some other way account for the cross-polarized field. A similar problem arises in the prediction of radar cross-sections for targets with a high degree of randomness. Kerr [5] and Berkowitz [6] both give short discussions.

We have measured spatial radiation patterns for the light transmitted by diffusers of various thicknesses. Both the parallel and cross-polarized output component intensities were measured for normally incident plane-polarized monochromatic illumination. In separate experiments, the spatial cross-correlation functions for speckle images of different polarizations and for various diffuser thicknesses were measured.

3.2 Depolarization in the Radiation Patterns

Consider a diffuser, D in figure (3-1) illuminated by a normally incident, monochromatic plane wave. For a polarized input, the field exiting the diffuser should contain both parallel and cross-polarized field components. Also, the field amplitude will be spatially randomized by the rough diffuser. Hence the radiation will extend over large angles θ, and it will be highly speckled. We can define a transmission matrix for the diffuser as follows:

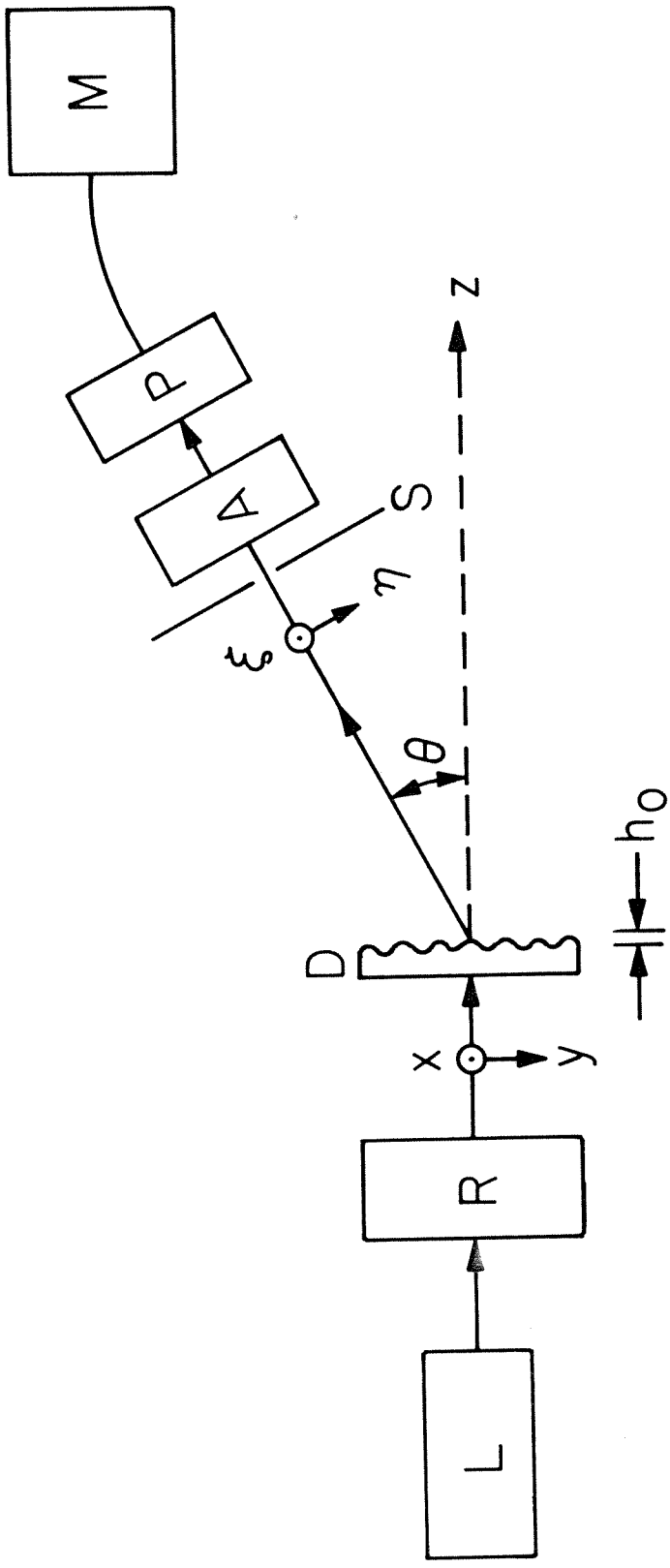

Fig. 3-1: Experimental setup for the measurement of the radiation pattern of the diffuser D. Polarization of the laser beam from L is controlled by the polarization rotator R. The receiver at an angle θ consists of a narrow slit S, a polarization analyzer A, a photodetector P and amplifier-meter M.

$$\begin{bmatrix} g_1 \\ \\ g_2 \end{bmatrix} = \begin{bmatrix} t_{xx} & t_{xy} \\ \\ t_{yx} & t_{yy} \end{bmatrix} \begin{bmatrix} E_1 \\ \\ E_2 \end{bmatrix} \tag{3.1}$$

where the input electric field vector $\underline{E}$ is given by

$$\underline{E} = \underline{e}_x E_1 + \underline{e}_y E_2 \ , \tag{3.2}$$

and the output field $\underline{g}$ is

$$\underline{g} = \underline{e}_x g_1 + \underline{e}_y g_2 \tag{3.3}$$

Speckle patterns can be calculated from the scalar field components g_1 and g_2 as in Chapter 2.

However, our interest in this section is to describe an experiment which gives one some information about the relative sizes of the transmission coefficients, i.e., the matrix elements in (3.1).

Beckmann [2] has given a description of backscattered radiation from a rough reflecting surface in terms of two components: A quasi-specular component reflected by "mirroring" elements of the surface whose normals point toward the radiation source and a diffuse component which is scattered into directions not parallel with the incident or reflected radiation. He predicts that the cross polarization in the quasispecular component of the scattered radiation will be zero, and that only the diffuse component will be depolarized.

By analogy to the rough reflector, it is expected that in transmission through a phase diffuser the portion of a beam which passes through undeviated will retain its original polarization and the portion which is scattered out of the direction of the incident beam will be cross polarized to some degree.

Since the analysis of Beckmann is done for the single reflection case, we would expect experimental agreement to the extent that our diffuser is thin enough to discount multiple scattering.

For the experiments, a series of diffusers of varying thicknesses, h_o in Fig. (3-1), was prepared from a single sheet of flashed opal glass. Starting with an initial diffuser of 500 μm thickness, we ground and optically polished an assortment of diffusers ranging in thickness from 5 μm to 500 μm.

The setup for measuring the radiation patterns of these diffusers consists of a laser, a polarization rotator, the diffuser, and a sensitive receiver mounted so as to facilitate precise measurements of the angle θ. The incident electric field is polarized along the x-axis. The analyzer A is adjusted to pass either the parallel (ζ-axis) or the crossed-polarization (η-axis). The slit S is chosen small enough to minimize error in the angular measurement, but still large enough to purposely <u>average</u> over several speckles.

The radiation patterns for the 50 μm and 500 μm diffusers are shown in Figs. (3-2) and (3-3) respectively.

The thinner diffuser has a large forward lobe of parallel-polarized radiation; the cross-polarized component is down by 33 db.

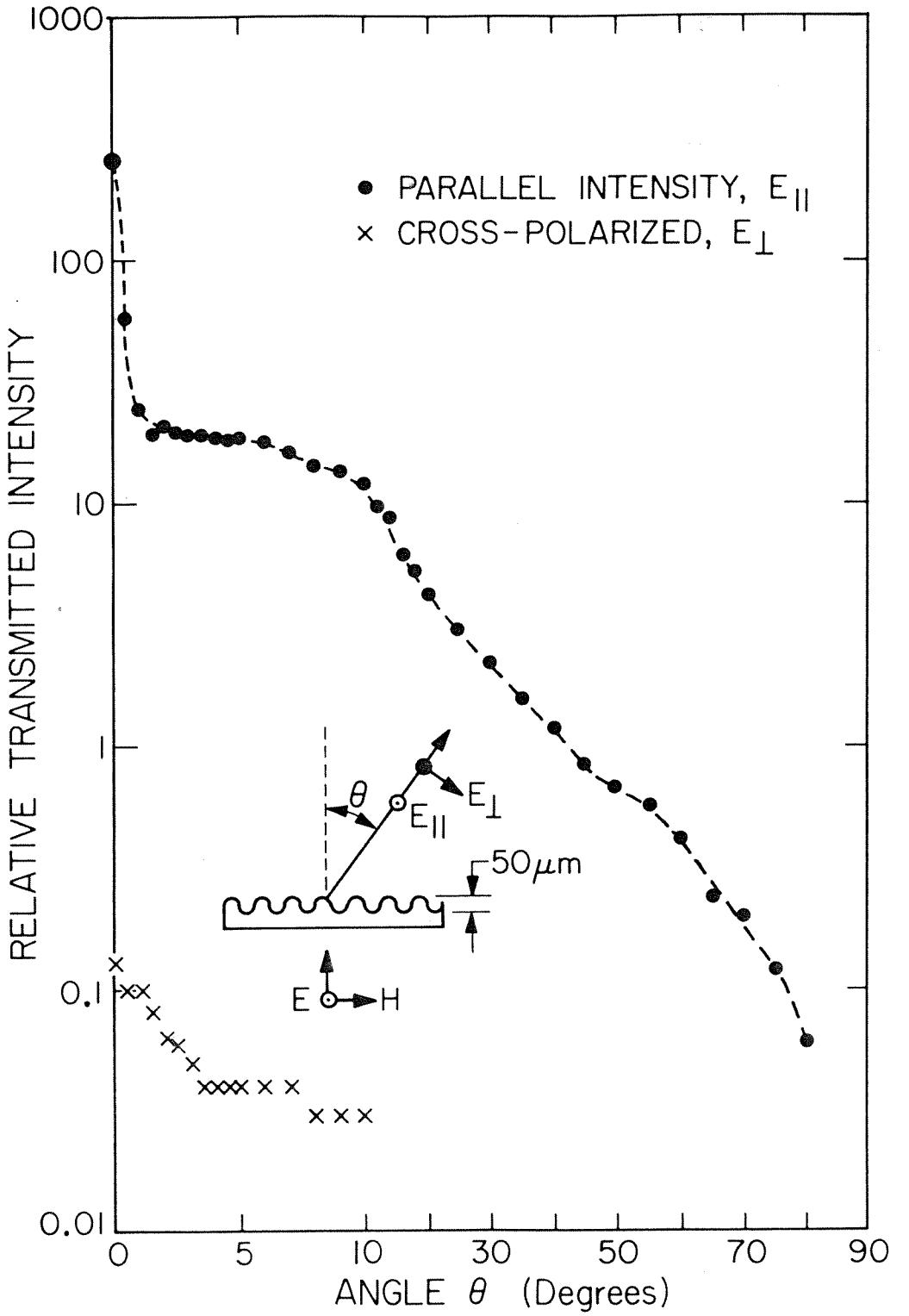

Fig. 3-2: Transmission of parallel and cross-polarized intensity through an opal glass diffuser of 50μm thickness. Incident light was plane polarized at 5750Å as shown in Fig. 3-1.

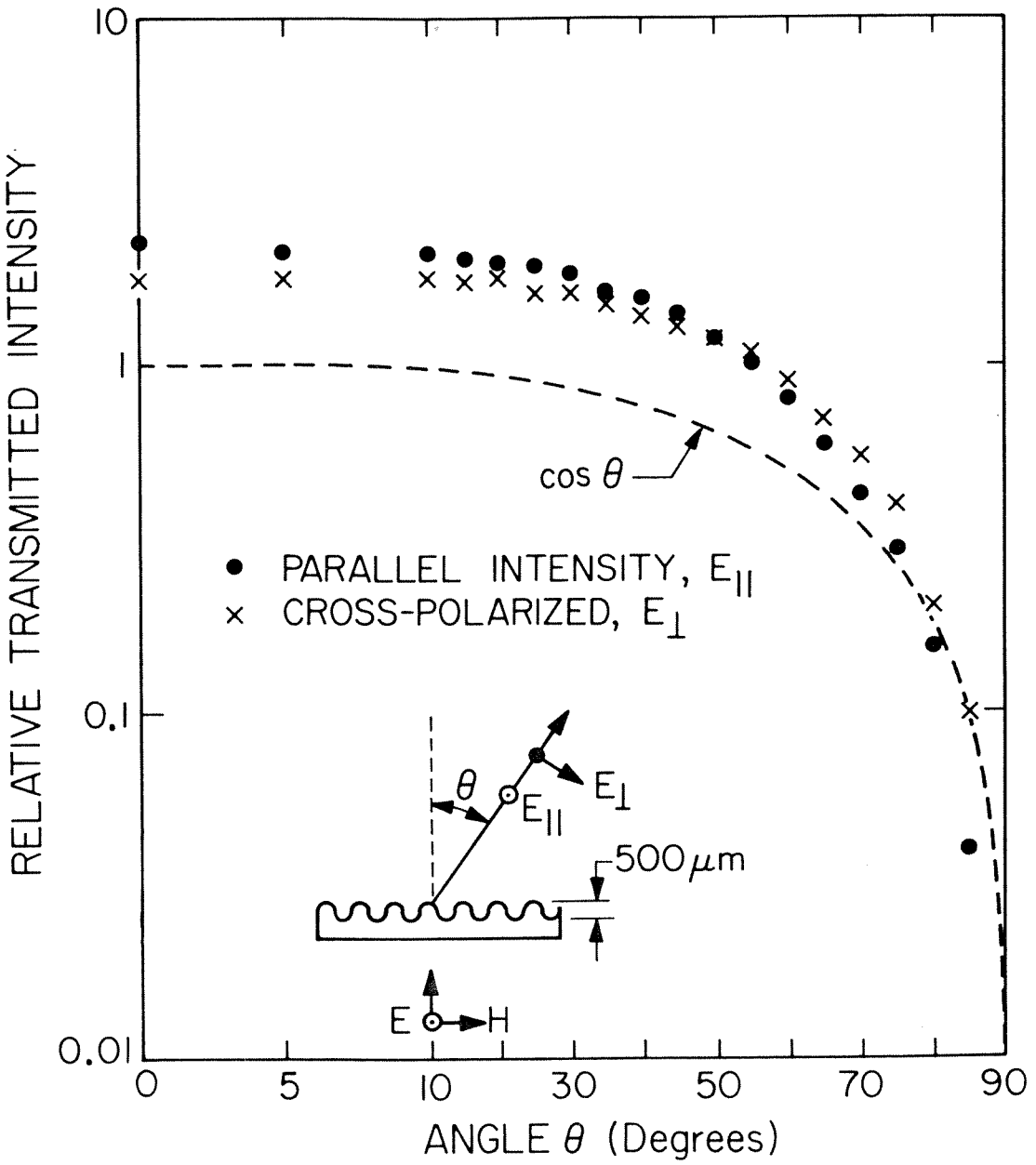

Fig. 3-3: Transmission of parallel and cross-polarized intensity for an opal glass diffuser of 500μm thickness.

The actual ratio may be somewhat larger since the polarizer-analyzer combination used was limited to an extinction ratio of 12,000. The thicker diffuser has almost equal radiation in either polarization. For comparison to radiation from a blackbody, the curve of cos θ is also shown in fig. (3-3). These results agree well with the theory and with corresponding data for bidirectional reflectance which were measured by Bair , et. al. for numerous surfaces at several optical wavelengths [7].

For normally incident radiation, the directly transmitted beam has a depolarization ratio, i.e., the ratio of the crossed to the parallel components in intensity, varying widely from 10^{-4} for the thin opal glass diffuser to unity for the 500 μm, as shown in fig. (3-4). Even at 100 μm, we note that the depolarization ratio, D, is only about 1/10. We have also measured the depolarization ratio for the intensity in transmission and reflection at an angle 30° from the normal (fig. 3-4). It is noticed that the depolarization of the reflected radiation is much greater than that for the transmitted beam. This is expected with the opal glass, since the "reflection" is not a surface effect, but results from multiple scattering in the bulk of the opalescent layer. From the geometry of the experiment, one would expect that radiation received in the reflected direction has undergone more scattering interactions than the transmitted light, thus more depolarization is observed.

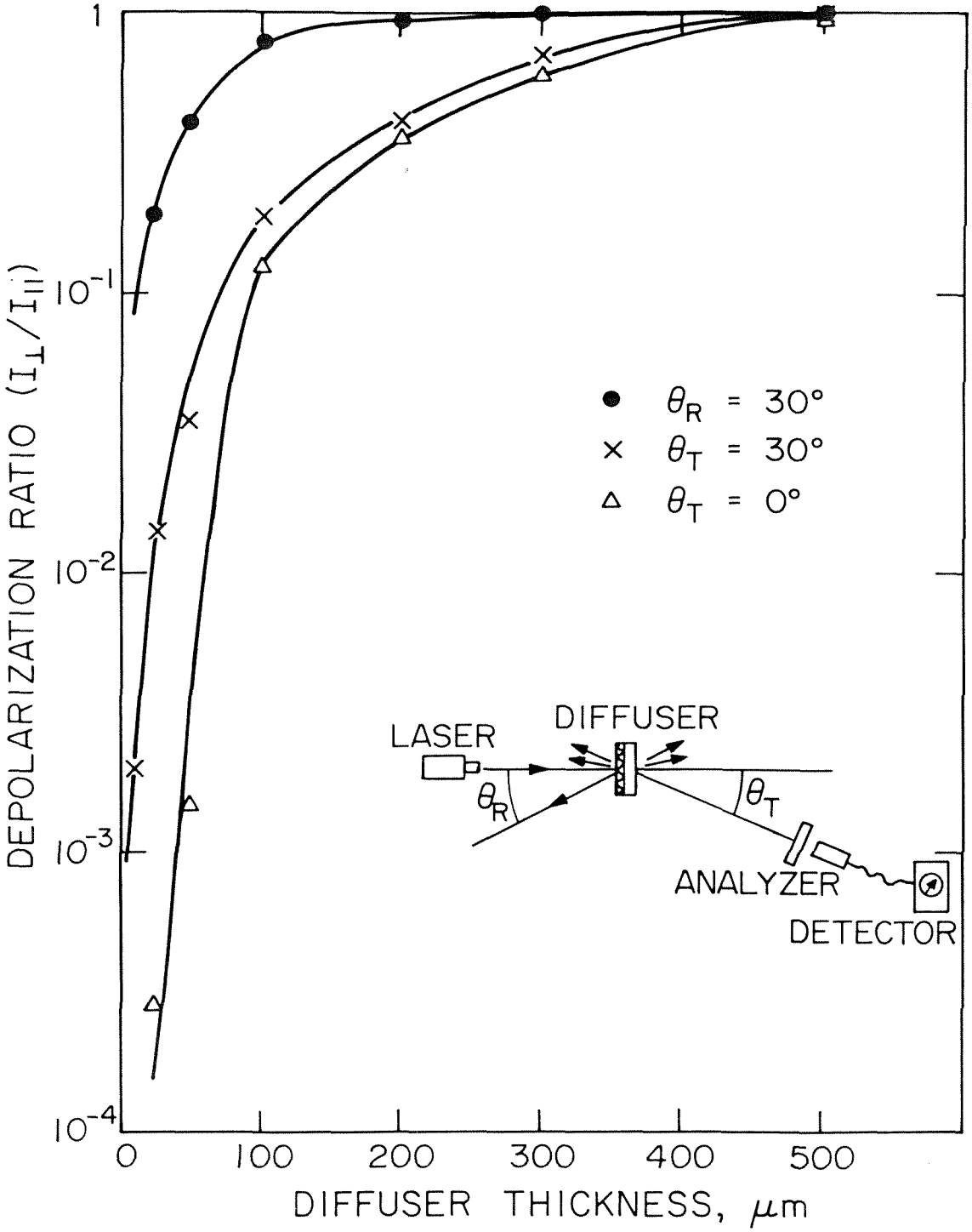

Fig. 3-4: The ratio of cross-polarized to parallel polarized intensity for plane polarized laser light interacting with a series of opal glass diffusers.

3.3 Polarization Effects in the Speckle Patterns

Chakraborty [6] has studied the cross-correlation between speckle patterns recorded photographically as the incident plane polarized field is rotated. He reports decreasing correlation as this angle increases from zero to ninety degrees, but apparently, no analyzer was used. The experiments described herein differ in that both the input polarization to the diffuser and the polarization of the radiation leaving the diffuser are controlled. Additionally, the depolarization ratio is highly dependent on the thickness of the diffuser.

Figure (3-5) illustrates the setup used for our experiments. The plane of polarization of the illumination from the laser L on the diffuser D is controlled by the rotator R and the appropriate component of the polarized term is of course highly speckled; the controlling aperture is associated with the microscope objective.

We have measured some characteristics of speckle patterns with various combinations of input and output polarizations. In these experiments, we have studied the image of a diffuser by recording the intensity detected by a scanning fiber optic probe as in fig. (3-5). In fig. (3-6), the autocorrelation functions of the intensity profiles, detected by the probe as it scans a length of the image, are given for two different sets of polarization configurations for a 500 μm diffuser. The curve labeled "polarized" is for the illumination in the y polarized mode and the analyzer set to pass only the y-polarized term.

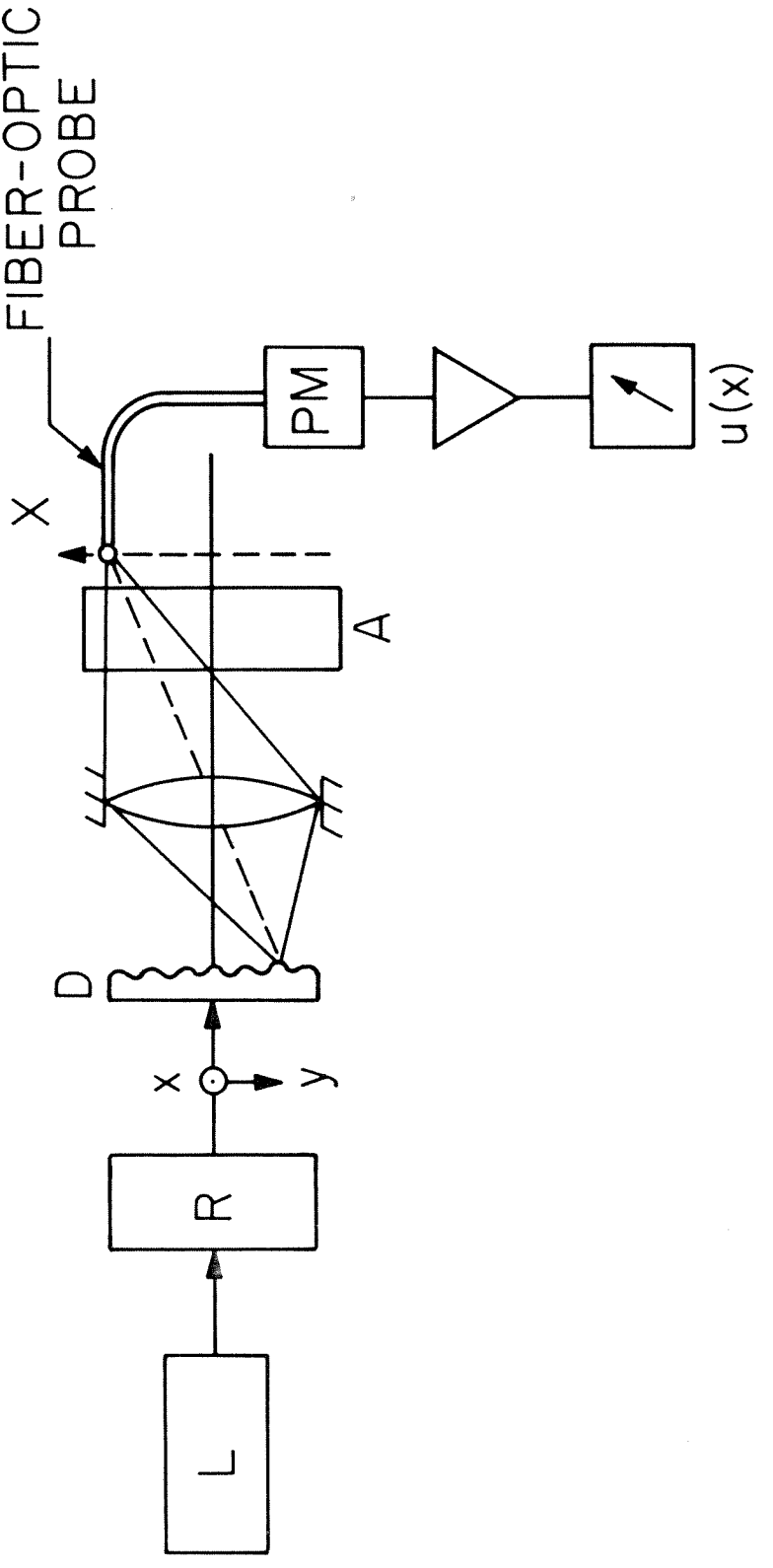

Fig. 3-5: The experimental setup for measuring intensities in the speckled image of a diffuser D for different polarizations of the diffuser illumination and the detected intensity. (L is a laser, R a polarization rotator, A an analyzer and PM a photomultiplier.) The fiber-optic probe can be moved in the x dimension by a micrometer.

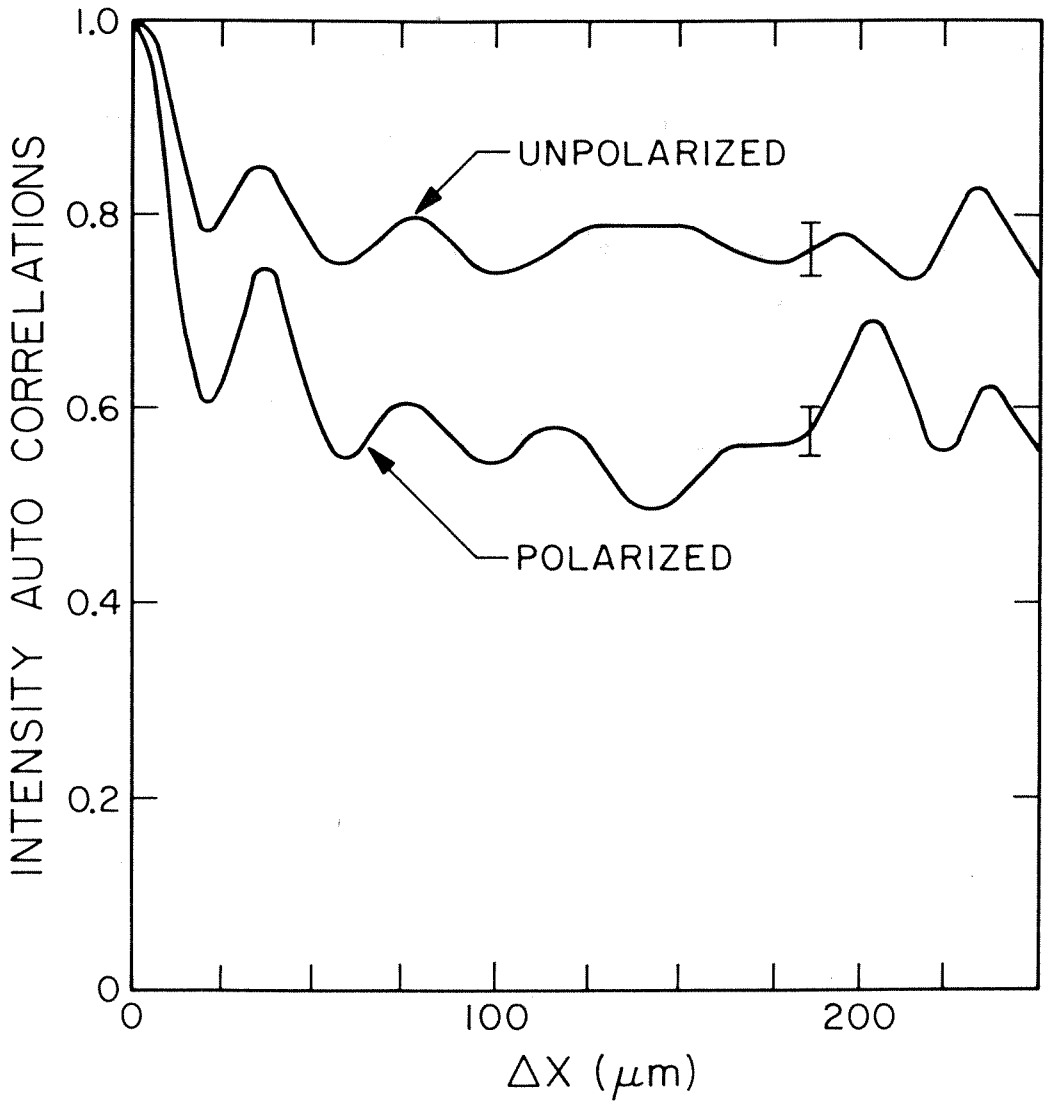

Fig. 3-6: Curves of the spatial autocorrelation of speckle intensity measured in the system of Fig. 3-5. The distance Δx has been referred to the input plane, an aperture of .94mm used in the image system and the 500μm thick opal glass diffuser used. As predicted, the correlation of the unpolarized pattern has a higher asymptotic value than that for the polarized pattern.

It is noted that the autocorrelation for the unpolarized case approaches a higher value asymptotically than the autocorrelation for the polarized case. The ratio of the asymptotic values is dependent primarily on the statistics of the speckle pattern. We note that what is meant in this case by unpolarized is that the intensity recorded is of random polarization. The introduction of the analyzer which selects a plane polarized component for viewing allows us to describe the polarization in terms of the orthogonal set (x,y). From this frame of reference we can proceed to calculate the difference in the asymptotes for the autocorrelations of fig. (3-6).

We have calculated the autocorrelations using the following:

$$R_u(K) = \frac{\sum_N I(N)I(N-K)}{\sum_N I(N)I(N)} \tag{3.4}$$

where I(N) is the intensity at the Nth displacement of the probe and K is the lag. If we consider the case for $K \to \infty$ in a random speckle pattern, we will be approaching the point of complete decorrelation. Now when I(N) and I(N-K) are completely decorrelated we make use of the fact that if two random variables x and y, are uncorrelated [7]

$$\langle xy \rangle = \langle x \rangle \langle y \rangle \tag{3.5}$$

where the symbol <> denotes the expected value. Therefore we can write

$$\sum_{N} I(N)I(N-K) = N \langle I(N) \rangle \langle I(N-K) \rangle \tag{3.6}$$

Since

$$\langle I(N-K) \rangle = \langle I(N) \rangle \tag{3.7}$$

we have the result

$$\sum_{N} I(N)I(N-K) = N \langle I(N) \rangle^{2} \tag{3.8}$$

Thus for the case $K \to \infty$ equation (3.4) becomes

$$R_{u}(\infty) = \frac{N \langle I(N) \rangle^{2}}{N \langle I^{2}(N) \rangle} \tag{3.9}$$

which we write

$$R_{u}(\infty) = \frac{\langle I \rangle^{2}}{\langle I^{2} \rangle} \tag{3.10}$$

The asymptote for the polarized case can then be written

$$R(\infty)_{X} = \frac{\langle I_{X} \rangle^{2}}{\langle I^{2}_{X} \rangle} \tag{3.11}$$

Now, for the unpolarized case the intensity at a given point N is the algebraic sum of intensities of the two orthogonal polarizations

$$I_u(N) = I_x(N) + I_y(N) \quad . \tag{3.12}$$

The asymptote for the unpolarized autocorrelation is therefore

$$\begin{aligned} R(\infty)_u &= \frac{\langle I_x + I_y \rangle^2}{\langle (I_x + I_y)^2 \rangle} \\ &= \frac{(\langle I_x \rangle + \langle I_y \rangle)^2}{\langle I_x^2 + 2I_xI_y + I_y^2 \rangle} \\ &= \frac{\langle I_x \rangle^2 + 2\langle I_x \rangle \langle I_y \rangle + \langle I_y \rangle^2}{\langle I_x^2 \rangle + \langle 2I_xI_y \rangle + \langle I_y^2 \rangle} \end{aligned} \tag{3.13}$$

We now make two assumptions which are demonstrated experimentally in the subsequent section. We assume that the speckle patterns for the x and y analyzer positions have the same statistics and that they are uncorrelated. Using these assumptions we write

$$\begin{aligned} \langle I_x \rangle &= \langle I_y \rangle \\ \langle I_x^2 \rangle &= \langle I_y^2 \rangle \\ \langle I_xI_y \rangle &= \langle I_x \rangle \langle I_y \rangle \end{aligned} \tag{3.14}$$

Using (3.14) in (3.13)

$$R_u(\infty) = \frac{4\langle I_x \rangle^2}{2\langle I_x^2 \rangle + 2\langle I_x^2 \rangle} \tag{3.15}$$

which is equivalent to

$$R_u(\infty) = R_x(\infty) \left(\frac{2}{1 + R_x(\infty)}\right) \tag{3.16}$$

Clearly by the way we have chosen to formulate the autocorrelation function $0 < R_x(\infty) < 1$; therefore $R_u(\infty)$ will always be greater than $R_x(\infty)$. For the curves of fig. 3-7, the formulation of (3.16) is in agreement within 4%. We reiterate that this formulation applies only to the case of the thick diffuser which produces completely random polarization.

A more general form for $R_u(\infty)$ which takes account of the statistics of the speckle pattern can be shown by utilizing equation (3.10):

$$R_u(\infty) = \frac{\langle I \rangle^2}{\langle I^2 \rangle} \tag{3.17}$$

Now

$$\langle I^2 \rangle - \langle I \rangle^2 = \sigma^2 \tag{3.18}$$

is definitive, therefore

$$R_u(\infty) = \frac{\langle I \rangle^2}{\langle I \rangle^2 + \sigma^2}$$

$$R_u(\infty) = \frac{1}{1 + C_R^2} \tag{3.19}$$

where C_R is defined as the ratio of the standard deviation of intensity to the average intensity in the speckle pattern. As we will show subsequently, C_R is a function of diffuser thickness and polarization of the viewing system.

We have made detailed one dimensional correlation measurements of the various speckle patterns created by different combination of input and output polarization. Using the system of Fig. (3-5) we recorded intensity versus displacement on a straight line section of the speckled diffuser image. The input polarization was controlled as well as the polarization reaching the image plane. An arbitrary axis x was established for the input and the parallel axis of the analyzer is also denoted by x. The notation we use is given by the input polarization and output analyzer position respectively: i.e. xx, xy, yx, yy. The correlations in fig. (3-7) were from data obtained by setting the scanning probe to a position (N) and by moving the polarizers and rotator, recording in order the intensities $I_{xx}, I_{xy}, I_{yy}, I_{yx}$ and then returning to I_{xx} for closure. Then the probe was moved to position N+1 and the operation repeated. 110-160 spatial samples spaced .04 mm apart were observed in this way. We found that the polarizers could be reset to produce a closure data point with much greater accuracy than by resetting the scanning micrometer. Although for readability, not all are shown in fig. (3-7), the autocorrelations for <u>each</u> of the polarization combinations are approximately the same. Since these functions are dependent upon the speckle contrast and the microscope aperture we would expect the similarity. We have shown in fig. (3-7) that there is no measurable correlation between any of the speckle patterns of different input/output polarizations. The pattern observed is completely determined by the particular group of scatters within a resolution diameter of the microscope. Therefore,

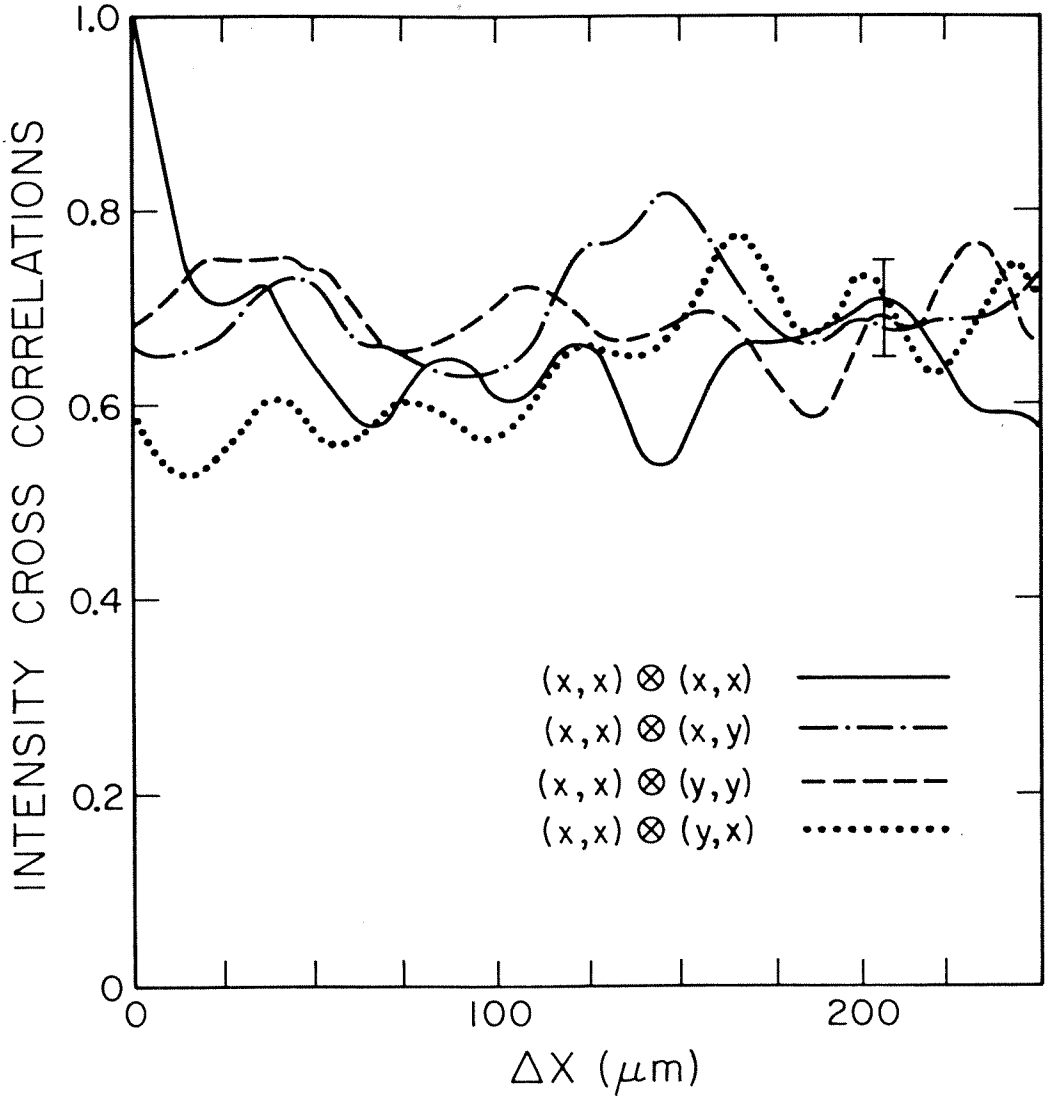

Fig. 3-7: Cross-correlations for speckle intensity in the image plane of Fig. 3-5 are shown for the 500μm diffuser. The notation is: (x,x) = (x polarized input, x polarized output) and ⊗ indicates the cross-correlation operation. (x,x) ⊗ (x,x) is an autocorrelation. Little or no correlation is seen between speckle of dissimilar polarization states

we would expect that the scatterers would interact differently with the different polarizations much as a glass flat placed in a polarized beam at a random orientation will interact with orthogonal polarizations in different ways.

References

1. P.Beckmann, A. Spizzichino: The Scattering of Electromagnetic Waves from Rough Surfaces (Pergamon Press Ltd., Oxford, 1963).
2. P. Beckman: The Depolarization of Electromagnetic Waves (The Golem Press, Boulder, 1968).
3. H. Hodara: Proc. IEEE 54, 3 (1966).
4. N. George, A. Jain: Applied Physics 4, 201 (1974).
5. Kerr, D. W.: Propagation of Short Radio Waves, McGraw-Hill, New York, 1951.
6. Berkowitz, R. S.: Modern Radar, John Wiley & Sons, New York, 1965.
7. M. E. Bair, D. C. Carmer, S. R. Stewart: Report No. 1652-24-T ERIM-Willow Run Laboratories, The University of Michigan, Ann Arbor (1970).
8. A. K. Chakraborty: Optics Communications 8, 366 (1973).
9. N. George, A. Jain: J. Opt. Soc. Am. 63, 480A (1973).
10. A. Papoulis: Probability, Random Variables and Stochastic Processes (McGraw-Hill, New York, 1965).

Chapter IV

STATISTICS OF SPECKLE

4.1 Introduction

In this chapter, a review of the theory predicting the statistics of intensity fluctuations in speckle patterns is presented. It is then demonstrated theoretically and experimentally that the statistics of speckle are highly dependent upon the roughness of the diffuser producing the speckle, as well as the polarization of the system for viewing the speckle.

In a space-invariant imaging system as shown conceptually in fig. (2-2), the electric field at a point in the image plane will be of the form

$$R = \sum_{r=1}^{N} e^{iah_r} \tag{4.1}$$

where h_r is a random variable and N is the number of iso-phasic regions in a resolution area of the imaging system. The statistics of this function were given by Lord Rayleigh in 1880 [1] in his paper "On the Resultant of a Large Number of Vibrations of the Same Pitch and of Arbitrary Phase." Translating Rayleigh's result into terms relating to speckle patterns, it is found that for large N, the electric field probability density function for an arbitrary phase will be

$$P(e_\theta) = \frac{1}{\sqrt{2\pi\sigma^2}} \; e^{-e_\theta^2/2\sigma^2} \tag{4.2}$$

which of course is Gaussian. It is also determined that the density function for electric field amplitude is

$$P(|e|) = \frac{|e|}{\alpha^2} e^{-|e|^2/2\alpha^2} \quad U(|e|) \tag{4.3}$$

where $U(|e|)$ is the unit step function and the density function is named for Lord Rayleigh. In a publication in 1918, Rayleigh [2] showed that the density function for intensity, ee^*, is

$$P(u) = \frac{1}{\alpha} e^{-u/2} \quad U(u) \tag{4.4}$$

It is noted that these results apply for large N, however it has been shown by Burch [3] and others that these density functions are accurate for N of order 10 or greater.

In studies of laser speckle patterns, the results above are generally accepted [4-7]. A direct result of equation (4.4) is that the contrast ratio of a speckle pattern, defined by

$$C_R = \frac{\sigma}{\langle u \rangle} \tag{4.5}$$

where σ is the standard deviation of intensity and $\langle \mu \rangle$ the mean of intensity, will always be equal to one. Frequently the density function of (4.4) and the resultant $C_R \equiv 1$ have been presented in a way indicating them to be definitive of laser speckle. However, Fujii and Asakura [7] have measured probability densities for speckle intensities from diffusers of different thicknesses and have seen that the density function depends upon the roughness of the diffuser. It is our purpose to explain these differences

analytically and to show experimentally the relationship between the probability density function and the contrast ratio to the diffuser characteristics.

4.2 Diffuser Characteristics and Statistics

We have studied speckle patterns produced by diffusers made of flashed opal glass of various thicknesses. For diffusers of this kind, there are three overlapping thickness ranges of interest which are explained physically as follows:

(1) Thick; able to produce local phase retardations greater than $\lambda/2$ and substantially randomize the polarization of a plane polarized input.

(2) Medium; able to produce local phase retardations of order $\lambda/2$, but not highly depolarizing.

(3) Thin; not capable of producing local phase retardations of $\lambda/2$ or greater and not able to depolarize a plane polarized input.

It is understood that these descriptions are appropriate only for the opal glass diffusers, since for other types of diffusers the relationship between the thickness or roughness required to produce large local phase variations and that required to cause significant depolarization may be entirely different.

We consider a thick opal glass diffuser. It has been observed that a plane polarized illumination beam incident on a

diffuser 500 μm thick will be completely depolarized by transmission through it. It has also been observed that for an incident beam polarized in the x-direction as in fig. (3-5), the speckle measured with the analyzer parallel to x and speckle measured with the analyzer perpendicular to x have the same average intensity and are uncorrelated. We refer to these two cases as xx and xy, respectively.

As previously mentioned, the electric field density function for either the xx or xy speckle patterns will be Gaussian. Therefore, the density function for the intensities in either case will be the negative exponential,

$$P_{xx}(u_{xx}) = \frac{1}{\alpha} \exp\,[-u_{xx}/\alpha]$$

$$P_{xy}(u_{xy}) = \frac{1}{\alpha} \exp\,[-u_{xy}/\alpha] \qquad (4.6)$$

where u_{xx} and u_{xy} are the intensities and α is the average intensity.

We now show that if the speckle pattern from a diffuser thick enough to cause significant depolarization is viewed without an analyzer, the intensity distributions will no longer follow the negative exponential and the contrast ratio (4.5) will be less than one.

In the un-analyzed viewing the intensity at each point is

$$u = u_{xx} + u_{xy} \qquad (4.7)$$

Thus [9]

$$P(u) = \int_0^u P_{xx}(u-u_{xy})\, P_{xy}(u_{xy})\, du_{xy} \qquad (4.8)$$

Using (4.6) we write

$$P(u) = \frac{1}{\alpha^2} \int_0^u \exp(-u/\alpha)\, du_{xy}$$

$$P(u) = \frac{u}{\alpha^2} \exp[-u/\alpha] \qquad (4.9)$$

This result has been shown by Burch [3] in the general context of superposition of two incoherent speckle patterns. The fact that the two orthogonal polarizations do not interfere optically makes our analysis analogous. For the density function (4.9) we calculate the average intensity,

$$\langle u \rangle = 2\alpha \quad , \qquad (4.10)$$

and the standard deviation

$$\sigma = \sqrt{2}\,\alpha \quad . \qquad (4.11)$$

Thus the contrast ratio will be

$$C_R = 1/\sqrt{2} \qquad (4.12)$$

for the speckle from the thick diffuser.

It is noted that this treatment is consistent with the experimental results of Fujii and Asakura [7]. In these experiments, the diffusers were sufficiently smooth so as not to depolarize the incoming illumination, [8] hence the resulting speckle patterns exhibit the characteristics of those viewed with an analyzer.

We have measured the probability density for intensity in

speckle patterns produced by the 500 μm thick opal glass. The intensity data were obtained using the experimental setup of fig. (3-5). Rather than scanning the speckle patterns with the fiber optic probe, we have in these experiments moved the diffuser in 1 mm. steps over a matrix of 160-300 points. In this way we ensured more complete randomization of the data, and fig. (4-1) shows complete decorrelation after a lag of one data point. Data were taken with the analyzer parallel to the input polarizer (fig. 3-5) and with the analyzer removed. Figure (4-2) shows the experimental density functions obtained by a computer histogram method from the data. The differences in the functions for the two cases is clear.

We now consider the statistics of speckle from thin diffusers. The analysis is formulated for the polarized viewing case since by our definition of "thin," the crossed polarized component will be very small. We choose a model for the thin diffuser by a physical argument which presumes that a proportion of the incident light is propagated as if unscattered, producing in essence an unspeckled beam with a speckle pattern superposed on it. This model is analogous to the problems of radar return from an assembly of random scatterers plus a steady target [10]. The density function for electric field at the arbitrary phase angle of the unscattered beam is a normal density of nonzero mean:

$$P(E_0) = \frac{1}{\sigma\sqrt{2\pi}} \exp[-(E_0 - \eta)^2/2\sigma^2] \qquad (4.13)$$

The probability density for electric field 90° out of phase with the

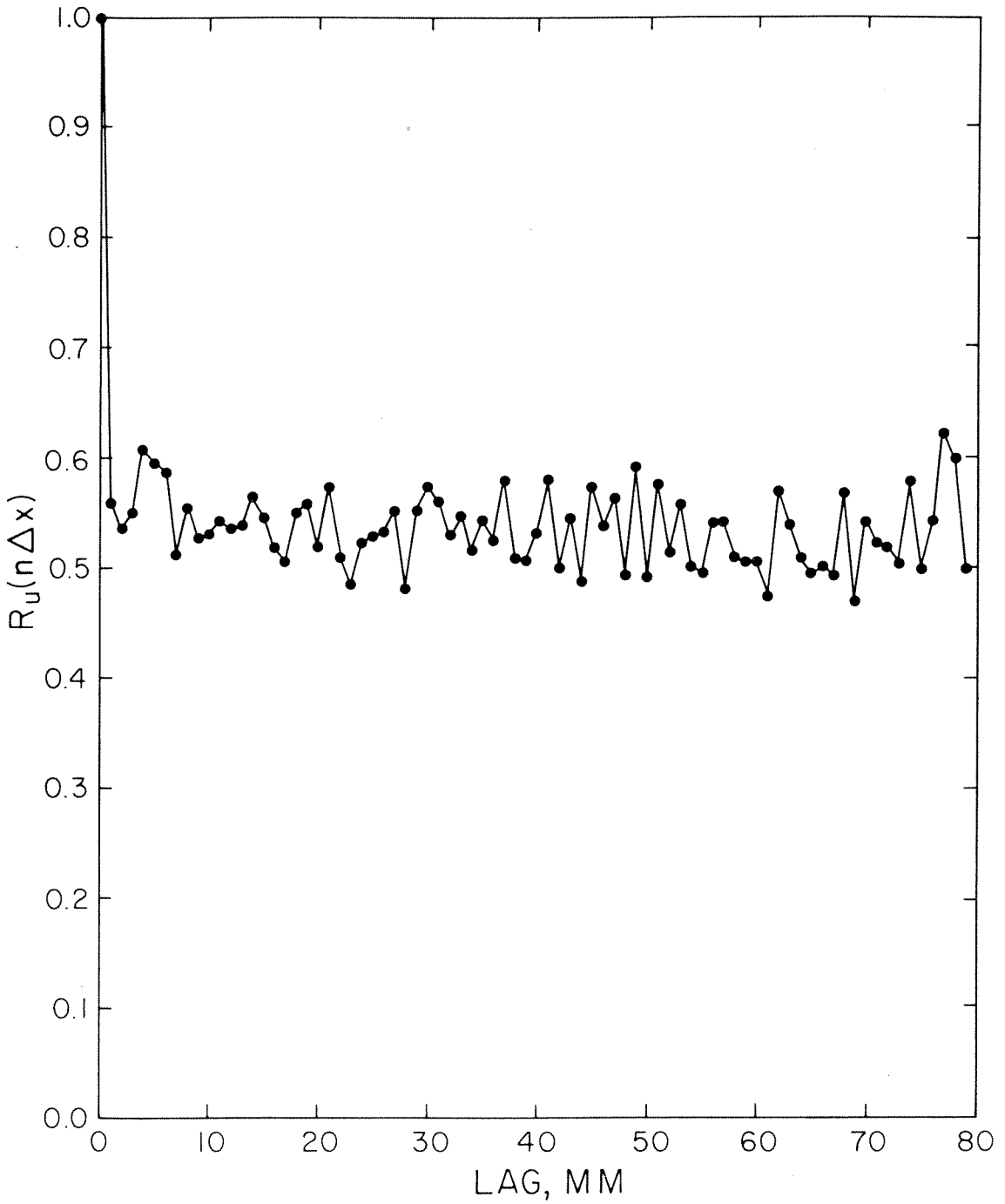

Fig. 4-1: Autocorrelation of speckle intensity obtained as in Fig. (3-5) by moving the 500 μm diffuser in 1 mm. steps while the fiber optic probe in the image plane was stationary. Complete decorrelation in one step is seen.

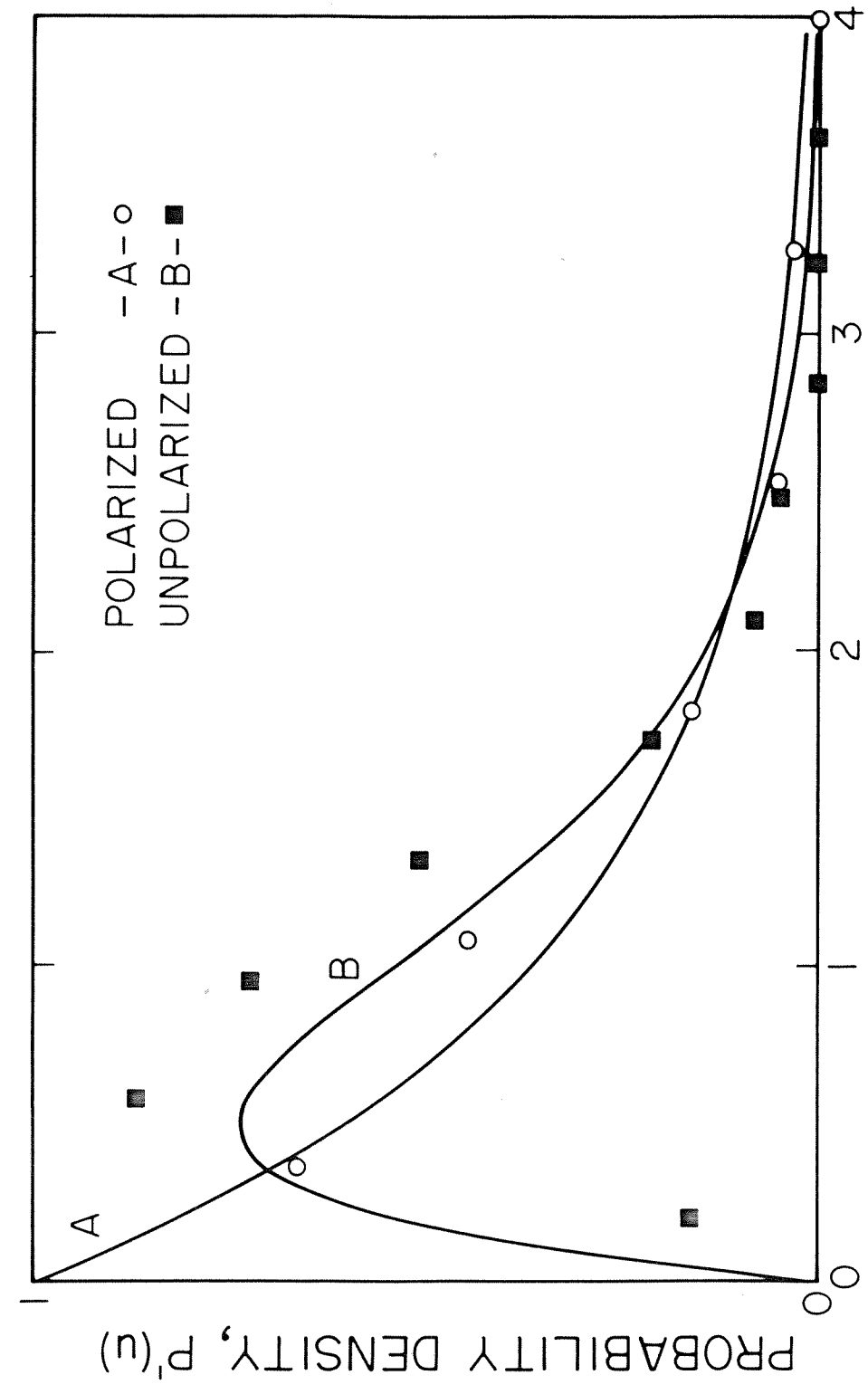

Fig. 4-2: Probability density functions for speckle intensity in the image of the 500μm diffuser. Curves A and B are theoretical plots while the data points are experimental values.

unscattered beam is normal of zero mean:

$$P(E_1) = \frac{1}{\sigma\sqrt{2\pi}} \exp[-E_1^2/2\sigma^2] \tag{4.14}$$

The resulting density for electric field amplitude is then [7,10,11]

$$P(|E|) = \frac{|E|}{\sigma^2} \exp[-(|E|^2 + \eta^2)/2\sigma^2] \tag{4.15}$$

$$\times\ I_0\left(\frac{|E|\eta}{\sigma^2}\right)\ U(|E|)$$

where I_0 is the modified Bessel functions of zero order. $P(|E|)$ is thus a joint density between a normal density of mean η and a normal density of zero mean. The density function for intensity u is found by the variable change

$$u = |E|^2 \tag{4.16}$$

so that

$$P(u) = \frac{1}{2\sigma^2} \exp[-(u + \eta^2)/2\sigma^2]$$

$$\times\ I_0\left(\frac{\sqrt{u}\,\eta}{\sigma^2}\right) \tag{4.17}$$

where we note that the parameters η and σ refer to the electric field. Rewriting (4.17)

$$P(u) = \frac{1}{2\alpha^2} \exp[-(u + \beta^2)/2\alpha^2]\ I_0\left(\frac{\sqrt{u}\,\beta}{\alpha^2}\right) \tag{4.18}$$

we solve for α and β in terms of parameters measurable in intensity. We find that

$$\langle u \rangle = \beta^2 + 2\alpha^2 \tag{4.19}$$

and

$$\langle u^2 \rangle = \beta^4 + 8\beta^2\alpha^2 + 8\alpha^4 \tag{4.20}$$

both of which reduce to the appropriate values for the negative exponential density when $\beta = 0$. Using (4.19) and (4.20) we determine the following:

$$\begin{aligned} 2\alpha^2 &= \langle u \rangle - \sqrt{\langle u \rangle^2 - \sigma^2} \\ \beta^2 &= \sqrt{\langle u \rangle^2 - \sigma^2} \end{aligned} \tag{4.21}$$

These parameters then are functions of the measurable average value and variance of the speckle pattern and it is again clear that when the contrast ratio is equal to one, then $\beta^2 \equiv 0$ which produces the negative exponential density from (4.18). In fig. (4-3) we have plotted normalized curves from equation (4.18) for 5 values of contrast ratio C_R where we have used the identities

$$\begin{aligned} 2\alpha^2 &= \langle u \rangle \left(1 - \sqrt{1 - C_R^2}\right) \\ \beta^2 &= \langle u \rangle \sqrt{1 - C_R^2} \end{aligned} \tag{4.22}$$

A series of experiments were performed to determine the form of the density function for opal glass diffusers of various thicknesses. Diffusers of 25 μm and 50 μm thickness were known [8] to have a large intensity lobe in the forward scattering direction, so the statistics of these samples were measured as before with polarized viewing and compared to those of the 100, 200 and 500μm samples. Figure (4-3) shows the density functions of the three diffusers measured as before by the histogram method and compared to the theoretical result (4.18).

In another series of experiments, we have measured the statistics for diffusers from 25-500 μm thick with the polarization analyzer removed from the system. From the results shown in fig. (4-4) it is seen that the density functions for the thin diffusers are nearly the same as those measured with the analyzer in place. However, in the medium thickness range ($\sim$ 100 μm) the contrast ratio is high because the phase changes are great enough to produce near nulls and the depolarization ratio is small. As the thickness approaches 500 μm the density function tends toward that of the two incoherently combined speckle patterns of equation (4.9).

4.3 Determination of Diffuser Thickness

Having established that the statistics, i.e., the probability density function for intensity, of speckle patterns are highly dependent upon the thickness of the diffuser as well as the polarization of the viewing system, we seek a convenient parameter related to

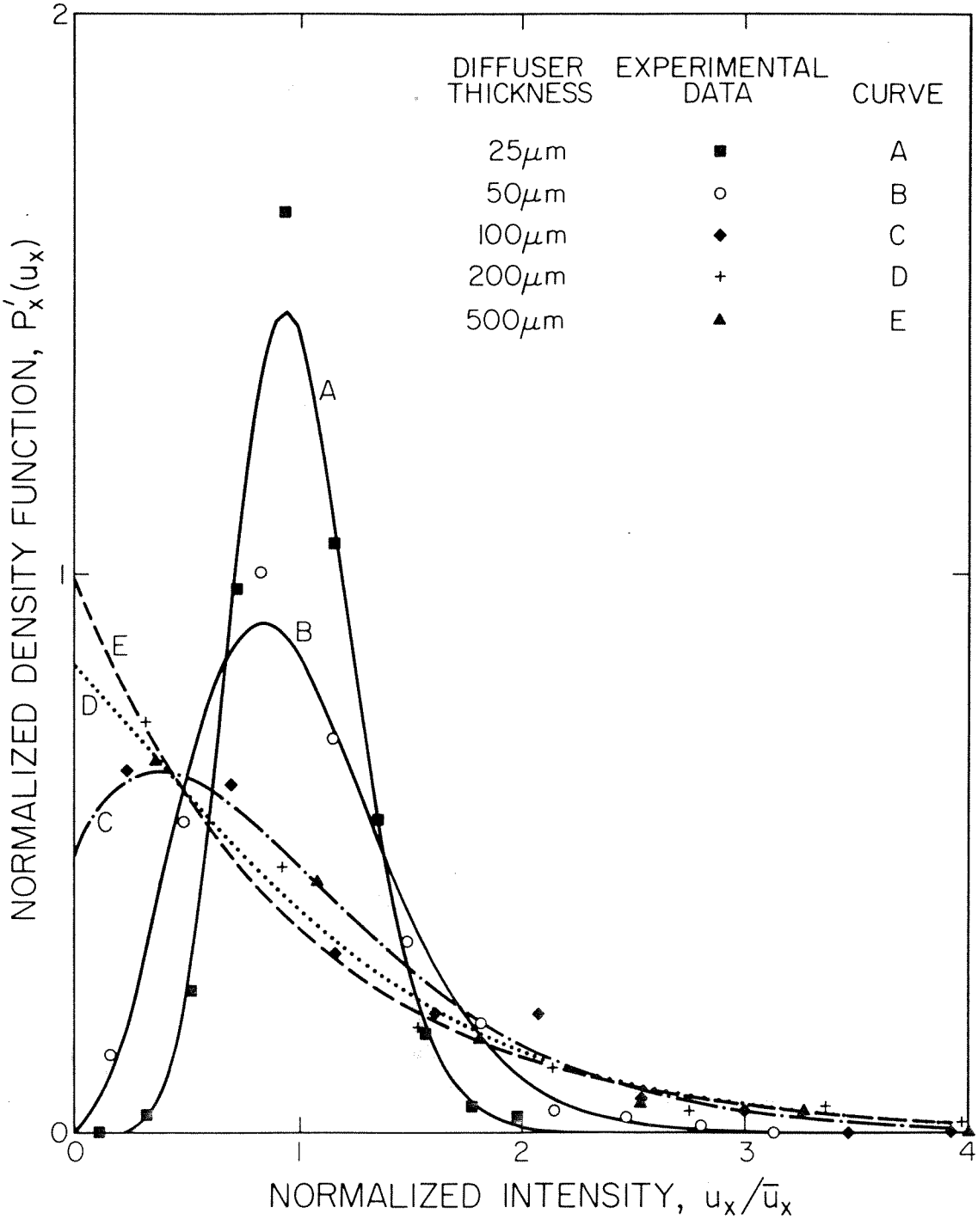

Fig. 4-3: Intensity density functions for a number of opal glass diffusers. The data were obtained as in Fig.(3-5) with the polarization analyzer set parallel to the illumination polarization.

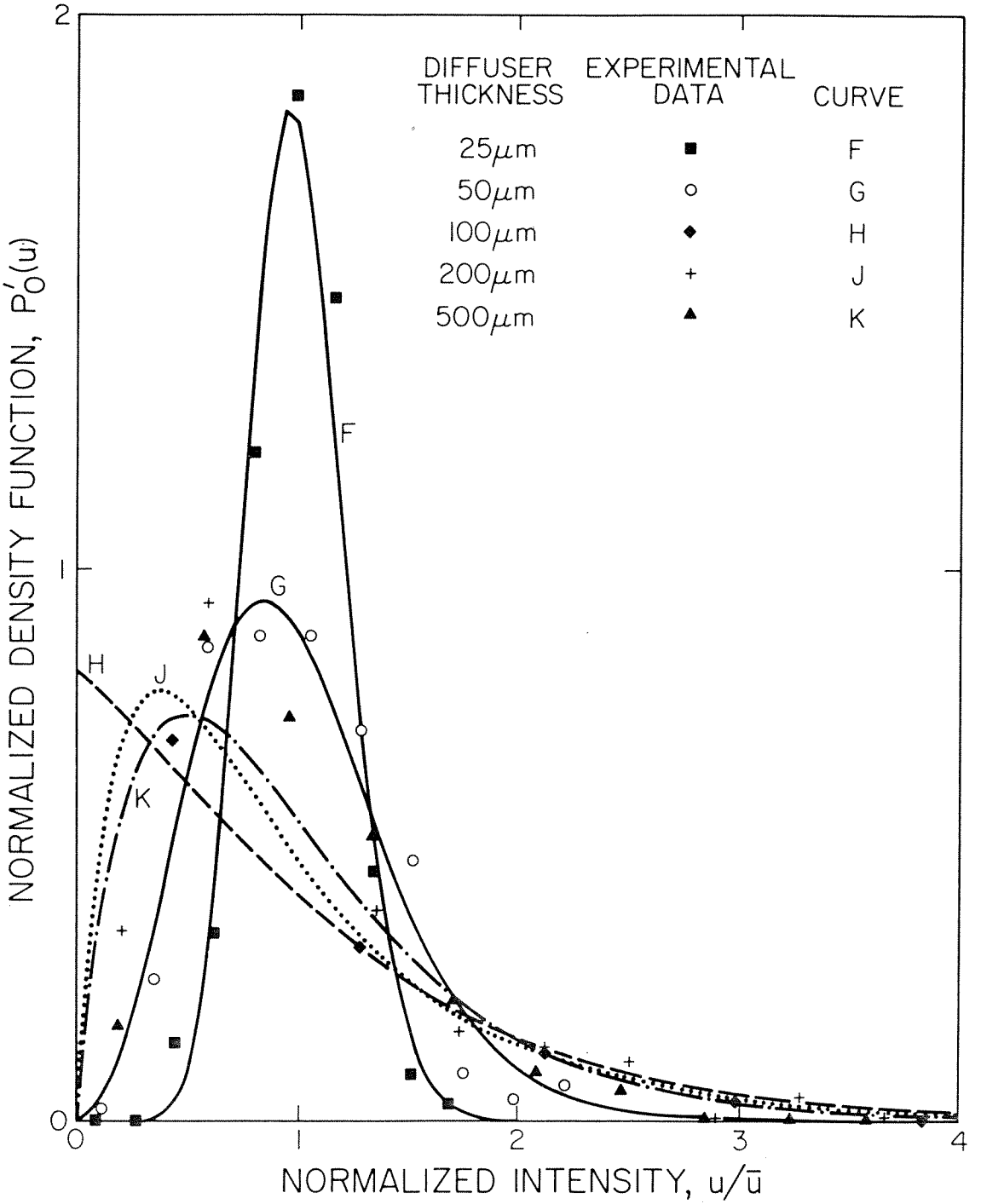

Fig. 4-4: Intensity density functions for a number of opal glass diffusers. The data were obtained as in Fig. (3-5) with the analyzer removed from the system.

the statistics which can be measured easily and which will provide direct information about the diffuser.

A logical choice of parameter is the contrast ratio $C_R = \langle\mu\rangle/\sigma$. Figure (4-5) gives plots of C_R vs diffuser thickness for polarized and unpolarized viewing. The differences between the curves enable a unique determination of the thickness of these opal glass diffusers over the range 0-500μ to be made from two measurements of contrast ratio.

It is also noticed that the curve C_R vs T for the polarized viewing can be expressed to within 5% over the entire thickness range as

$$C_R = 1 - \exp[-T/73] \tag{4.23}$$

where T is the thickness in μm. A slightly different dependence of C_R on diffuser roughness (for a different diffuser model) has been predicted by Jain [12].

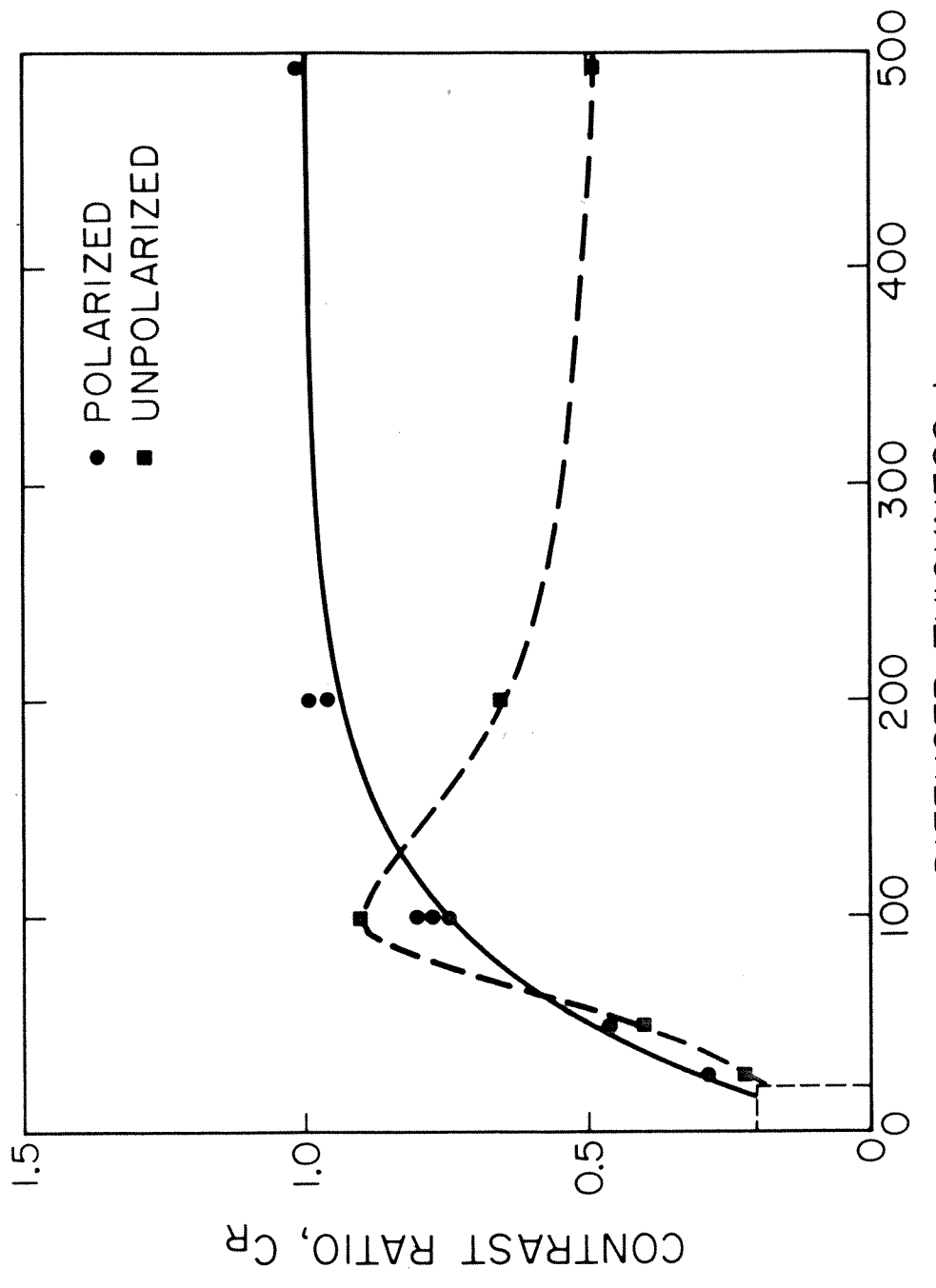

Fig. 4-5: Contrast ratio of the speckle intensity, $C_R = \sigma/\bar{u}$ as a function of diffuser thickness for a series of opal glass diffusers.

References

1. Lord Rayleigh: Phil. Mag. X (1880).
2. Lord Rayleigh: Phil. Mag. XXXVI (1918).
3. Burch, UJ. M.: Optical Instruments & Techniques, Oriel Press, 1970.
4. Collier, Burkhardt and Lin: Optical Holography, Academic Press, New York, 1971.
5. Goodman, J. W.: Proc. IEEE 53 (1965).
6. Dainty, J. C.: Optica Acta 17 (1970).
7. Fujii, H. and Asakura, T.: Optics Comm. 11 (1974).
8. George, N., Jain, A. and Melville, R.: in press.
9. Papoulis, A.: Probability, Random Variables and Stochastic Processes, McGraw-Hill, New York (1965).
10. Berkowitz, E.: Modern Radar, John Wiley & Sons, New York (1965).
11. Kerr, D.: Propagation of Short Radio Waves, McGraw-Hill, New York (1951).
12. Jain, A.: Ph.D. Thesis: A Wavelength Diversity Technique for Smoothing of Speckle, California Institute of Technology, 1974.

Chapter V

Measurements of Space and Wavelength Dependence of Speckle

5.1 Design of the Experiments

We have measured the spatial and spectral behavior of the image of a coherently illuminated diffuser as in figure (5-1). As we subsequently show, if the diffuser is properly chosen the image is a random speckle pattern. The illumination source used was a continuous wave tunable dye laser with a linewidth of less than 1/2Å. The dye laser along with a compensation system for power fluctuation and beam steering is fully described in Appendix A. The imaging system used was a Leitz binocular microscope. The limiting aperture of the system was controlled by use of a series of specially made circular pinholes which were mounted in the microscope objective. Speckle intensities in the image plane were measured with a scanning micrometer eyepiece and photomultiplier system. The Gamma Scientific Model 700-10 scanning micrometer replaces one of the normal microscope eyepieces. A movable fiber optic probe of 50 μm diameter samples intensity in the image plane of the objective and transmits the optical signal through a flexible fiber bundle to the photomultiplier. An RCA 4463 PM tube with S-20 response provided response flat to within 10% over the wavelength range in the experiments. A mechanical chopper was used in the illumination beam and the signals from the photomultiplier were detected and measured with a lock-in amplifier phase locked to the chopper. A signal-to-noise ratio of approximately 10:1 was observed at all signal levels in these experiments.

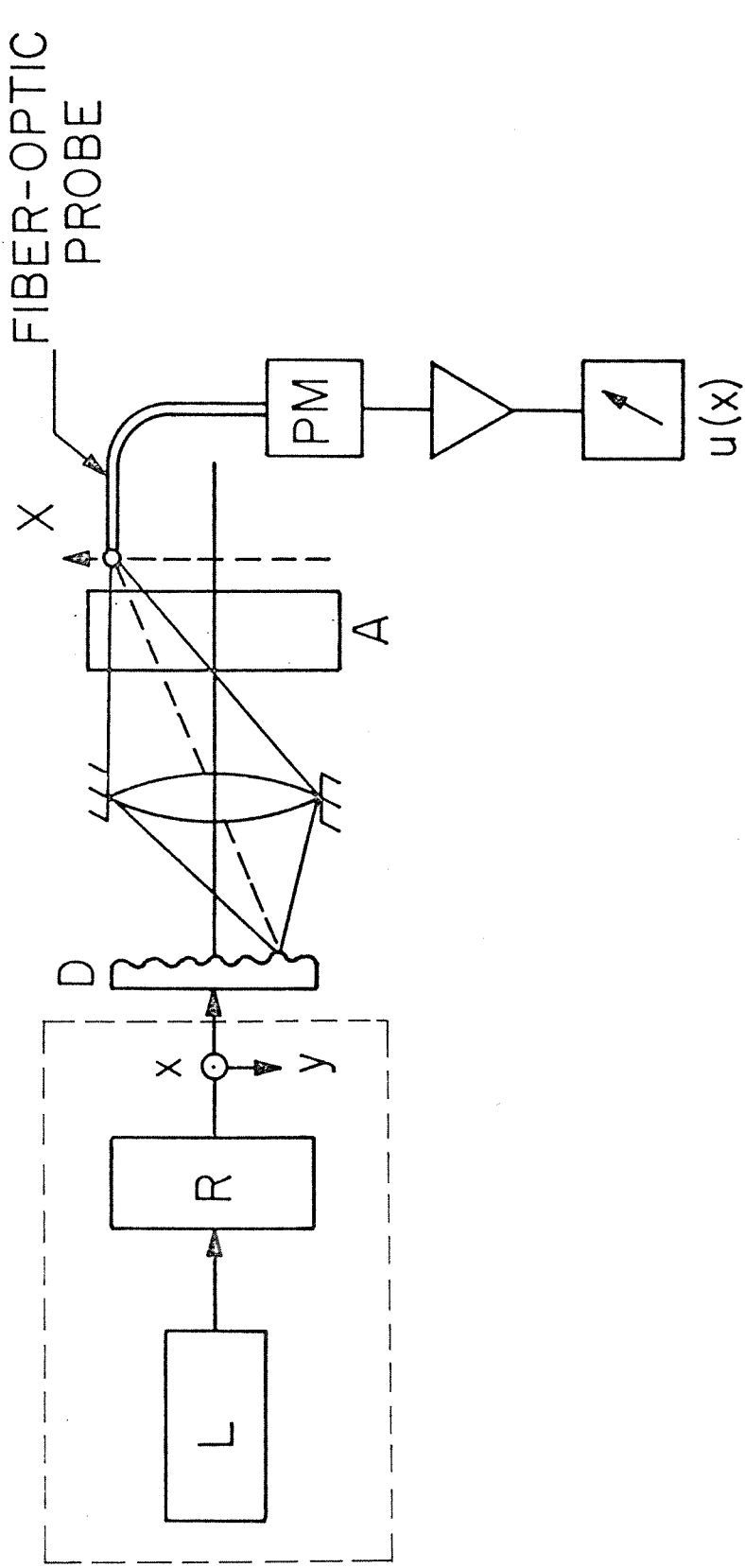

Fig. 5-1: Optical system for measuring speckle intensity. The dashed box represents the compensated laser system (Appendix A), D the diffuser, A an analyzer and PM the photomultiplier.

The fiber optic probe and photomultiplier system provide extremely linear response to intensity over a great range of power and has been employed specifically because of this. Another technique, which has been employed in a number of experiments found in the literature, is the recording of speckle patterns on photographic film and making subsequent measurements from the film. Unfortunately, photographic film is inherently nonlinear in response to exposure (intensity x time) and the nonlinearity is further complicated by its sensitivity to the film processing parameters. In Appendix B we have discussed this problem in some detail and conclude that even with an idealized film characteristic and ideal processing, very careful compensation must be employed to make accurate speckle measurements from photographic records. We have therefore avoided the use of photographic film altogether in these experiments.

In all of the measurements described here the illumination beam was plane polarized and a polarization analyzer parallel to the sense of the input polarization was incorporated in the objective carrier (nosepiece) of the microscope. The limiting aperture of the system was maintained small enough at all times so that the average speckle diameter was at least 250 μm, or five times the fiber optic probe diameter.

5.2 Choice of Diffusers

In the experiments, we desire to examine the behavior of purely random speckle patterns. However, in the study of speckle in an imaging system we may expect to find the image of the diffuser surface in addition to the speckle as the output of the optical system. We

would then be faced with the problem of separating the speckle behavior from the deterministic portions of the diffuser image. For this reason, we have used diffusers in these experiments for which the sizes of the phase scatterers are below the resolution limit of the microscope. Thus, none of the surface detail of the diffuser appears in the image plane.

We have found that common flashed opal glass has no resolvable features in our image system and yet produces heavily speckled output. Figure (5-2) shows microscope photographs of opal glass and Kodak fine-ground glass both illuminated in transmission by white light. The surface features of the ground glass are clearly resolved, while the opal glass appears as a milky-white blur with no apparent surface features. In figure (5-3) images of the same diffusers illuminated by the dye laser at 5700Å are shown. Although both images are heavily speckled, surface detail of the ground glass is well resolved and is clearly evident. The image of the opal glass shows nothing but the purely random speckle pattern. As previously described (Section 3.2) we have prepared opal glass diffusers of several different thicknesses for use in these experiments. As we shall indicate, the thickness of the opal glass corresponds to surface roughness of a diffuser such as ground glass.

Opal glass may be considered as producing local random phase variations in the cross-section of the illumination beam because of local random index of refraction differences in the material. Opalescent glass consists of a two-phase imiscible oxide system. The optical scattering property is caused by many tiny droplets of one

(a)

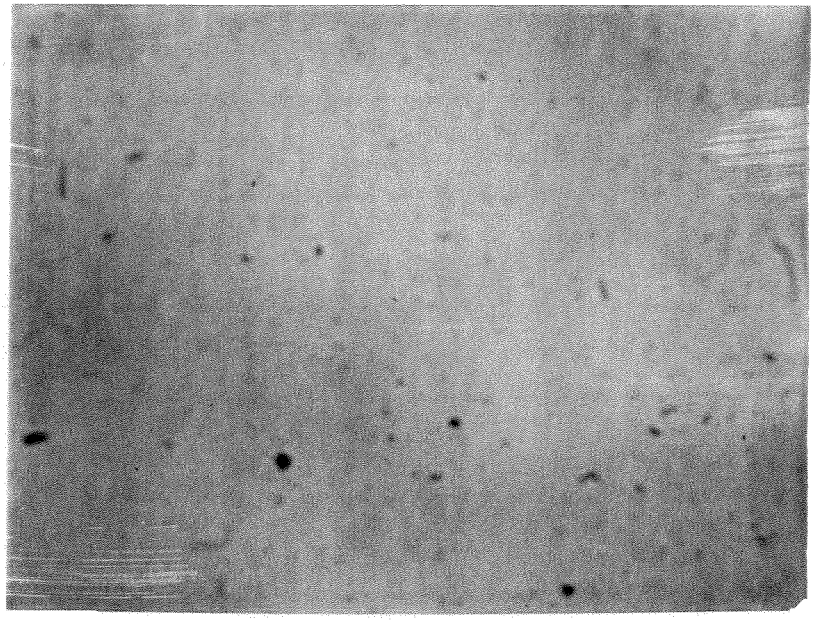

(b)

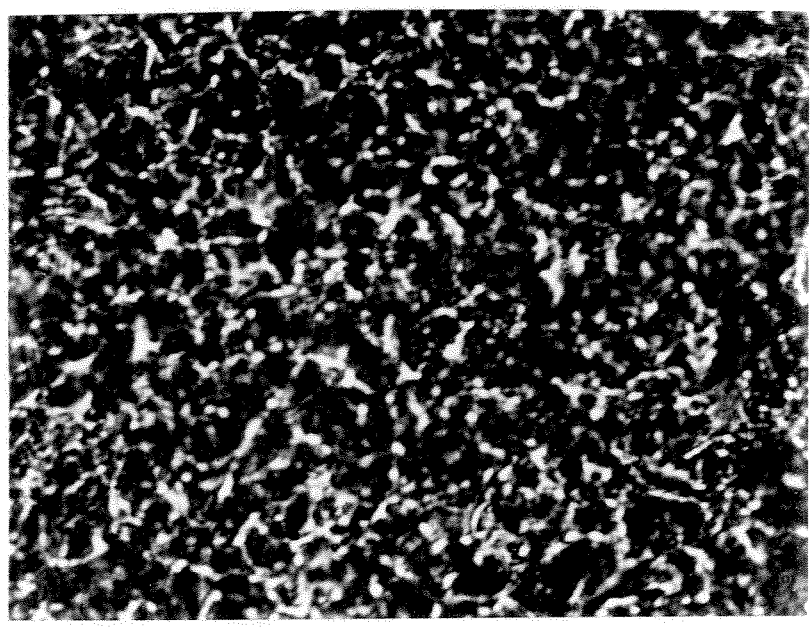

Fig. 5-2: Microscope photographs at 50x magnification in white light. (a) is the image of the opal glass surface and (b) is ground glass.

(a)

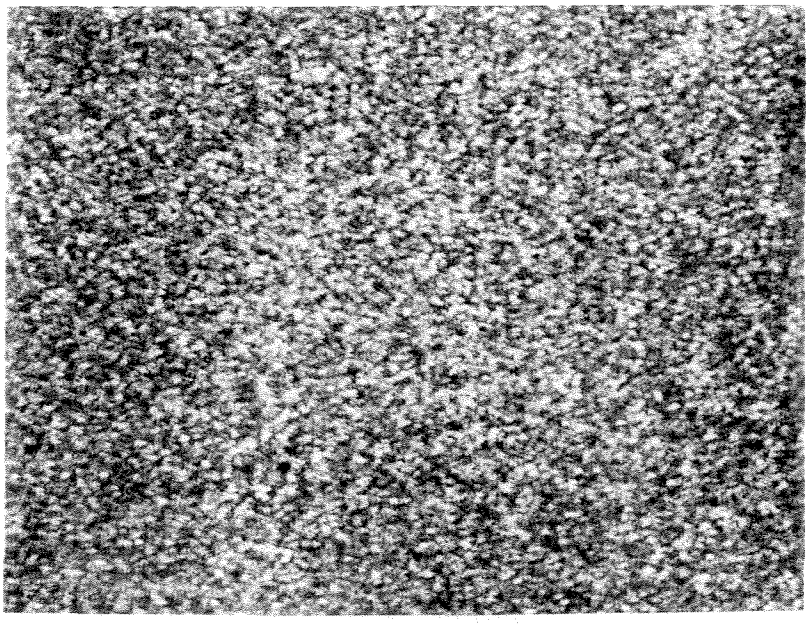

(b)

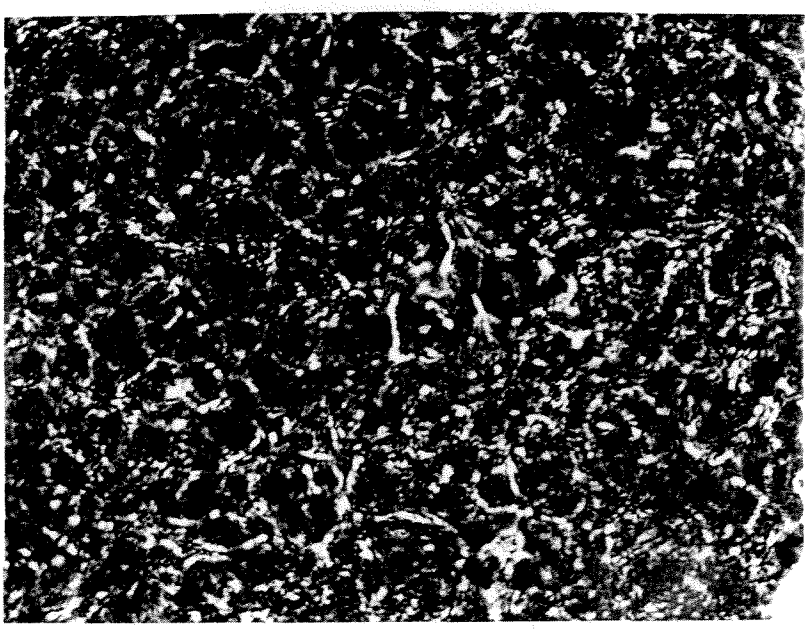

Fig. 5-3: Microscope photographs at 50x magnification with laser illumination at 5700A. (a) is the image of the opal glass and (b) is the ground glass.

phase suspended in the bulk phase [1]. The droplets or domains in an opalescent glass are typically from 0.1 to 0.5 μm in size, are nearly spherical [1,2] and are randomly distributed throughout the bulk of the glass. Using a scanning electron microscope, we made a *photograph [figure (5-4)] of the surface of a typical opal glass* sample at 10,000X magnification. The scattering centers are approximately spherical in shape and are about 0.5 μm in diameter.

In optical terms, the opal glass is a medium of bulk index of refraction n_1, containing many small regions of a slightly different index n_2. Qualitatively, we expect that the maximum optical phase difference we might observe between any two points in the cross-section of a beam after transmission through opal glass will be a function of the overall thickness of opalescent layer as well as the concentration of the scattering centers. In our experiments, since the diffusers have been prepared by varying the thickness of pieces cut from a larger piece of opal glass it is reasonable to expect that the maximum phase differences will be a function of the sample thickness. In addition we hypothesize that speckle produced by phase variations in transmission through a rough surfaced material such as ground glass with standard deviation of surface heights $\sigma(h)$ will be similar to speckle from opal glass of thickness $T >> \sigma(h)$. A physical argument to support this hypothesis is based on the fact that at the interface between a rough surface and air the difference in the index of refraction will be about .5, whereas in opal glass the index difference between the scattering droplets and the bulk material is $\Delta n << .5$. Experimentally we find that the first order statistics

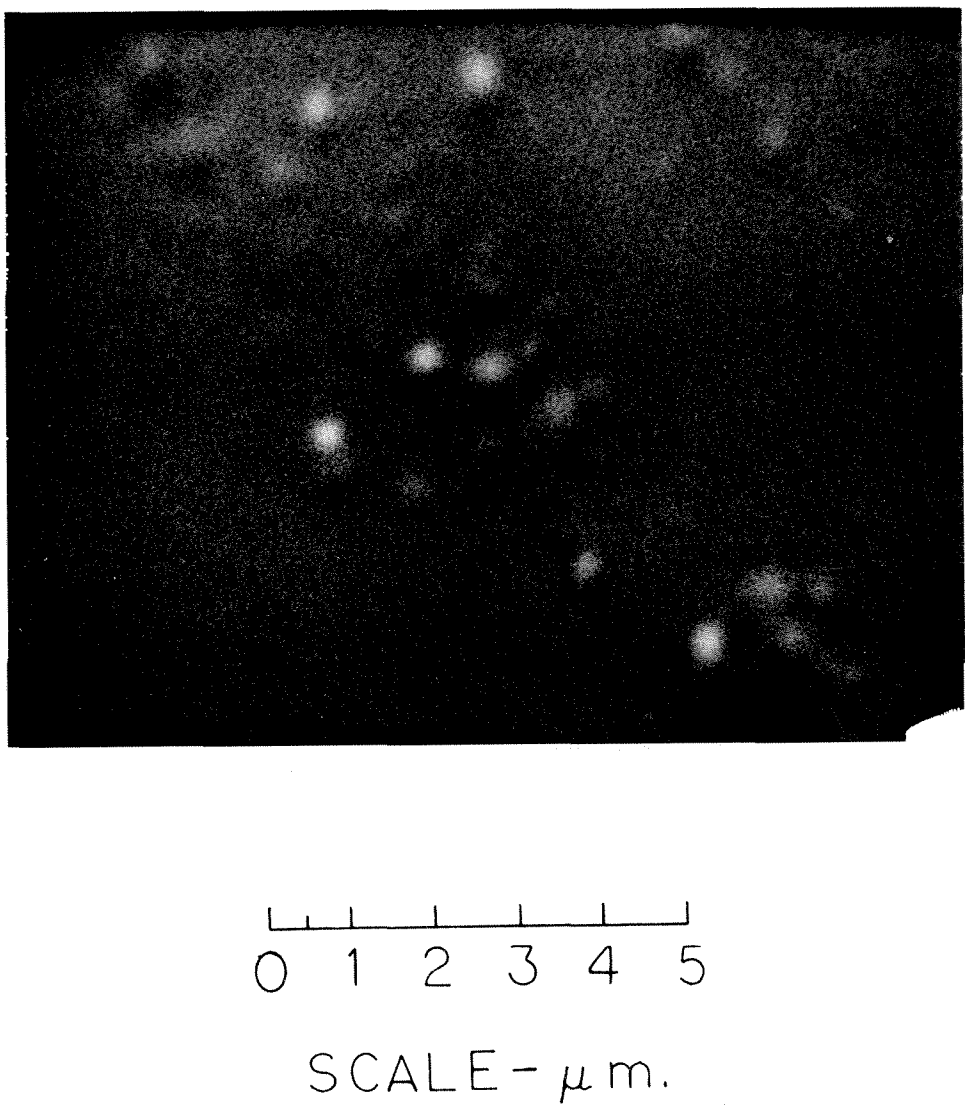

Fig. 5-4: Electron microscope photograph of opal glass surface at 10000x magnification.

which we have measured for the speckle from an opal glass 100 μm thick are similar to statistics for speckle from ground glass of .5 μm average surface roughness [3].

5.3 Spatial Autocorrelation Function

We have measured the spatial autocorrelation function of speckle intensity with the system of figure (5-1). Recalling the formalism of Chapter II, where we have called the autocorrelation $R_u(\Delta x,\eta_1,\eta_2)$, we define the spatial autocorrelation as $R_u(\Delta x,\eta_1,\eta_1)$ in which we maintain the optical frequency (wavelength) constant. In the experiment, the wavelength of the dye laser was maintained constant and the intensity of the speckle pattern was measured by scanning the pattern in one dimension along a straight line with the fiber-optic probe. The scan was made in a stepwise manner so that the resulting data set was in the form of a sampled function. Figure (5-5) is a computer plot of one of the experiments. The autocorrelation of the sampled function was calculated in the computer using the equation

$$R'_u(K) = \frac{\sum_N I(N)\, I(N-K)}{\sum_N I(N)\, I(N)} \qquad (5.1)$$

as a basis. $I(N)$ is the intensity at the N^{th} probe displacement and K is the lag. Figure (5-6) is a typical autocorrelation R'_u vs. Δx .

We have made several measurements of the spatial autocorrelation for each diffuser thickness at each available aperture size. For each of the curves similar to figure (5-6) the lag, Δx , required for the function to go from the maximum value to the projected asymptotic value was measured. This lag we arbitrarily call the decorrelation

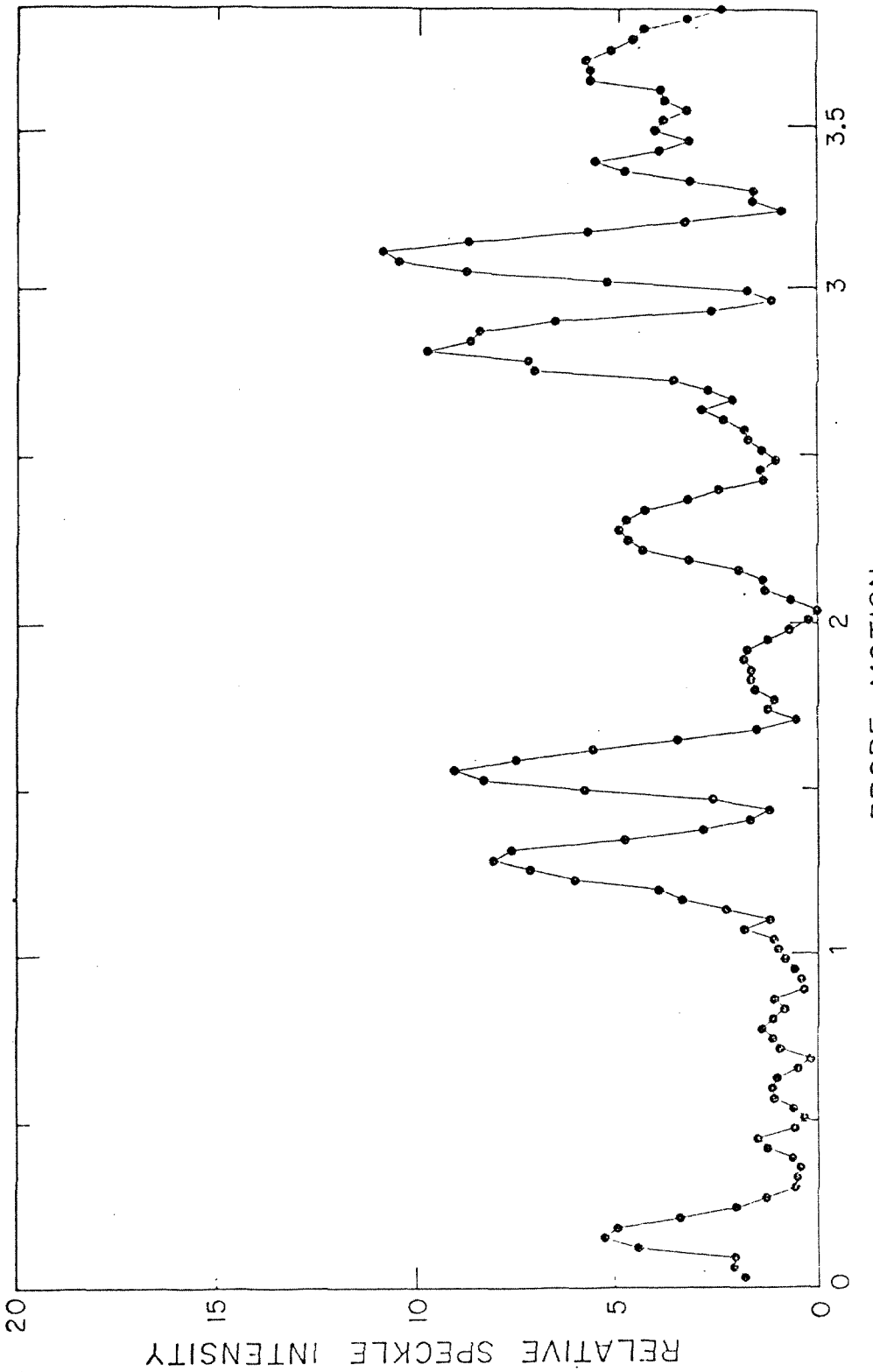

Fig. 5-5: Plot of intensity vs. probe motion for a typical experiment. The sampled data are used to compute the autocorrelations and the histograms for first order statistics.

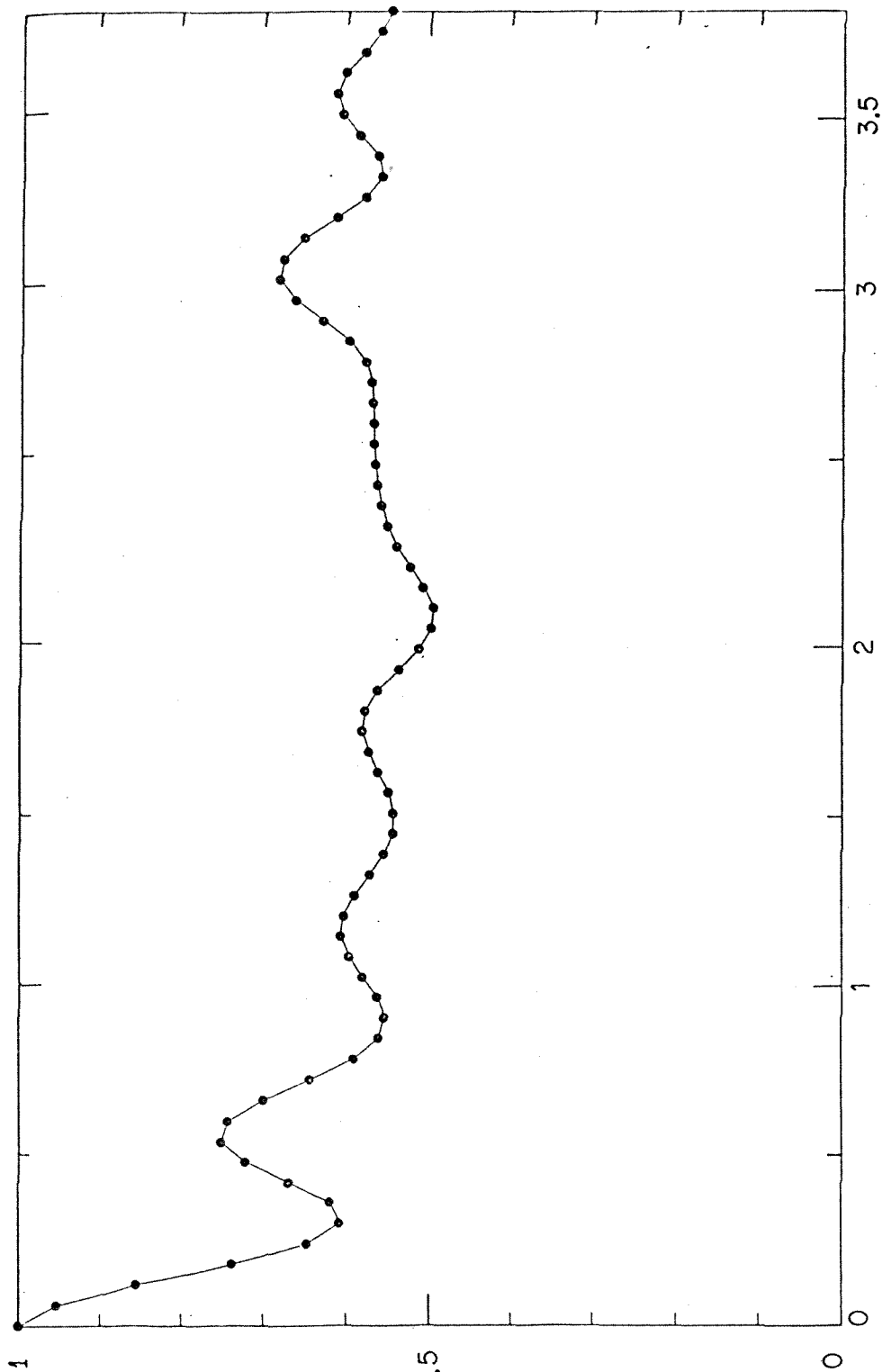

Fig. 5-6: Spatial autocorrelation of speckle intensity for probe motion in the image plane at fixed wavelength.

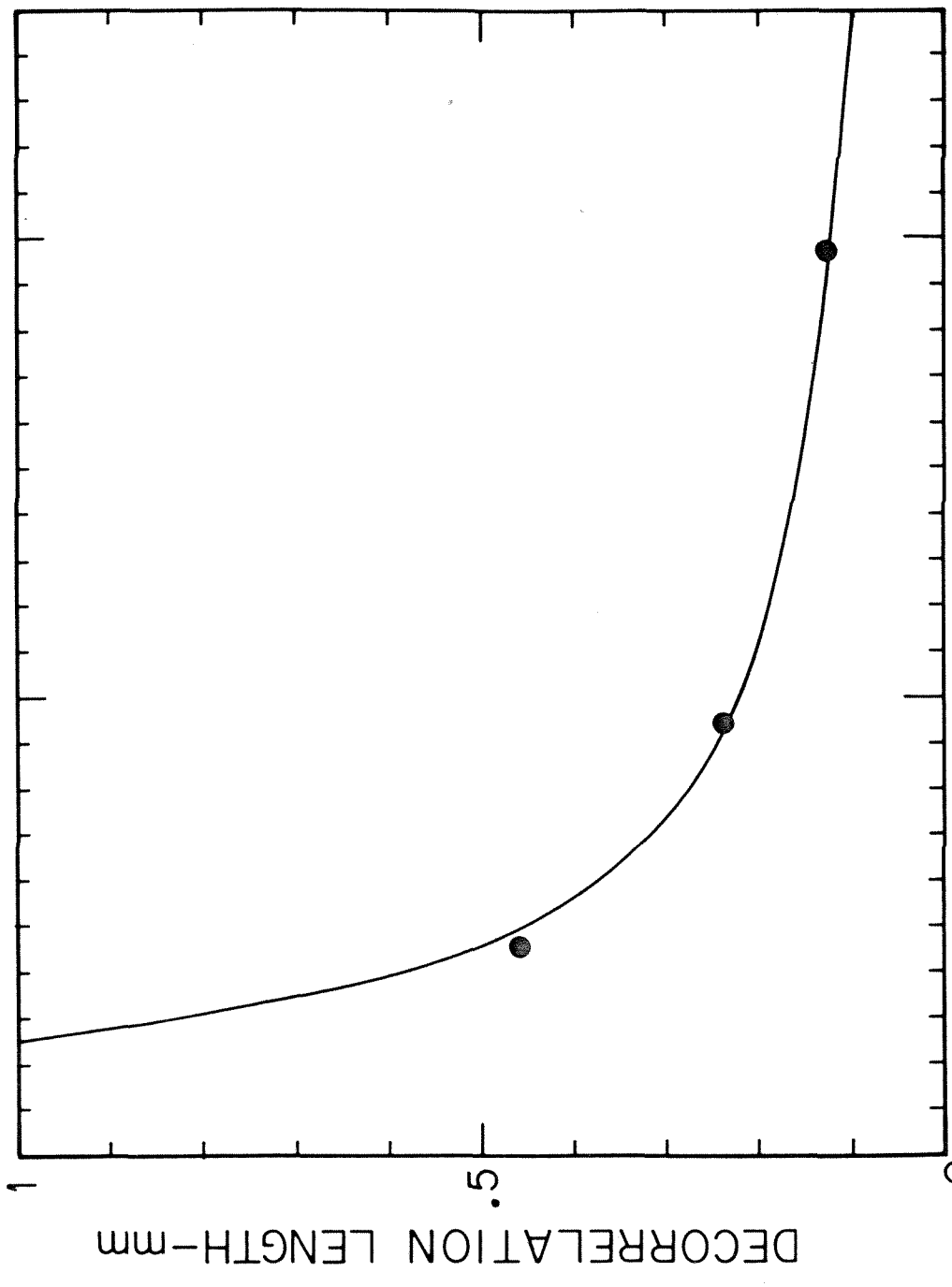

Fig. 5-7: Decorrelation distance $\Delta\xi_o$ vs. pupil diameter d. Data points are plotted with the curve $\Delta\xi_o d$ = constant fit at d = 1.96mm.

length. We found that the decorrelation length with respect to the spatial variable was independent of the thickness of the diffuser sample and of the particular portion of the diffuser viewed. However, the decorrelation length is strongly influenced by the limiting aperture of the optical system. Figure (5-7) gives the decorrelation length as a function of aperture size for three different apertures. Each experimental point shown results from the average of four to ten measurements. A curve representing a constant times the inverse of the aperture size is drawn through one experimental point and shown for comparison. The theoretical results of Chapter II for the thin diffuser also show that the spatial decorrelation of speckle is inversely dependent upon aperture size.

5.4 Spectral Autocorrelation Function

In an experiment similar to that for the measurement of the spatial character of the speckle pattern, we have measured the autocorrelation of speckle intensity as a function of the illumination wavelength. This function we define by $R_u(0,\eta_1,\eta_2)$. The measurements were made with the fiber optic probe fixed in position, and the illumination wavelength was varied by tuning the dye laser in two Angstrom unit steps over a 250-300Å range. Thus, the data obtained represented a sampled function of intensity vs. wavelength. A typical plot of intensity vs. wavelength is shown in figure (5-8). Using a similar computer code to that previously described, plots of the autocorrelation function as a function of the lag $\Delta\lambda$ in Angstroms were made. Figure (5-9) shows the autocorrelation vs. $\Delta\lambda$ for 3 different diffuser thicknesses. From these autocorrelation functions we have measured the decorrelation wavelength

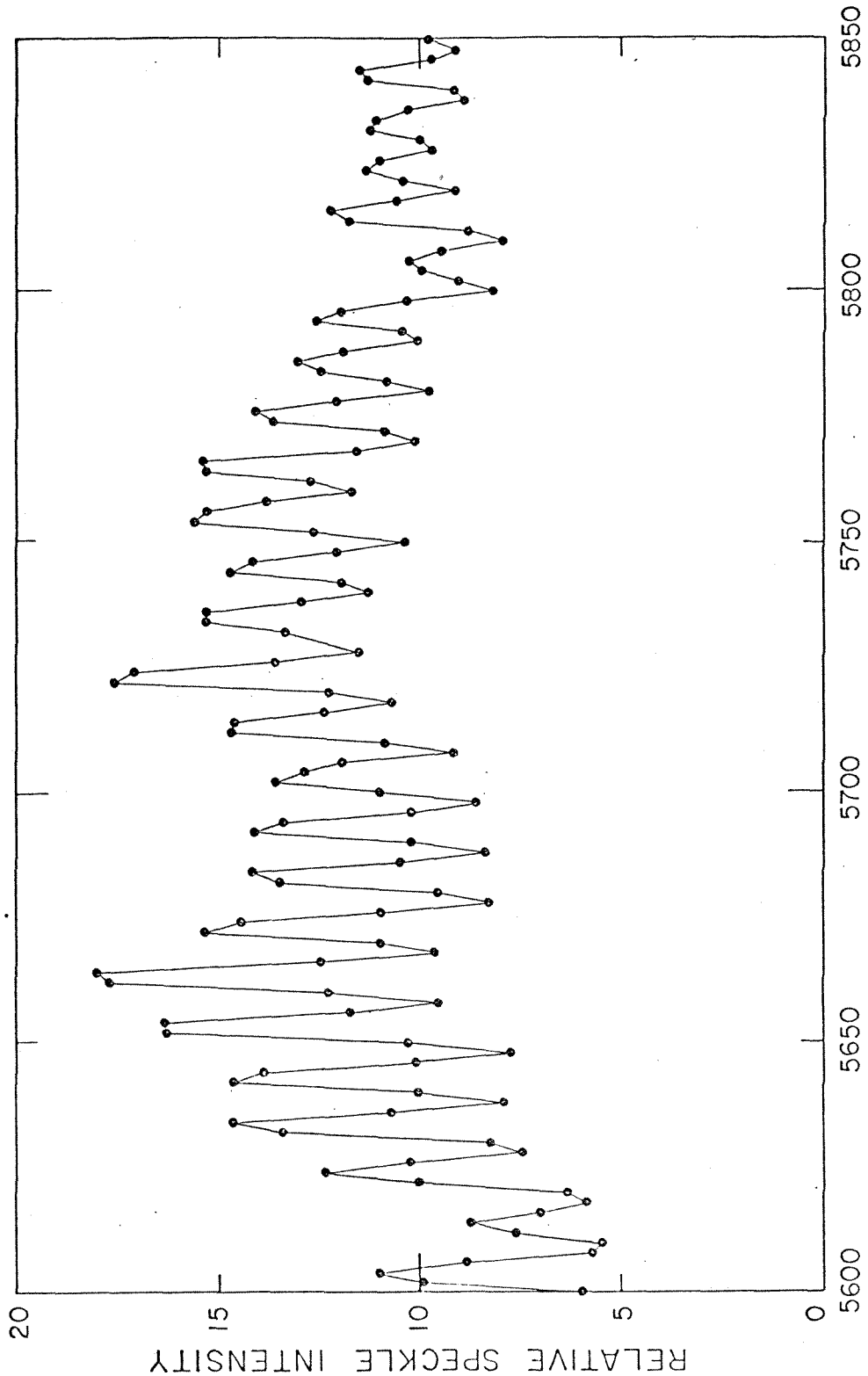

Fig. 5-8: Intensity as a function of wavelength with probe position fixed. Points represent the sampled data.

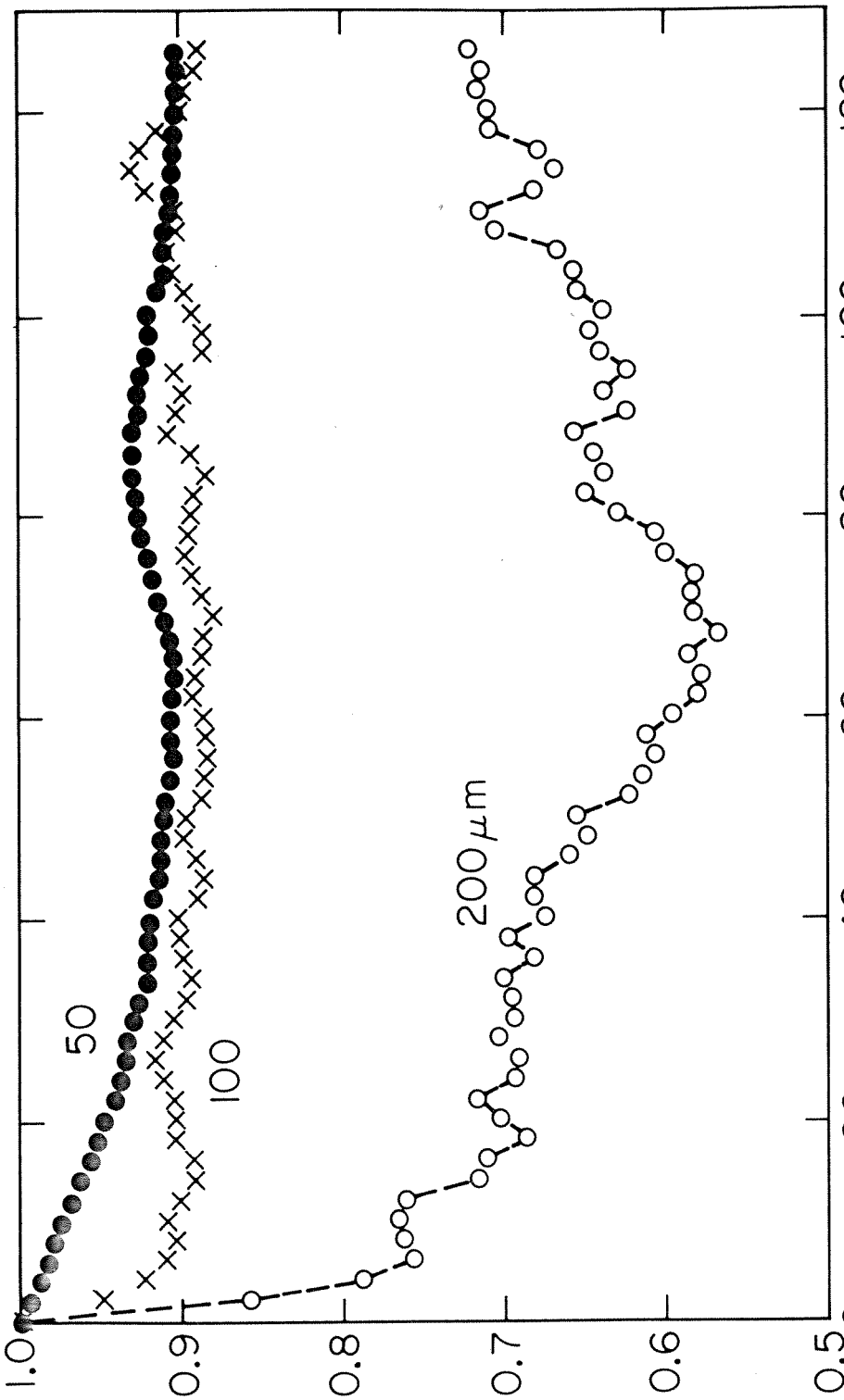

Fig. 5-9: Autocorrelation of speckle intensity vs. wavelength interval for 50,100 and 200μm thick opal glass diffusers.

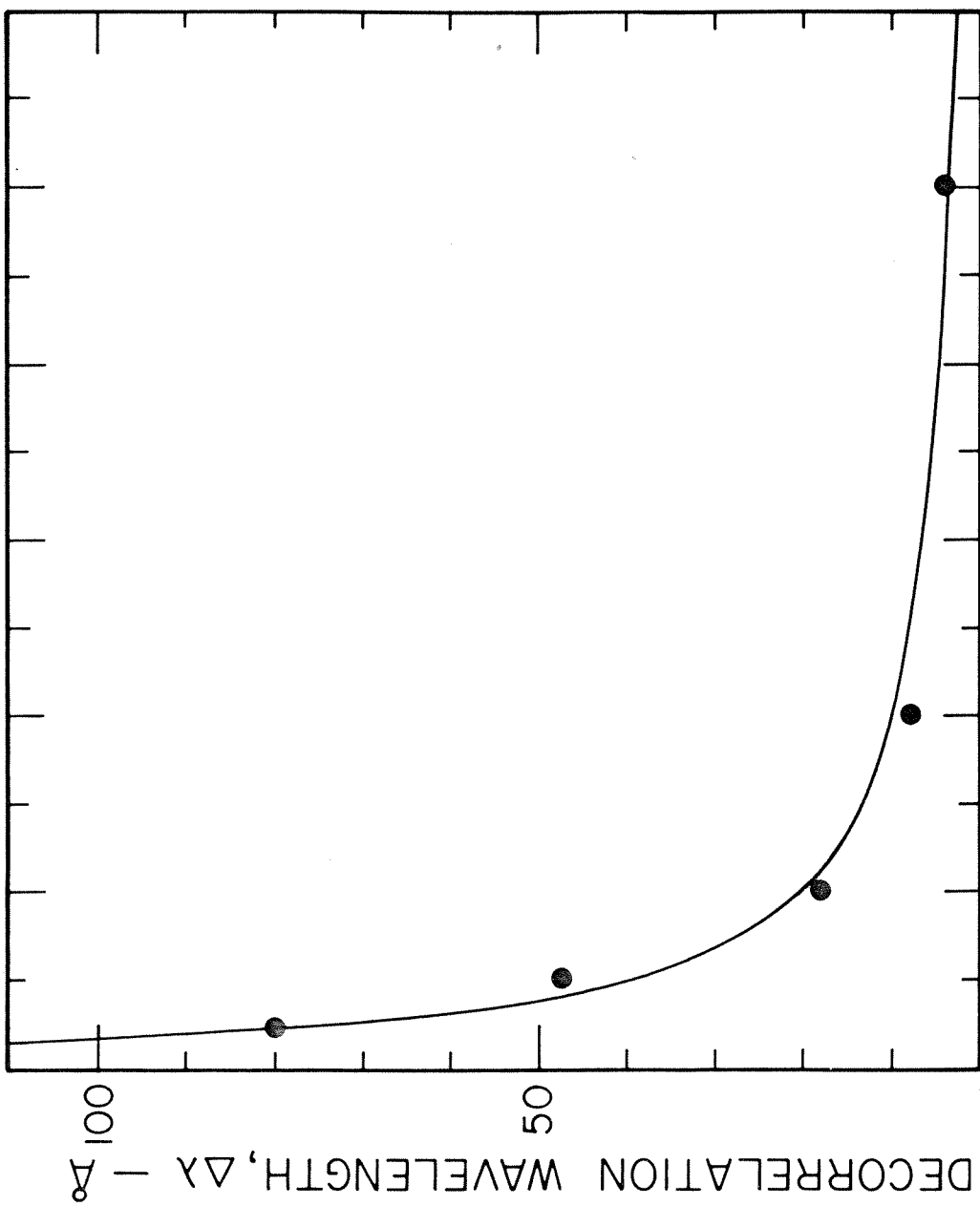

Fig. 5-10: Decorrelation wavelength as a function of diffuser thickness. Points are experimental data. The curve is drawn for $\Delta\lambda T$ = constant and fit at T = 500μm.

defined as the wavelength span required for the autocorrelation to go from the maximum value to the asymptotic value.

The decorrelation wavelength was seen to be independent of the aperture dimension. Figure (5-10) shows the decorrelation wavelength as a function of diffuser thickness. Again, each experimental point represents an average over 4-10 separate measurements. The curve shown in the figure is a one point fit to diffuser thickness 500 μm and goes as inverse thickness. We note that the theory for the wavelength diversity required to decorrelate two speckle patterns predicts dependence proportional to inverse roughness.

5.5 Summary of Results and Conclusions

In this section, we summarize the essential results of the theory and experiments described in this thesis.

In Chapter II, we have given a theory for the autocorrelation of speckle intensity in a space-invariant linear system as a function of spatial and wavelength variables. Calculations of the autocorrelation function for a number of speckle-producing diffusers of different surface characteristic were made and digital computer plots of these autocorrelation functions vs. either spatial or wavelength variables were presented. The central result of all of these calculations is seen in equations (2.2), (2.44), (2.64), (2.74) and (2.75) and in figures (2-4) through (2-9). From these we theorize that the spatial character of the autocorrelation of speckle depends on the limiting aperture of the optical system, while the spectral behavior of the autocorrelation depends upon the roughness of the diffusing medium.

In Chapter III we have examined the effect of the polarization of the diffuser illumination and the use of a polarization analyzer in viewing the speckle pattern. We have measured the extent to which a plane polarized beam is depolarized by passage through opal glass diffusers of various thicknesses. The influence of input and output (with respect to the diffuser) polarization on the autocorrelation function was also studied. Cross-correlations of speckle patterns observed with various combinations of input/output polarizations were measured. From these polarization studies, we conclude that in order to assess experimental speckle information correctly, the polarization of the illumination entering and exiting the diffuse surface must be controlled by the experimenter.

Chapter IV describes theory and measurements of the first order statistics of speckle in the imaging system. We determined that the density function for speckle intensity depends upon the polarization of the viewing system and upon the roughness of the diffuser. These results are given in equations (4.8) and (4.18) and shown in figures (4-2), (4-3) and (4-4). In addition, it was shown that a measurement of the speckle contrast ratio C_R, defined as the ratio between the standard deviation of intensity and the mean of intensity could be used to determine the thickness of the opal glass diffusers used in our experiments. Thus, measurement of speckle characteristics may be useful for remote determination of surface roughness or diffusivity.

Finally, in Chapter V we have measured the spatial and spectral autocorrelations of speckle and have shown experimental results. We see that the experimental results are in essential agreement with the

theory of Chapter II.

Table (5-1) gives a summary of some experimental results which are primarily functions of the diffuser characteristics. All of these results have application toward use of speckle measurements to study diffusers and diffuse surfaces. These results appear elsewhere in this work with more detailed explanation and analysis.

Diffuser Thickness h_o, μm	Polarized		Depolarization Ratio $D = u_\perp / u_\parallel$	Unpolarized		Decorrelation Wavelength $\Delta\lambda$, Å
	C_R	$R'_u(\infty)^\dagger$		C_R	$R'_u(\infty)^\dagger$	
25	.27	.93	2.8×10^{-4}	.22	.95	80
50	.46	.83	1.5×10^{-3}	.45	.83	48
100	.78	.62	.12	.91	.54	18
200	.98	.51	.35	.68	.68	8
500	1.00	.50	1.0	.52	.79	4

†The same data are used for C_R and $R'_u(\infty)$. The relationship is given by $R'_u(\infty) = 1/1 + C_R^2$.

Table 5-1: Summary of experimental results for opal glass diffuser series. These data are compiled from figures shown and discussed in detail elsewhere in the text.

References

1. Holland, L.: The Properties of Glass Surfaces, Chapman and Hall, London (1964).

2. Volf, M. B.: Technical Glasses, Sir Isaac Pitman & Sons Ltd., London (1961).

3. Fujii, H. and Asakura, T.: Optics Comm. 11 (1974).

APPENDIX A

THE TUNABLE DYE LASER

A.1 Description of the Dye Laser System

In the experiments reported herein, we have used a Spectra Physics Model 370 Tunable Dye Laser to illuminate various diffusers and produce laser speckle patterns. A mixture of methanol and water containing the dye Rhodamine 6G was used as the lasing medium. Rhodamine 6G absorbs radiation in the 4800 to 5300Å band and provides laser gain from 5400 to 6300Å. A Spectra Physics Model 165 Argon Ion Laser was used to irradiate the dye cell and was generally operated at 1 watt output. A collimating lens inside the dye laser cavity was set to provide the minimum linewidth across the 5600 to 6000Å region. At the setting chosen for the collimating lens, the laser manufacturers estimate of linewidth is about 1/2Å and we observed linewidths narrower than 1/2Å across the 5600 to 6000Å spectrum. When operated in this mode, the dye laser provided continuous wave output from 60-200 mw in the wavelength band of interest.

A.2 Measurements of Dye Laser Characteristics

In using the dye laser for speckle experiments, there were several operating parameters which were considered crucial to the accuracy of the experimental data. We therefore measured several of these parameters and where necessary have introduced suitable compensation into the experimental layouts.

Output Power: We have measured the power output from the dye laser as a function of wavelength with 1 watt of optical pumping from the argon laser. Power was measured using a Coherent Radiation Model 910 Laser Power Meter and wavelength monitored with a Jarrel Ash 1/2 meter grating spectrometer. Figure (A-1) shows the plot of power vs. wavelength and it is seen that the power varies by about 3:1 over the 5600 to 6000Å region.

In the speckle experiments in which the dye laser was tuned through a band of wavelengths we installed a power monitoring system and a neutral density wedge to compensate for the variation in laser power and to maintain constant intensity of illumination on the diffuser samples.

Linewidth: It is noted in the manufacturers instructions that the linewidth of the dye laser is very sensitive to the resonator alignment. In addition, the alignment of the resonator may vary as the output wavelength is changed. At a given wavelength, minimum linewidth should be observed when the resonator is aligned for maximum output power. We have measured the effect of wavelength tuning and resonator alignment on the laser linewidth. Using the Jarrel-Ash 1/2 meter grating spectrometer, we have measured linewidth at a given wavelength. Then, we have tuned to a wavelength 50Å away and without any further adjustment have measured the linewidth at the new wavelength. Upon re-aligning the resonator for maximum power, another linewidth measurement was made. Figure (A-1) shows the result of this process in the 5600 to 6000Å band. Generally, a slight

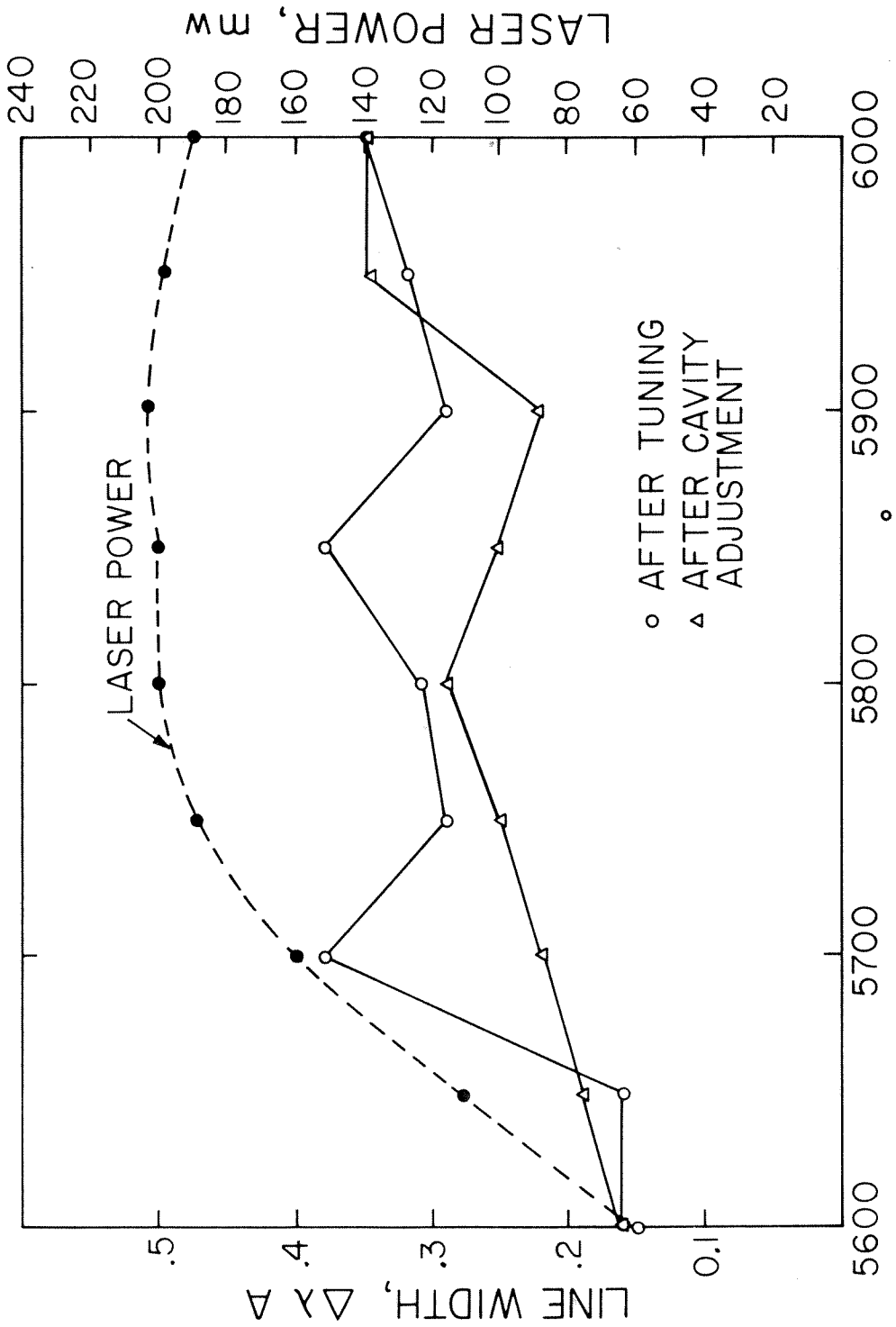

Fig. A-1: Linewidth and laser power variation with selected wavelength output. Linewidth is shown after tuning to a new wavelength and again after making a fine adjustment to the laser cavity to maximize output. The points are connected only to make the data more readable.

improvement (line narrowed) can be made by adjustment of the resonator after tuning to a new wavelength, however the linewidths observed were all under 0.4Å which exceeds the estimate of the manufacturer for the operating conditions used.

In experiments in which the narrow linewidth was important we have adjusted the resonator after wavelength changes of 25 to 50Å.

Tracking of the Laser Wavelength Indicator: The wavelength indicator on the Model 370 Dye Laser is marked in 25Å increments and is mechanically driven from a knurled thumbwheel. One revolution of the thumbwheel changes the wavelength indication by 25Å. We have measured the tracking and accuracy of the indicating system after carefully aligning the indicator at 5800Å with the reference spectrometer. We found that we were able to reset wavelengths to within 2Å at any wavelength by adding reference marks to the thumbwheel and the tracking accuracy is such that wavelength changes as shown on the laser indicator are accurate to within 10% across the entire 5600-6000Å band. At the center of this band where most of our data for the wavelength decorrelation of speckle were obtained, the accuracy of the system is within 5% for 200Å changes in wavelength.

Beam Steering: It was determined that as the wavelength was changed and when the cavity was aligned for peak power output the direction of the laser beam was shifted very slightly. Since it is critical in the speckle experiments that the illumination of the diffusers remain stationary in position and direction to a very close approximation, we have taken the precaution to isolate the laser from

the experiment by a mirror and pinhole spatial filter arrangement as shown in Figure (A-2). In this setup, the 12μm diameter spatial filter defines the spatial source for the illumination beam as "seen" by the diffuser. Using a power monitor in the output of the spatial filter, if the output of the laser shifts slightly, the mirror is re-positioned to give maximum power through the pinhole.

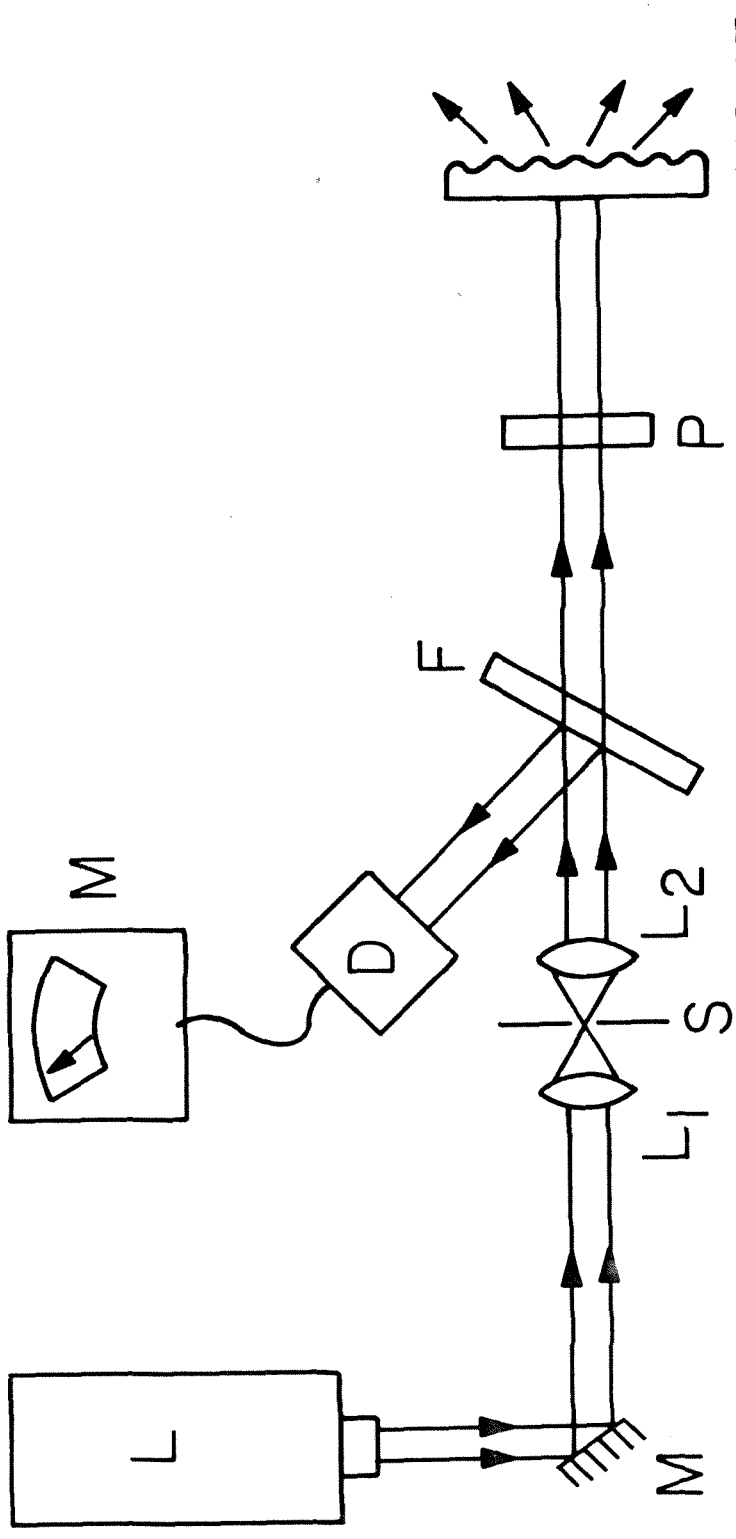

Fig. A-2: Illumination system compensated for laser power fluctuation and beam steering. The beam from laser L is reflected from moveable mirror M and passed through the collimator L_1, S, L_2: L_1 and L_2 are microscope objectives and S is a 12μm pinhole spatial filter. A fraction of the collimated beam is reflected from the glass flat F onto detector D. At P a polarizer or polarization rotator is positioned.

APPENDIX B

Speckle Measurements with Photographic Film

B.1 Introduction

In the main body of this work, we have measured speckle intensity with a fiber optic probe and photomultiplier. This system is a very nearly ideal intensity (square-law) detector and data obtained from it are usable directly in the various first and second order statistical measurements we have made.

However, it is sometimes more convenient to record speckle patterns on photographic film and subsequently to measure first order statistics or autocorrelations from the film. One advantage of this technique in the measurement of autocorrelations is that it permits parallel processing of a large number of speckles in two dimensions, whereas with the probe system an enormous matrix of data points would have to be manipulated in the computer to produce comparable results. A significant disadvantage in the use of film is that it is inherently nonlinear in its response to incident radiation. In this section we present data from a computer simulation of the effect of recording a speckle pattern on either of two commonly used laboratory films to make a negative and then reprocessing the negative to make a positive transparency from which speckle statistics and autocorrelations might be measured.

B.2 Effect of the Photographic Process on First Order Statistics

We have used intensity data observed with the fiber optic probe and have simulated the recording of the data on film such that for each

value of intensity an intensity transmittance, τ , will be formed. An idealized transmittance vs. exposure curve is given by

$$\tau = \left[\frac{(ut)^{\gamma} + \alpha^{\gamma}}{(ut)^{\gamma} + \beta^{\gamma}}\right]^{\Gamma/\gamma} \cdot f \qquad (B.1)$$

where u is the measured intensity, t is exposure time, and α , β , γ , Γ and f are empirically chosen to provide the best fit to the film characteristic published by the manufacturer. The simulation was done using the characteristics of a high contrast film, Kodak 649F and a medium contrast film, Kodak Plus-X Pan. We find that the values $\alpha = 4.6$, $\beta = .48$, $\gamma = 3.42$, $\Gamma = 2.5$ and $f = .0022$ in (B.1) give an excellent fit to 649F curves for very short development times. The values $\alpha = 5.45$, $\beta = .00695$, $\gamma = 3$, $\Gamma = .53$ and $f = .0158$ simulate the Plus-X film. In addition, we have normalized the intensity data and assumed exposure time to match the center of the most linear region of the film characteristic. The array of points τ_i corresponding to u_i then represents a photographic negative. Again using equation (B.1) we insert the values τ_i in place of u and calculate a new array of points. This third data set represents a positive transparency of the speckle intensity.

Now, using the three sets of data we have calculated the density function for intensity for each. Figure (B-1) shows the three densities derived from the original data and from the two film process simulations with 649F. We see that this high contrast film tends to make the intensity binary, that is, the transmittance of the film is either very high

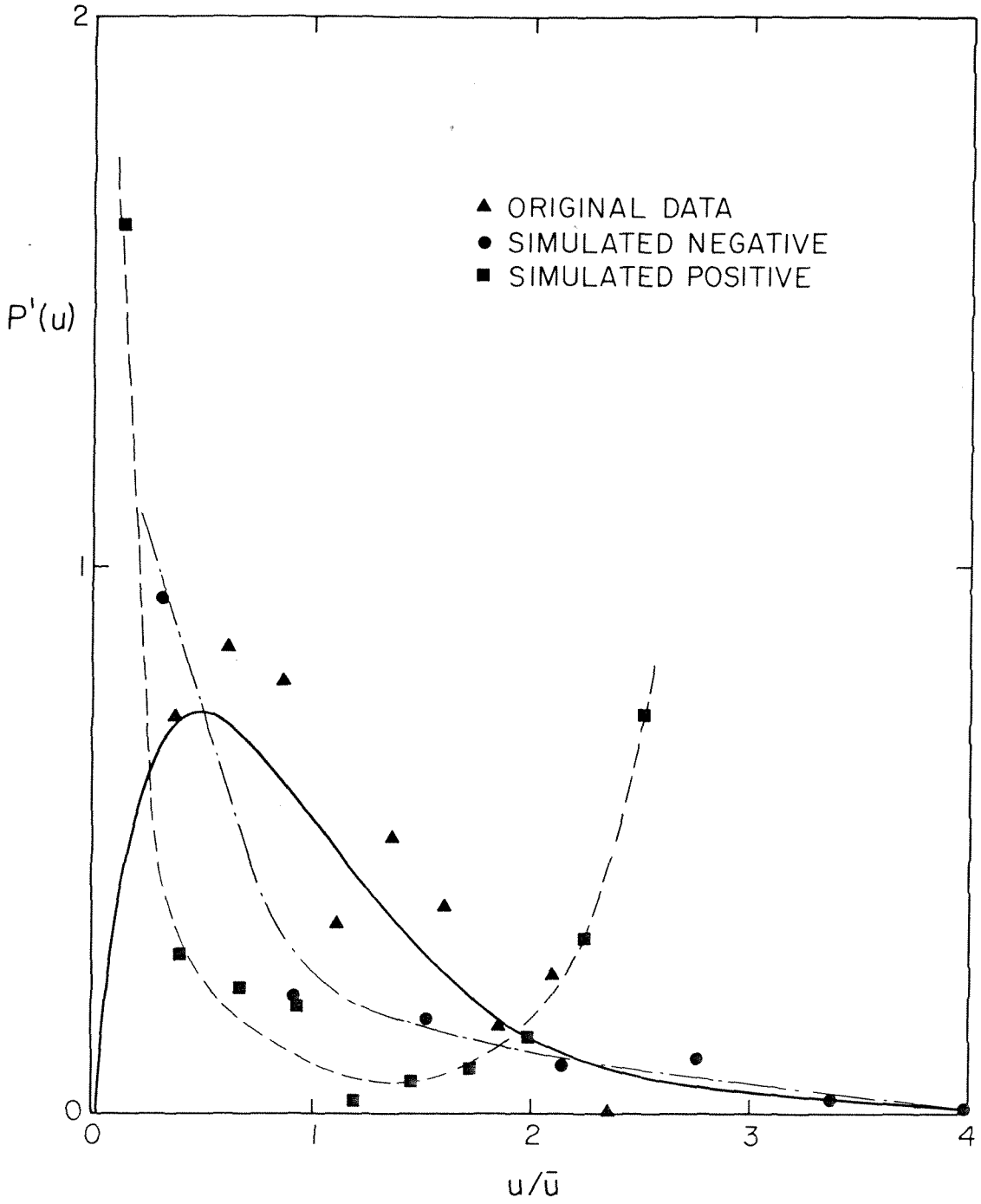

Fig. B-1: Probability density functions for speckle intensity u, normalized to average intensity $\bar{u}$. The plotted points are from experimental data and from a computer simulation of the recording of the data on Kodak 649-F film. The solid curve is from the theory (Ch.IV).

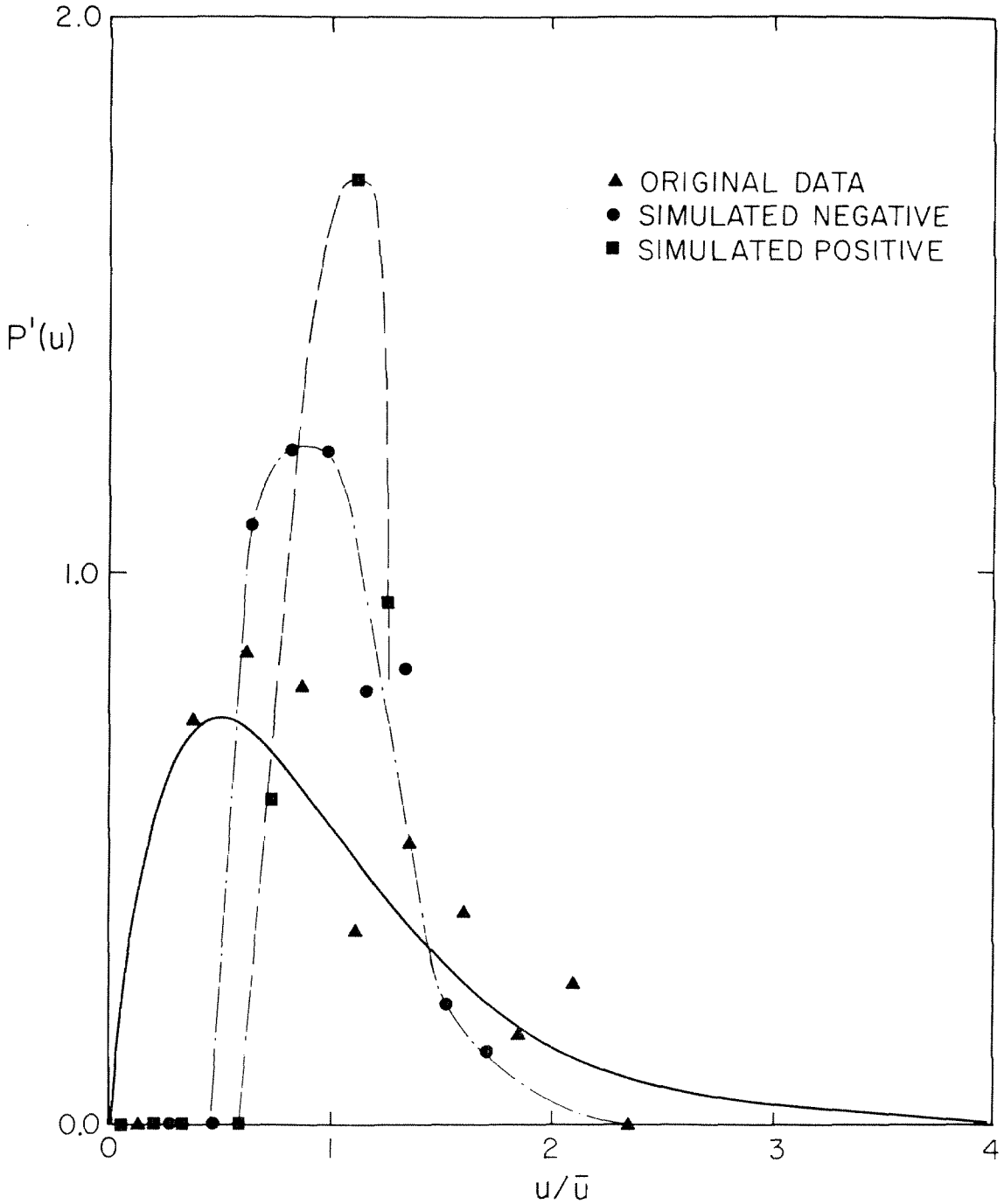

Fig. B-2: Probability density functions for speckle intensity u, normalized to average intensity $\bar{u}$. The plotted points are from experimental data and from a computer simulation of the recording of the data on Kodak Plus-X film. The solid curve is from the theory (Ch.IV)

or very low with few values in the middle range. In Figure (B-2) the effect of the lower contrast Plus-X film is seen. In this case the intensities tend to be grouped around the average value after two film steps.

Thus we see that in order to make correct measurements of the first order statistics from speckle patterns which have been recorded on film it is imperative that very careful compensation for the film transfer characteristic must be made.

B.3 Effect of the Photographic Process on the Autocorrelation Function

In optical processors, as described in Appendix C, photographic transparencies of two-dimensional functions such as speckle patterns are generally used as the input to the system. The output of the processors of interest to us in this context is the convolution product of two transparencies or the self-convolution of one transparency. If, as in the case of speckle patterns, the transparencies represent real functions, the output of the processor is the cross-correlation of two functions or the autocorrelation of a function.

We have simulated the way in which the photographic process influences the measurement of autocorrelations in an optical processor. Thus, using the data representing the original intensity, the photographic negative and the positive transparency for each of the two films, 649F and Plus-X, we have calculated the autocorrelation of each data group. Figure (B-3) shows the autocorrelations as modified by the 649F film curve and Figure (B-4) shows the same autocorrelations as modified by the Plus-X film characteristic. We notice that the

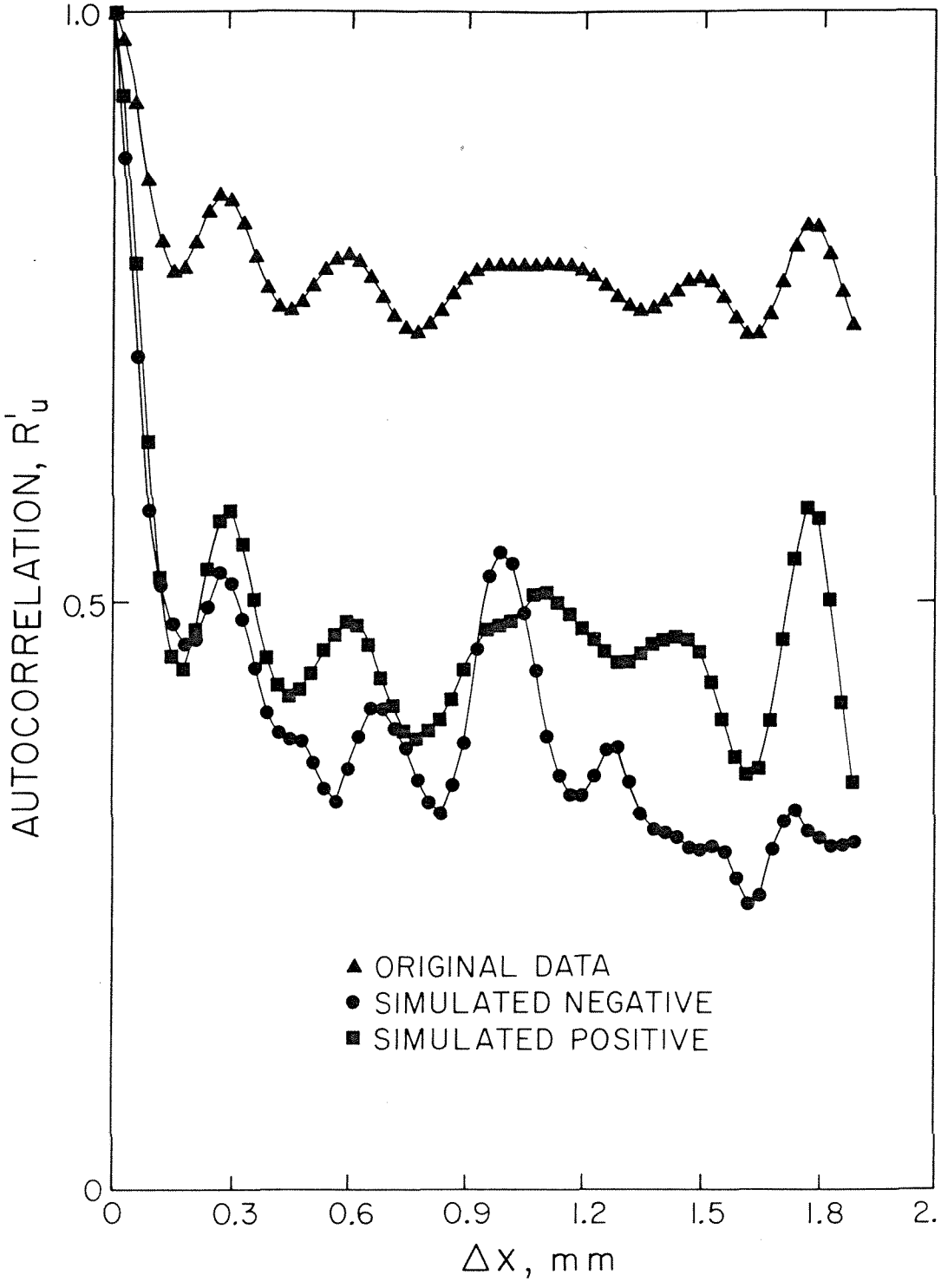

Fig. B-3: Spatial autocorrelation functions for speckle intensity. The plots are from experimental data and from a computer simulation of the recording of the data on Kodak 649-F film. The curves for the processed data drop to a lower level, indicating increased contrast in the speckle (Ch. III).

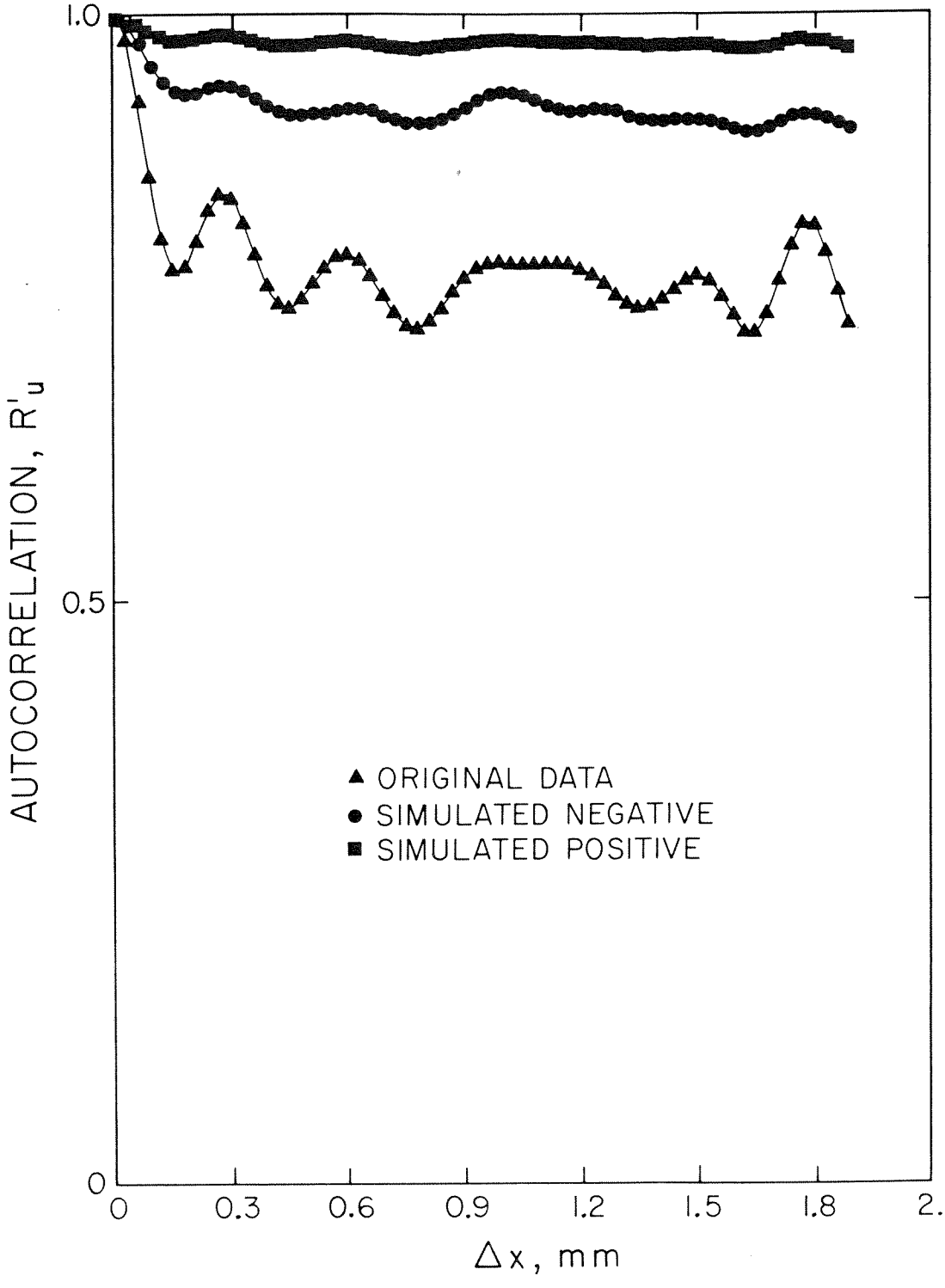

Fig. B-4: Spatial autocorrelation functions for speckle intensity. The plots are from experimental data and from a computer simulation of the recording of the data on Kodak Plus-X film. The curves for the processed data remain at a high level, indication decreased contrast in the speckle (Ch. III).

asymptotic value of the autocorrelation R_u is strongly influenced by the film process. This results from the changes in the first order statistic and hence the contrast of the recorded speckle pattern. The higher contrast is seen as a reduction in the asymptotic value of R_u, while lower contrast has the reverse effect. Thus, the use of uncompensated transparencies in an optical processor will generally not permit accurate measurement of the autocorrelation of speckle intensity. However, the film process does preserve the spatial form of the autocorrelation as seen by the oscillatory period observed in the curves, so that for measurements of the spatial characteristics of speckle patterns uncompensated transparencies may be used.

Appendix C

OPTICAL PROCESSORS

C.1 Introduction

In the study of the properties of two dimensional functions, such as speckle patterns recorded on photographic transparencies, we consider optical systems which measure the convolution product of two spatial functions. These systems also measure auto and cross-correlations of functions when input functions are real valued.

We examine two different systems which might be used for these purposes. The first allows us to look at the convolution of two functions displayed as a two dimensional image. In doing so, we can determine immediately the existence of periodic or deterministic functions on the transparency which are almost totally obscured in normal imaging. This system provides a qualitative look at the functions and allows us to accept or reject transparencies for further and more laborious measurement. The second system enables us to evaluate the convolution of functions in two dimensions to a high degree of accuracy. Data are taken point-by-point and the results plotted by digital computer techniques.

C.2 Image of the Convolution Product

We examine images of the convolution of two transparencies in a manner given by Kovasnay and Arman [1]. Although the system used in this technique is frequently referred to as an autocorrelator, it is

better described as a system for performing a convolution [2]. As will be shown, the autocorrelation is obtained as a result of the characteristics of the input to the system and not strictly from the action of the system.

To analyze the operation of the system we refer to figure (C-1), and we use the notation of Goodman[2]. S is a distributed, incoherent source; lenses L_1 & L_2 are a matched pair of focal length f_1, and D is the output plane at the focal distance from L_2. The intensity transmittance of an input function, $\tau(x,y)$ is defined by

$$\tau(x,y) = \frac{\text{Intensity transmitted at } (x,y)}{\text{Intensity incident at } (x,y)} \qquad (C.3)$$

and d is the distance between τ_1 & τ_2. The geometry of the system is such that light rays from the point $(-x_s,-y_s)$ on the source emerge from L_1 as a parallel beam at an angle θ with the optic axis, where

$$\theta = \tan^{-1} \frac{x_s}{f} \qquad (C.2)$$

Therefore, if we choose the optic axis as the common origin of coordinates for τ_1 and τ_2, a ray which intercepts τ_1 at $(-x,-y)$ will intercept τ_2 at $(-x + \frac{x_s}{f} d, -y + \frac{y_s}{f} d)$. When all of the rays which traverse the system are brought into focus at plane D at $(x_D = x_s, y_D = y_s)$ the intensity at x_s, y_s is given by

$$I(x_s,y_s) = k \int_{-\infty}^{\infty}\int \tau_1(-x,-y)\tau_2(\frac{x_s}{f}d - x, \frac{y_s}{f} d - y)dxdy \qquad (C.3)$$

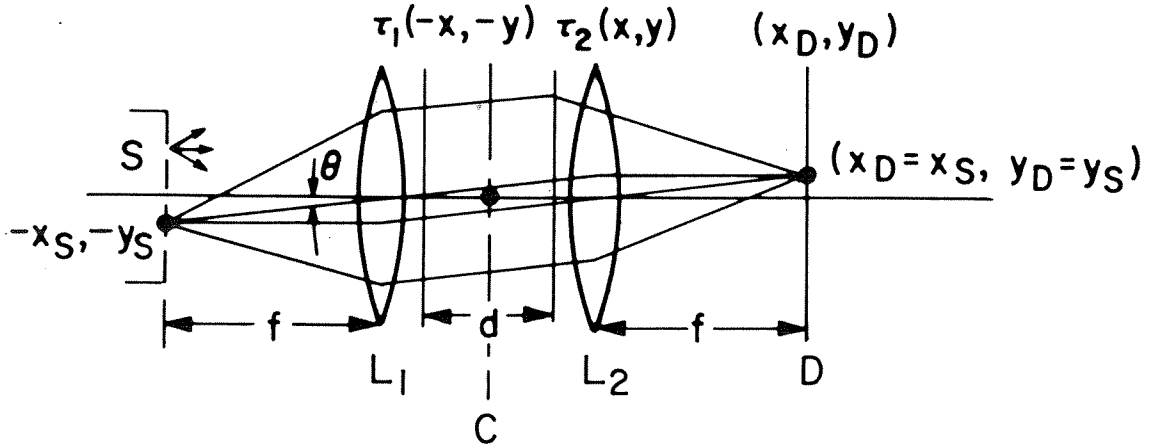

Fig. C-1: Optical system for viewing the convolution of two transparencies of intensity transmittance τ. S is an extended white-light source, L_1&L_2 lenses of focal length f and D is the image plane for the convolution.

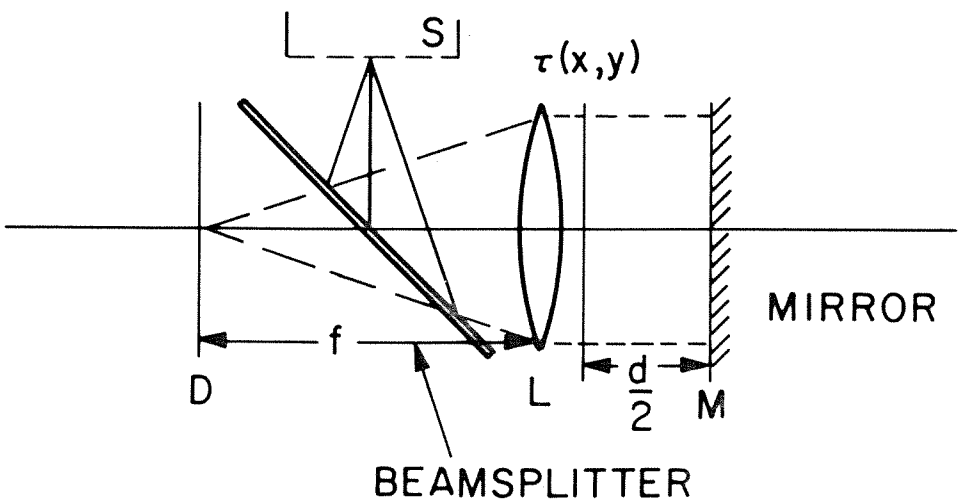

Fig. C-2: Improved system for viewing the self-convolution of a transparency τ. The mirror is placed at plane C of Fig. (C-1) and the beamsplitter is used so that the source S can be moved out of the image plane D.

Thus, if we insert either τ_1 or τ_2 in a reflected geometry, i.e., $\tau(-x,-y)$ then (C.3) will be the convolution of the functions τ_1 and τ_2 where the effects of finite aperture are included in the functions τ and the integration is over the infinite limits.

We write the autocorrelation of a function g

$$R_{gg}(x,y) = \iint_{-\infty}^{\infty} g(x_o,y_o)g^*(x - x_o,y - y_o)dx_o dy_o \qquad (C.4)$$

Then from equation (C.3), we see that if we choose $\tau_1 = \tau_2$ and both are real, the intensity in the output will be

$$I(x_s,y_s) = k \iint_{-\infty}^{\infty} \tau(x,y)\tau^*(\frac{d}{f} x_s - x, \frac{d}{f} y_s - y)dxdy \qquad (C.5)$$

or

$$I(x_s,y_s) = k\, R_{\tau\tau}\,(x_s,y_s) \qquad (C.6)$$

Figure C-2 shows an improved system used to obtain the autocorrelation functions. Because of the symmetry about the axis C in figure (C-1), we see that the output of this system is the same as we have shown in equation (C.6) except for a multiplicative fractional constant introduced by the beam-splitter. The system of figure (C-2) is simpler for autocorrelations because we do not have to duplicate the functions and careful spatial registry of the two function spaces is not required.

C.3 Measurement of the Convolution Product

We measure the convolution of two spatial functions in a coherent optical processor. Since this system is linear in electric

field amplitude and not in intensity, we characterize the inputs to the system in terms of field amplitude transmission function, t(x,y). These functions are defined such that

$$t(x,y) = \frac{\text{amplitude transmitted at } (x,y)}{\text{amplitude incident at } (x,y)}$$

It is noted that in a photographic transparency the function t(x,y) is related to the intensity transmittance $\tau(x,y)$ by the relation [2]

$$t(x,y) = \pm\sqrt{\tau(x,y)}\ \exp\{i\phi(x,y)\} \qquad (C.7)$$

where $\phi(x,y)$ is a phase variation introduced by the recording medium.

Figure (C-3) shows the system. An expanded and collimated laser beam passes through the transparency t(x,y) at plane 1. A carefully matched pair of lenses, L_1 & L_2, forms the inverted image t(x,y) at plane 3. At plane 3, another transparency t or s(x,y) is placed. This second transparency is mounted in a precision x-y translation stage which can provide measureable motions of the order of 1μm. The output of the system is taken from lens L_3 through the spatial filter in the output focal plane.

In the analysis of the system we make use of repeated application of the Fresnel zone approximation to Sommerfeld's formula [2]. In a generalized imaging system, the output field amplitude $u(x,y)e^{i\omega t}$ is given by

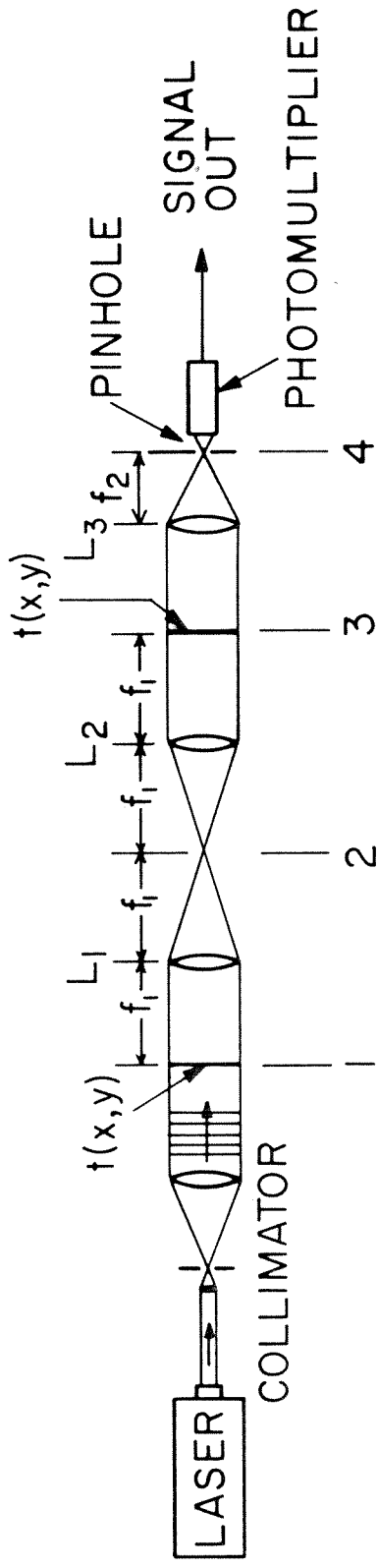

Fig. C-3: Coherent optical processor. Lenses L_1 and L_2 have identical focal length f_1. L_3 has focal length f_2. Transparencies of amplitude transmittance $t(x,y)$ are placed on precision x-y translators at planes 1 and 3. A pinhole spatial filter approximately the size of the impulse response of L_3 is located in plane 4. The convolution is obtained by moving one of the transparencies and measuring the photomultiplier signal as a function of the transparency position.

$$u(x,y) = \frac{-\exp\left\{\frac{-i2\pi}{\lambda}(s + s')\right\}}{\lambda^2 ss'} \int_{-\infty}^{\infty}\int\int\int\int d\xi d\eta du dv \;\; u(\xi,\eta) \qquad (C.8)$$

$$\cdot\, T(u,v)\, \exp\left\{\frac{-i\pi}{\lambda s'}\left[(u - \xi)^2 + (v - \eta)^2\right]\right\}$$

$$\cdot\, \exp\left\{\frac{-i\pi}{\lambda s}\left[(x - u)^2 + (y - v)^2\right]\right\}$$

Where (ξ,η) is the input field and $T(u,v)$ is the transmission function of the lens which includes the spherical phase factor. The $e^{i\omega t}$ dependence is suppressed.

In the system of figure (C-3), we make the infinite aperture approximation, i.e.:

$$T(u,v) = \exp\left\{\frac{i\pi}{\lambda f}(u^2 + v^2)\right\} \qquad (C.9)$$

and we assume a unit amplitude plane wave illumination at plane 1. The field at plane 1 is then $t(x,y)$. Applying equation (C.8), we find the field at plane 2 to be

$$u(x_2,y_2) = \frac{-\exp\left\{\frac{-i2\pi}{\lambda}(f_1 + f_1)\right\}}{\lambda^2 {f_1}^2} \int_{-\infty}^{\infty}\int\int\int\int dx_1 dy_1 dx_a dy_a \; u(x_1,y_1)$$

$$\cdot \exp\left\{\frac{i\pi}{\lambda f_1}\left[(x_a^2 + y_a^2) - (x_a - x_1)^2 - (y_a - y_1)^2\right.\right.$$

$$\left.\left. - (x_2 - x_a)^2 - (y_2 - y_a)^2\right]\right\} \qquad (C.10)$$

We integrate over the lens plane variables (x_a, y_a) giving the result:

$$u(x_2,y_2) = \frac{\exp\left\{-i\left(\frac{4\pi f_1}{\lambda} + \frac{\pi}{2}\right)\right\}}{\lambda f_1} \iint_{-\infty}^{\infty} dx_1 dy_1 t(x_1,y_1) \exp\left\{i\frac{2\pi}{\lambda f_1}(x_2x_1 + y_2y_1)\right\} \tag{C.11}$$

We apply this result a second time to find the fields at plane 3.

$$u(x_3,y_3) = \frac{\exp\left\{-i\left(\frac{8\pi f_1}{\lambda} + \pi\right)\right\}}{\lambda^2 f_1^2} \iiiint_{-\infty}^{\infty} dx_1 dy_1 dx_2 dy_2 \; t(x_1,y_1)$$

$$\cdot \exp\left\{i\frac{2\pi}{\lambda f_1}\left[(x_2x_1 + y_2y_1) + (x_3x_2 + y_3y_2)\right]\right\} \tag{C.12}$$

Integration over the x_2, y_2 variables yields

$$u(x_3,y_3) = \exp\{-i(4kf_1 + \pi)\}$$

$$\cdot \iint_{-\infty}^{\infty} dx_1 dy_1 \; t(x_1,y_1)\delta(x_1 + x_3)\delta(y_1 + y_3) \tag{C.13}$$

where $k = \frac{2\pi}{\lambda}$ and δ is the dirac delta function.

Therefore at plane 3 we have the field

$$u(x_3,y_3) = t(-x_3,-y_3) \exp\{-i(4kf_1 + \pi)\} \tag{C.14}$$

which is the same as the field at plane 1 with reflected geometry and phase delay.

At plane 3 we insert a second transparency of amplitude transmission $s(x_3,y_3)$. This function is mounted in the precision x-y

translation stage enabling us to form $s(x_3-x,y_3-y)$. The field immediately past plane 3 is then given by

$$u'(x_3,y_3) = t(-x_3,-y_3)s(x_3-x,y_3-y)\exp\{-i(4kf_1 + \pi)\} \tag{C.15}$$

Application of equation (C.11) gives the field at plane 4:

$$u(x_4,y_4) = \frac{\exp\{-i(2kf_2 + \frac{\pi}{2})\}}{\lambda f_2} \exp\{-i(4kf_1 + \pi\} \cdot \iint_{-\infty}^{\infty} dx_3dy_3\ t(-x_3,-y_3)s(x_3-x,y_3-y) \cdot \exp\left\{\frac{ik}{f_2}(x_4x_3 + y_4y_3)\right\} \tag{C.16}$$

Now at plane 4 we have placed the pinhole spatial filter, so that to a close approximation the only field which passes to the photodetector is that characterized by $x_4 = y_4 = 0$. Thus, the field seen by the photodetector is

$$u_p = \frac{\exp\{i(4kf_1 + 2kf_2 + \frac{3\pi}{2})\}}{\lambda f_2} \cdot \iint_{-\infty}^{\infty} t(-x_3-y_3)s(x_3-x,y_3-y)dx_3dy_3 \tag{C.17}$$

If we place one of the transparencies in the system with reflected geometry we will make the field at the photodetector proportional to

the convolution of t and s:

$$u_p = K \iint_{-\infty}^{\infty} t(x_3,y_3)s(x_3-x,y_3-y)dx_3dy_3 \qquad (C.18)$$

If the functions are real, then the intensity at the photodetector will be proportional to the cross-correlation of the intensity transmittances of the transparencies t and s.

REFERENCES

1. Kovasnay, L.S.G. & Arman, A.: Rev. Sci. Inst. 28, 793 (1957).

2. Goodman, J.W.: Intro to Fourier Optics, McGraw-Hill, N.Y. (1968).